

**THE SEARCH FOR SUPERNOVA LIGHT ECHOES FROM THE
CORE-COLLAPSE SUPERNOVAE OF AD 1054 (CRAB) AND AD 1181**

**THE SEARCH FOR SUPERNOVA LIGHT ECHOES
FROM THE CORE-COLLAPSE SUPERNOVAE OF
AD 1054 (CRAB) AND AD 1181**

By

BRITTANY JUNE MCDONALD, B.Sc.

A Thesis
Submitted to the School of Graduate Studies
in Partial Fulfillment of the Requirements
for the Degree
Master of Science

McMaster University
©Copyright by Brittany June McDonald, 2012.

MASTER OF SCIENCE (2012)
(Physics)

McMaster University
Hamilton, Ontario

TITLE: The Search for Supernova Light Echoes from the Core-Collapse Supernovae of AD 1054 (Crab) and AD 1181

AUTHOR: Brittany June McDonald, B.Sc.(McMaster University)

SUPERVISOR: Dr. Doug Welch

NUMBER OF PAGES: x, 123

Abstract

A deep, wide-field survey was conducted to hunt for the light echo systems associated with SN 1054 (Crab) and SN 1181 as an initial step to acquiring spectra and the prospect of extracting lightcurves of these historical, core-collapse supernovae. Images were acquired by the Canada-France-Hawaii Telescope's MegaCam during the 2011A and 2011B semesters for fields adjacent to SN 1054 and SN 1181, respectively. A total of 367 Sloan g' fields for the Crab and 195 Sloan r' fields for SN 1181 were imaged twice, with a minimum of one month separation.

Examination of 13,880 and 11,052 difference images for the Crab and SN 1181, respectively, revealed no light echoes with surface brightnesses brighter than $24.0 \text{ mag/arcsec}^2$ (the threshold for being able to acquire useful spectra). Based on our non-detections and assuming similar dust properties to nearby (detected) supernova light echo systems (Tycho and Cas A), we conclude it is unlikely that either SN was a Type II-L outburst but cannot provide constraints on other sub-types.

We further examined the known light echo locations for Tycho and Cas A and found a statistically-significant correlation between CO brightness temperature and the presence of scattering dust. However, the spacing of grid points in existing CO surveys is too sparse to be useful even a few degrees away from the galactic plane. We have yet to identify a search strategy based on survey data which is superior than random field placement.

Acknowledgements

First and foremost I would like to thank my supervisor, Dr. Doug Welch, for his guidance, support, and positivity - he was a constant source of motivation! Doug - your perpetual enthusiasm for astronomy is truly inspiring and contagious! I am so grateful to have worked on such an exciting and interesting research project with you. I don't know how to adequately express my thanks for all of the spectacular opportunities you have provided me with over the last two years. I would additionally like to express my gratitude towards my group member, Brendan Sinnott, who was a constant help and mentor throughout my research. I would like to thank my other committee members: Dr. Christine Wilson and Dr. Laura Parker - you have been inspirational throughout my entire journey in astronomy and your input and advice are truly valued.

Most importantly, I would like to thank all my loved ones for their unwavering supply of love and support throughout this process - you have stood by me with encouragement and patience when I have needed it the most.

1	Introduction to Supernovae	1
1.1	Types of Supernovae	1
1.1.1	Thermonuclear Supernovae (Type Ia)	2
1.1.2	Core-collapse Supernovae	8
1.2	The Milky Way’s Historical Supernovae	11
2	Introduction to Light Echoes	19
2.1	Finding Light Echoes	20
2.1.1	The First Light Echo Discoveries	20
2.1.2	Discovering Light Echoes using Difference Imaging	22
2.2	Light Echo Formalism and Analysis	25
2.2.1	Geometry	25
2.2.2	Dust Scattering	27
2.2.3	Apparent Proper Motion	28
2.2.4	Light Echo Profile	29
2.2.5	Light Echo Spectroscopy	29
3	The Ancient SNe of 1054 AD (Crab) & 1181 AD	33
3.1	The Crab Supernova	33
3.2	Supernova 1181 AD & Radio Source 3C 58	35

4	Observations, Reductions and Searching	37
4.1	Reduction and Difference-Imaging Technique	37
4.2	Imaging at KPNO	39
4.3	Imaging at CFHT	41
4.3.1	CFHT & the Crab SN	42
4.3.2	CFHT & SN 1181 AD	43
4.4	Inspecting the Difference Images for LEs	45
5	Implications of Non-Detection	51
5.1	Dust	51
5.2	Distance Reliability	56
5.2.1	The Distance to the Crab Nebula	57
5.2.2	The Distance to the Radio Source 3C 58	57
5.3	Age Reliability	61
5.3.1	The Age of the Crab SN	62
5.3.2	The Age of 3C 58	64
5.4	Type	67
5.5	Expected Brightness	68
6	Discussion and Conclusions	73
6.1	Light Echo Visibility in our Survey	73
6.2	Conclusions	76
	Appendices	81
A	CFHT MegaCam Program 11AC033 Observed Fields	81
B	CFHT MegaCam Program 11BC021 Observed Fields	95
C	W_{CO} Values for Light Echo Fields	103
	References	105

LIST OF FIGURES

1.1	The Supernova Classification Tree	2
2.1	Light Echoes and Superluminal Motion	21
2.2	Difference-Imaging Example	23
2.3	Light Echo Geometry	26
4.1	Observing strategy for 11AC033 MegaCam program at CFHT (searching for Crab LEs)	44
4.2	Observing strategy for 11BC021 MegaCam program at CFHT (searching for SN 1181 LEs)	46
4.3	Positions on sky of the brightest Tycho and Cas A LEs found in the 2011B MegaCam data	48
4.4	Close-up of Tycho and Cas A LEs found in the 2011B MegaCam data	48
4.5	Difference images showing a few of the brightest LEs found in the 2011B MegaCam data.	49
5.1	Distribution of W_{CO} for fields with known Tycho and Cas A LEs.	53
5.2	Distribution of W_{CO} for the fields from the 11BC021 MegaCam program (SN 1181 LE search) that we <i>did not</i> detect LEs in.	54
5.3	MegaCam 11BC021 observing field locations and positions of known bright Cas A and Tycho LEs on Dame et al. (2001) W_{CO} map	55

- 5.4 Comparing the observing strategy used for our SN 1181 LE MegaCam survey, which assumed a 2 kpc distance, to the area covered if we had assumed 3.2 kpc 62

LIST OF TABLES

1.1	Sub-types of Core-Collapse Supernovae	10
1.2	Summary of the Milky Way's Historical SNe	13
4.1	General MOSAIC-1.1 Characteristics at the KPNO 4-Meter	40
4.2	Summary of our group's LE programs at KPNO	40
4.3	General MegaPrime/MegaCam Characteristics at CFHT	42
4.4	New Tycho and Cas A LEs found in the MegaCam 11BC021 data.	50
5.1	Summary of recent studies that have determined distances to Galactic SNRs associated with spiral arms	60
5.2	Summary of Age Estimates for 3C 58	65
5.3	Summary of Core-collapse SN Surveys	68
5.4	Average Absolute Peak Magnitudes of Core-collapse Sub-types	68
5.5	Tycho SN and LE Properties	70
5.6	Surface brightness estimates for a SN 1181 LE in MegaCam	70
5.7	Surface brightness estimates for a 3C 58 LE in MegaCam assuming age of 4000 yrs	71
5.8	Surface brightness estimates for a Crab SN LE in MegaCam	71
6.1	The probability of LE detection for the SN 1181	74
6.2	The probability of LE detection for a 4000 yr old SN that created 3C 58	74

6.3	The probability of LE detection for the Crab SN	75
A.1	CFHT MegaCam Program 11AC033 Observed Crab Fields	93
B.1	CFHT MegaCam Program 11BC021 Observed SN 1181 Fields	101
C.1	W_{CO} Values [K km/s] for Light Echo Fields	104

CHAPTER 1

INTRODUCTION TO SUPERNOVAE

1.1 Types of Supernovae

Supernovae (SNe) are stellar explosions involving the collapse or disruption of a star. At peak brightness, these explosions have luminosities of at least 100 million times that of the Sun with a fading period that lasts for many weeks afterward (Doggett & Branch, 1985). Much of the star's material is ejected into the surrounding interstellar medium at velocities reaching up to 10,000 km/s, leaving behind a supernova remnant (SNR) bound by the expanding shock wave. A young SNR ($< 50,000$ yrs old) often has a complex multi-wavelength structure due to the interaction of the star's ejected material with that of the interstellar medium.

SNe represent the end state of several different evolutionary scenarios beginning with a variety of stellar progenitor systems. Figure 1.1 shows the SN classification tree with the basic division of types based on the presence or absence of certain features in SN spectra taken near maximum light (Minkowski, 1941; da Silva, 1993). The primary division is thermonuclear (Type Ia) vs. core-collapse (Type Ib, Ic, and Type II) explosions. Spectra, lightcurves, and even environment help delineate SN into types and sub-types.

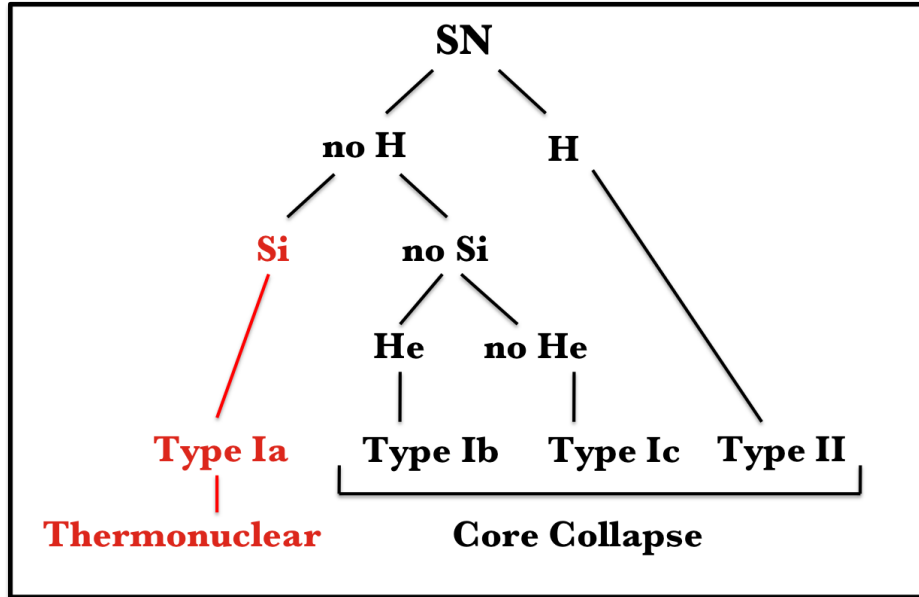


Figure 1.1 The supernova classification tree showing the basic division of thermonuclear vs. core-collapse explosions based on the presence or absence of certain features in their spectra taken near maximum light. This figure is adapted from Leibundgut (2008).

1.1.1 Thermonuclear Supernovae (Type Ia)

Type Ia SNe are believed to be thermonuclear explosions of a white dwarf (WD) star that has accreted mass from a binary companion and has undergone a runaway nuclear fusion reaction (Hillebrandt & Niemeyer, 2000). WDs are degenerate dense objects that are comprised of carbon and oxygen (CO WD). They represent the endpoint of stars within the mass range between about 0.07 and $10 M_{\odot}$ (Fontaine et al., 2001; Heger et al., 2003). WDs are supported by electron degeneracy pressure - not energy derived from nuclear fusion.

The standard model for SNe Ia is a carbon-oxygen WD that is accreting mass (from a binary partner) to the point that carbon is ignited just before the Chandrasekhar mass limit of $1.38 M_{\odot}$ (Hillebrandt & Niemeyer, 2000). The ignition creates a runaway thermonuclear reaction that rips through the WD, ultimately completely unbinding it in a matter of seconds and creating the SN explosion. The details of this process are still a matter of debate. There is good evidence that the exploding star is a WD (neither H or He is seen in type Ia spectra; Leonard (2007)) but the characteristics of the binary companion are a current subject of

dispute. These issues along with observations of SNe Ia, and the importance that they have had for cosmology will be discussed below.

Observations of SNe Ia Type Ia SNe are classified by the lack of hydrogen in their spectra (distinguishing them from Type II SNe) and a characteristic, singly-ionized silicon line at 615 nm during peak brightness (further classifying them as Type Ia; Wheeler & Harkness (1990)). Other elements found in SN Ia spectra at maximum light are neutral and ionized lines of intermediate-mass elements Ca, Mg, S, and O. The spectral evolution of SNe Ia are thought to represent the expansion and thinning of the SN, exposing different layers of the nucleosynthesis-enriched ejecta at various times (Hillebrandt & Niemeyer, 2000). Late-time spectra (~ 1 month after maximum light) are dominated by emission lines from iron-peak elements (Ni, Co, and Fe) that are thought to have been synthesized in the dense inner regions of the WD. The luminosity of SNe Ia results from the radioactive decay of first ^{56}Ni to ^{56}Co , then ^{56}Co to ^{56}Fe (Hillebrandt & Niemeyer, 2000). The spectral and photometric properties of individual SNe Ia are almost indistinguishable (Hamuy et al., 1996b). In the B-band, SNe Ia have typical rise times of about 20 days (Riess et al., 1999) peaking at a magnitude of:

$$M_B \approx M_V \approx -19.30 \pm 0.03 \quad (1.1)$$

The peak magnitudes of SNe Ia have a dispersion of $\sigma_M \leq 0.3$ (Hamuy et al., 1996a). It is important to note that empirical corrections are made for SNe Ia lightcurve shape and colour in order to obtain Equation 1.1. These consistent values make SNe Ia *standard candles* in astronomy and they remain important distance indicators (particularly due to their high intrinsic luminosity).

Type Ia SNe & Cosmology Due to their visibility at great distances, SNe Ia have become one of the best extragalactic distance indicators with a range greater than 1000 Mpc and a precision of 6% in distance (Jacoby et al., 1992). As was mentioned earlier, corrections must be made in order to obtain accurate distance estimates because individual SNe Ia do have some of the following intrinsic differences. There is still some dispersion in peak luminosity such that the brighter ones have broader light curves. However, it has been found

that the peak luminosity of SNe Ia are correlated with the rate of rise and fall in their brightness (Phillips, 1993). Therefore, the width of their light curves can be measured and used to correct the peak luminosity (see the 'stretch factor' method by Perlmutter et al. (1999) or the $\Delta m_{15}(B)$ parameterization by Phillips (1993) for more details). Differences in peak luminosity can also be affected by colour due to reddening from dust (Riess et al., 1996; Conley et al., 2007). These differences are corrected for by fitting various lightcurve models to observations (Jha et al., 2007; Guy et al., 2007). The standardization process above has been highly refined and now only subtle, systematic errors are thought to be responsible for any non-cosmological differences in magnitude.

The importance that SNe Ia have had to cosmology cannot be understated. The magnitude of SNe Ia should drop predictably as a function of redshift based on the rate of expansion of the universe described by the Hubble constant H_0 , and the other model parameters of the cosmological model of the universe. In 1998, distance determinations of distant Type Ia led to the unexpected result that the universe's expansion is accelerating with time. The findings were led by two independent groups - the Supernova Cosmology Project (SCP) (Perlmutter et al., 1999) and the High-z Supernova Search Team (Schmidt et al., 1998). They both observed more than 50 high-redshift SNe and were able to construct a Hubble diagram (distance vs. redshift) that extended out to $z = 1$ (distances for many local SNe already existed). After correcting for intrinsic factors (see above) and systematic errors, the results of their investigations showed that the distant SNe were dimmer than would be expected (i.e. larger than expected distances) if the universe was expanding at a constant rate or slowing down (as was previously expected). The best fit to the 1998 SN data implies that we are currently living in an epoch where the vacuum energy density ρ_Λ is larger than the mass energy density ρ_m indicating that the cosmic expansion is accelerating. This effect has since been deemed 'dark energy' - energy with negative pressure (Turner & Tyson, 1999). In units of critical density ρ_c , we can define the parameters $\Omega_\Lambda = \rho_\Lambda/\rho_c$ and $\Omega_m = \rho_m/\rho_c$.

Overall, three independent sets of observations in cosmology have worked together in determining the current normalized mass and vacuum energy densities: (1) distant SNe Ia

constrain $\Omega_\Lambda - \Omega_m$ and $\Omega_\Lambda > 0$ (Knop et al., 2003); (2) galaxy cluster inventories have constrained Ω_m (Allen et al., 2002); and (3) the cosmic microwave background (CMB using WMAP data; Spergel et al. (2003)) indicates a flat universe $\Omega_\Lambda + \Omega_m = 1$. All three studies are consistent with each other for an accelerating, flat universe. The values of Ω_Λ and Ω_m which best fit the above constraints have converged and we now estimate that:

$$\Omega_\Lambda \approx 0.7 \quad \Omega_m \approx 0.3 \quad (1.2)$$

SNe Ia Explosion Theory Primary arguments in favour of the current standard model are: (1) there are no observed compact objects associated with Type Ia SNRs; (2) the spectral and photometric properties of this distinct sub-type are very homogeneous and specific (recall the observations section for SNe Ia); (3) simulations of this model fit well with the observed light curves as well as the spectra of typical Type Ia SNe.

A specific issue with the standard SNe Ia model is the speed at which thermonuclear burning occurs in the WD. Burning that occurs supersonically (detonation) vs. a subsonic burning (deflagration) should create very different outcomes. Supersonic burning gives no time for the WD to expand and thus the high density should result in the synthesis of *only* iron-peak elements (a property we do not observe in spectra or lightcurves for SNe Ia; Arnett (1969)). Intermediate elements would be created via subsonic burning at a lower density (Nomoto et al., 1984), in agreement with many observations but fails to produce the high velocities required for the explosion (Mazzali et al., 2005) and leaves too much O and C unburned according to 3D-simulations (Gamezo et al., 2005). The resolution of this issue likely lies in a situation that begins with deflagration and transitions to detonation (Khokhlov, 1991). Although the physics is still not completely understood, some multi-dimensional simulations have been successful at producing the SN explosion using this method via the breaking of spherical symmetry by turbulent instabilities (Kasen et al., 2009; Röpke & Hillebrandt, 2005). Such simulations have also recently revealed that breaking of spherical symmetry is likely a critical factor in determining the width-luminosity relation for SNe Ia (Kasen et al., 2009). Explosions using more deflagration produce dimmer SNe Ia while those dominated by detonation produce brighter SNe Ia due to higher abundance

of ^{56}Ni produced. Therefore, the relative importance and partition of deflagrations, detonations and asymmetry must be considered when determining distances to SNe Ia using observations of their lightcurves (Kasen et al., 2009).

The SNe Ia Progenitor Question Although it is universally accepted that the primary exploding star in a SNe Ia is a WD, the properties of the secondary star remain uncertain. Unlike core-collapse SNe, SNe Ia progenitor stars have never been convincingly detected in pre-explosion images (Maoz & Mannucci, 2008; Li et al., 2011a). There are two primary models for the SN Ia binary system that have been investigated in the literature and both will be described here.

- **Single Degenerate (SD):** Binary partner is a non-degenerate main sequence or red giant star that loses mass to a carbon-oxygen WD via either Roche lobe overflow, or a wind (Whelan & Iben, 1973). There are many theoretical and observational issues that have arisen with this model. According to theory, the mass accretion rate on the the WD needs to be very specific (between 10^{-7} and $10^{-8} M_{\odot} \text{yr}^{-1}$) in order to both continue hydrogen burning on the surface and to maintain the accumulation of mass towards the Chandrasekhar limit (Nomoto, 1982). This specific, steady burning should generate super-soft X-rays that can be observed (van den Heuvel et al., 1992). Unfortunately the rate of super-soft X-ray sources observed simply does not match what we should expect based on the SN Ia rate if a connection did exist (Di Stefano, 2010; Gilfanov & Bogdán, 2010). Observational searches for signatures of the companion star have also not been very successful. For example, in the SD scenario, the partner should have survived the explosion and be detectable in the SNR (Wang & Han, 2010). The survivor associated with the Tycho SN has not yet been discovered (Ruiz-Lapuente, 2004; Fuhrmann, 2005; González Hernández et al., 2009; Kerzendorf et al., 2009). The lack of any H or He in late-time observations of SNe Ia (from the companion’s stellar winds) is also a primary problem for the SD model (Leonard, 2007).
- **Double Degenerate (DD):** The merger and explosion of two WDs after losing energy and angular momentum to gravitational waves (Iben & Tutukov, 1984; Webbink, 1984).

Simulations of this scenario using two equal-mass WDs have been successful in producing subluminous SN Ia (Pakmor et al., 2010). The key to obtaining normal or even overluminous SNe Ia via this process (using more massive equal-mass WDs) is still being investigated as the complicated 3-D simulations that are required have only recently been achieved. The Galactic SN Ia rate has also recently been found to agree with the local WD merger rate assuming that sub-Chandrasekhar mass mergers can also produce a SN Ia (Maoz & Mannucci, 2011).

Recently, the Palomar Transient Factory (PTF) survey was able to detect a SN event (SN 2011fe in M101 at 6.4 Mpc) less than a day after its explosion. SN 2011fe was detected so early that research teams have been able to put direct observational constraints on the progenitor system of this normal Type Ia SN. Li et al. (2011a) used pre-explosion imaging to exclude a luminous red giant as the companion. Nugent et al. (2011) and Brown et al. (2012) used very early observations in the optical and UV to rule out the presence of SN shocks from any ejecta colliding with a companion. Specifically, they ruled out red-giants along with most massive main-sequence stars. Chomiuk et al. (2012) used ELVA (Expanded Very Large Array Project) to obtain radio observations of SN 2011fe and infer a mass loss rate from the progenitor system. Based on these constraints, they ruled out SD progenitor models for this SN. Overall, evidence supporting a DD model as opposed to a SD model has been growing. It seems the long-favoured progenitor paradigm of an accreting WD from a MS or RG star simply cannot account for all - or possibly any - SNe Ia. As we enter the 'synoptic survey era' (large numbers of SNe Ia observations), there is every indication that the progenitor problem will be conclusively resolved.

The Future of SNe Ia Research Third-generation surveys such as the Palomar Transient Factory, Pan-STARRS, the Dark Energy Survey, and Skymapper, are already producing valuable observational results with a promise of large subsamples which can be compared. Fourth-generation surveys are also on the horizon such as the Large Synoptic Survey Telescope and potential space missions. New techniques in SNe Ia theory such as 3D-modelling are beginning to yield results. In terms of the SNe Ia explosion mechanism, their use as standard candles, and their progenitors, the next decade holds real promise for our complete understanding of these events.

1.1.2 Core-collapse Supernovae

Contrary to thermonuclear explosions, core-collapse explosions represent the death of a single massive star ($M > 8 \pm 1 M_{\odot}$) (Smartt, 2009). These stars are massive enough to produce elements all the way to iron and nickel during the slow evolution phase of the star. The fusion of iron and nickel are not energetically favoured (Fewell, 1995) and thus, once this point has been reached, fusion is impeded in the star and pressure is lost. Once pressure is lost, the star begins to *collapse*, resulting in higher and higher densities. Pressure from electron degeneracy alone cannot counter the gravity and the cataclysmic implosion continues. Neutron degeneracy pressure soon (within seconds) halts further collapse in the core, resulting in the in-falling material bouncing off the 'proto-neutron star' (Smartt, 2009). A subsequent outward shock wave is responsible for removing the outer layers of the star and creating the supernova explosion. The extreme temperatures and densities in the collapsing core produce neutrinos with a total energy of 3×10^{53} ergs (Smartt, 2009). The deposition of a small fraction of this energy is thought to be the primary energy source that helps drive the outward shockwave, expelling the star's envelope material (Janka et al., 2007). The remaining neutrinos escape the explosion and, in the case of SN 1987A, these neutrinos were detected on Earth (Hirata et al., 1987), confirming our standard model of core-collapse SNe (CCSNe). The finer details of the explosion mechanism are a subject of dispute and will be discussed in more detail in the next section. Often a compact remnant (either a neutron star or a black hole) remains from the inner iron core along with expanding material from the surrounding layers. Core-collapse supernovae are responsible for the production of elements more massive than iron which can be generated given the extreme conditions during the explosion (Smartt, 2009).

Observations of CCSNe There are three primary sub-classifications of CCSNe: Type Ib, Type Ic, and Type II (see Figure 1.1). SNe II are defined by strong H lines in the spectra, SNe Ib lack H but contain He lines, and lastly SNe Ic lack both H and He lines (da Silva, 1993). CCSNe spectra also do not contain the singly-ionized silicon absorption line that is observed in the spectra of SNe Ia. Beyond this basic sub-classification more subdivisions exist for CCSNe based on the diversity of observed light-curves and spectra. Unlike SNe Ia, CCSNe of a given sub-classification can have very diverse properties. CCSNe have a B-band peak

magnitude roughly 1.5 mag fainter than SN Ia, covering a wide range of 5 mag (Richardson et al., 2002). They are primarily observed in star-forming regions of galaxies which is consistent with the idea that the progenitors are young, massive stars (Smartt, 2009). The various sub-divisions of CCSNe have been theoretically and observationally linked to the degree of stripping of the progenitor star (Smartt, 2009). Type I b/c supernovae show no evidence of H ejected indicating that the exploding star did not have a H atmosphere at the time. See Table 1.1 for the summary of core-collapse types and their properties.

There are a few exotic objects that have been recently linked with CCSNe: (1) long duration gamma-ray bursts (GRBs) are thought to represent the most energetically extreme CCSNe and a few have been observationally linked with Type Ic-BL SNe indicating that their progenitor was highly stripped (Woosley & Bloom, 2006); (2) a new class of 'ultrabright' CCSNe have been observed with average peak magnitudes brighter than -21mag in the optical and very peculiar spectra that are difficult to type (Chomiuk et al., 2011; Quimby et al., 2011) - they are among the most luminous SNe ever discovered and there is much dispute over what is powering their lightcurves. How exactly these oddities fit with our current model of CCSNe is still an open question and a hot topic in the field. Their higher luminosities may make their detection and characterization by light echo techniques achievable for longer durations at greater distances than "normal" SNe.

Progenitors of CCSNe The progenitor stars of SNe II-P have been well-constrained based on pre-explosion imaging to be red super-giants (RSG) (Smartt et al., 2004; Van Dyk et al., 2003). This result agrees well with observations of SNe II-P outbursts and the theory that they stem from progenitors that have maintained most of their H-envelope. The puzzle currently lies in the progenitors of SNe I b/c. Only ten pre-explosion images exist for these outbursts and there is no detected progenitor in any of them Smartt (2009). The observations put constraints on the theory that the SNe Ib/c progenitors are giant Wolf-Rayet stars (Gaskell et al., 1986) and indicate that there must be another progenitor channel. The constraints have spurred theories supporting lower-mass stars within interacting binaries as the progenitor system whose magnitude limits cannot be ruled out (Podsiadlowski et al., 1993).

Type of CCSNe	Property
Type II-P	Strong H lines in spectra and plateau phase in light curve.
Type II-L	Strong H lines in spectra and linear decay after peak brightness.
Type IIb	Begins with spectra like Type II (H lines) but evolves to display He lines while H lines fade and then disappear.
Type IIn	Narrow H emission lines which usually have multiple components of velocity.
Type Ib	Distinct signatures of He but no H - also O, Mg and Ca lines.
Type Ic	No He or H lines - but have O, Mg and Ca lines
Type Ic-BL	Broad-lined Ic SNe (large kinetic energies) - have been associated with long gamma-ray bursts (GRBs)

Table 1.1 Sub-types of core-collapse supernovae and their spectral and photometric properties described by Smartt (2009). Going from the top to the bottom of the table represents higher degrees of stripping of the progenitor star based on our current perspective of CCSNe.

CCSNe Explosion Theory Modelling of core-collapse supernovae have made significant progress during the last ten years with a move towards three-dimensional simulations. The primary issue with the standard model for ordinary CCSNe lies in a fraction of a second after the initial bounce from the collapse, where the shock has stalled approximately 200 km from the centre (this is deemed the *standing accretion shock*; Fryer et al. (2005)). As described earlier in this section, the standard model suggests that neutrino energy deposition from the collapsing proto-neutron star re-energizes the standing shock wave, pushing the rest of the star off and creating the supernova. Computer simulations, however, have rarely been able to re-launch the stalled shock using only neutrino energy deposition (Fryer et al., 2005). Whether the problem is missing physics (rotation and magnetic fields are not usually included in simulations), computational difficulty or both is currently unclear.

There is strong evidence from simulations that breaking of spherical symmetry is the key ingredient in overcoming the stalled shock (Fryer et al., 2005). A popular model that

incorporates this is the “stationary accretion shock instability” (SASI) which enhances neutrino deposition and helps explain observational evidence of asymmetric explosions as well as neutron star kicks (Blondin et al., 2003; Foglizzo et al., 2007). Another new and upcoming model that uses breaking of symmetry are jet-driven explosions which use rotation, magnetic fields and energetic outflows (jets) as the central engine for the explosion (as opposed to simply neutrinos) (Fryer et al., 2005). The answer may lie in a combination of both, using 3-D neutrino radiation magnetohydrodynamic simulations, which have yet to be performed!

There are few techniques to directly and indirectly *observe* asymmetry in a SN (CCSN or SN Ia) explosion: (1) SNR observations - symmetry in terms of the nebulosity; (2) SN spectropolarimetry; and (3) SN light echoes. Overall, observational and theoretical research on asymmetries appears to be the most promising path for resolving the remaining mysteries of both CCSNe and SNe Ia.

It is alarming to realize that the fundamental “central engine” of a core collapse outburst is still under debate. Future observations of remnants, outbursts, and light echoes as well as advances in core collapse theory will hopefully settle the issues at hand.

1.2 The Milky Way’s Historical Supernovae

Although thousands of *extragalactic* SNe have been observed during telescopic times, the last known SN event to have been observed in our own Milky Way (MW) galaxy was Kepler’s SN - it was recorded by the unaided eye in 1604 AD. The most reliable estimate of the Milky Way’s SN rate is about one SN every 80 years (Cappellaro et al., 1999). Cappellaro et al. (1999) utilized visual and photographic methods to count the number of SN events in local galaxies similar to the MW. In order to reduce the effects of galaxy inclination and extinction, simple empirical bias corrections were applied. The reason the actual *observed* SN rate in our own galaxy is much lower than this derives from dust obscuration - the majority of SNe (those from massive stars) will occur close to the Galactic plane, shielding our view of the event. Overall, the SN community has been patiently waiting for a Galactic SN sighting

to locally test our SN theories. Until one of these events occur, our information on Galactic SNe rely on historical records from pre-telescopic sightings.

Literature from pre-telescopic times describes a variety of celestial events including the appearance of *guest stars* (temporary stars). The majority of these historical records are from four distinct regions: (1) East Asia (China, Japan and Korea); (2) Babylon; (3) Europe and; (4) the Middle East. The most recorded guest star sightings are from East Asia, where official astronomers existed as early as 200 BC (specifically in China) (Stephenson & Green, 2002). Guest stars were described as being either fixed or moving and are thought to have mostly corresponded to three different types of Galactic astronomical events: comets, novae, and supernovae (Stephenson & Green, 2002). In order to decipher the type of event as well as the position it had in the sky, astronomers have had to carefully translate and interpret ancient descriptions. The distinction between a comet and a nova/supernova resides in whether or not the guest star was described as stationary. In the case of novae vs. supernovae, novae are generally shorter in duration - novae can fade by two magnitudes from their peak in a few days up to a few months (Warner, 2003), while SNe typically take many months and sometimes up to several years to fade significantly (Stephenson & Green, 2002).

The last five guest star sightings that have since been classified as SN events (through interpreting historical descriptions and the modern discovery of their individual remnants), are deemed the *Milky Way's Historical Supernovae*. Table 1.2 gives a summary of these events based on their associated SNR and reported apparent magnitude at the time of discovery. Each historical SN is identified by the year of its discovery. Although some associations are still under dispute, the guest star positions have been connected with well-known remnants in our galaxy. The reported V_{max} values in Table 1.2 are very rough estimates that Stephenson & Green (2002) have inferred from the apparent magnitudes of known stars and planets that the guest star was compared to at its peak.

It is important to note that Table 1.2 does not include the Galactic SN event that created the young (~ 345 yrs old) Cassiopeia A remnant - the outburst has not been credibly identified in any known historical documents (Stephenson & Green, 2002). The five historical

SNe and details about the Cas A remnant are described in more detail below.

Historical SN	Associated SNR	Reported V_{max}
SN 1604	3C358 (Kepler's SNR)	-3.0
SN 1572	3C10 (Tycho's SNR)	-4.5
SN 1181	3C58	0
SN 1054	Crab Nebula	-3.5
SN 1006	G327.6+14.6	-7.5

Table 1.2 Summary of the Milky Way's historical SNe (Stephenson & Green, 2002).

SN 1604 (Kepler's SN) This event is the most recent Galactic SN to have been observed. It was recorded in China, Korea and Europe in AD 1604 and remained visible for a full year (Stephenson & Green, 2002). More notably, it was observed by Johannes Kepler who subsequently wrote a book on the event, describing its position and brightness changes in great detail. Therefore, this SN and its remnant have since been named after Kepler. Its position was favourable for a quick discovery because it appeared close to the ecliptic and a triple planetary conjunction (Mars, Jupiter and Saturn) - thus this was an area already being carefully watched by astronomers. Using the European and Korean estimates of brightness, Clark & Stephenson (1977) pieced together the light curve of SN 1604. The SN had a peak magnitude close to -3.0 and was identified by Clark & Stephenson (1977) as a Type I based on the light curve's shape. Stephenson & Green (2002), however, have argued that the light curve shape was simply too ambiguous to assign a classification given the similarity of Type I and Type II SN light curves (Schaefer, 1996). The guest star's position is well-known (the Europeans recorded it to ± 1 arcmin precision) and the remnant of Kepler's SN was first identified optically in 1943 (Baade, 1943) and then in the radio in 1957 (catalogued as 3C358, Baldwin & Edge (1957)). Kepler's SNR is now generally accepted as the remnant of a Type Ia SN, based on the O/Fe ratio observed in the X-ray spectrum (Reynolds et al., 2007). Its distance, however, is very poorly constrained and there are conflicting estimates: (1) $3.0 < D_{SNR} < 6.4$ kpc from H I absorption (Reynoso & Goss, 1999), H α line width, and proper

motion measurements (Sankrit et al., 2005); (2) $D_{SNR} > 7$ kpc based on the non-detection of TeV gamma-rays (Aharonian et al., 2008).

SN 1572 (Tycho’s SN) This event was recorded in China, Korea and Europe in AD 1572 (Stephenson & Green, 2002). It is thought that SN 1572 was a significantly brighter event than Kepler’s SN. Astronomers described its brightness as being comparable to Venus (magnitude of -4.5) since it was visible during daylight hours (Stephenson & Green, 2002). Tycho Brahe was among the Europeans to have observed this event and he recorded it in detail. In fact, his description of diminishing brightness and position were so accurate, that there is *no doubt* in the community that the event was indeed a SN and that its remnant is G120.1+1.4 (in the constellation Cassiopeia). The remnant was first identified in the radio in 1952 (Hanbury Brown & Hazard, 1952) and has since been catalogued as 3C10. In 2008, Tycho was classified as a SN Ia event based on the optical spectrum of scattered light echoes discovered from the original outburst (Krause et al., 2008b). The precise distance to Tycho’s SNR is uncertain, with recent studies suggesting a value between 2.5 and 3 kpc (Tian & Leahy, 2011).

SN 1181 This event was recorded by Chinese, Japanese, and Korean observers in AD 1181 (Stephenson & Green, 2002). After it was observed, there were no SN candidates recorded for almost four centuries (until Tycho’s SN in 1572). SN 1181 appeared in the constellation of Cassiopeia. The maximum brightness of the 1181 guest star is hard to decipher from the historical records due to vague descriptions. Stephenson & Green (2002) infer that it was likely no fainter than magnitude 0 due to the fact that each separate set of accounts discovered the new star within days of each other, indicating it was fairly bright. The Japanese also described the guest star as having ‘had rays’ and the Chinese describe it as ‘large’. The radio source 3C 58 was first suggested to be the remnant of SN 1181 by Stephenson (1971). Based on historical records, the SN was described as being close to (within 1 degree of) the fifth star in *Chuanshe* (a faint star group designated by Chinese astronomers). There are two stellar candidates whose coordinates are close enough to be considered the “fifth star” in *Chuanshe*: SAO 12076 and 53 Cas. As it turns out, the radio source 3C 58 lies about 0.7 degrees and 0.5 degrees from SAO 12076 and 53 Cas, respectively. Other SNR candidates in this region

have yet to be discovered and for many years, astronomers were confident that 3C 58 was the remnant of SN 1181. Surprisingly, more recent observations of 3C 58 (the remnant's expansion rate, evolution, and energy) indicate that there may not be a connection after all with SN 1181, rather 3C 58 may be the remnant of a considerably older SN event (~ 4000 yr) (Fesen et al. (2008), Table 3). The focus of this thesis specifically involves SN 1181 and the search for its light echoes. Therefore, the SN 1181-3C 58 connection and the debate surrounding it will be discussed in greater detail in later sections. A pulsar (J0205+6449) has been observed in the remnant 3C 58, indicating that the SN which created it was a core-collapse event (Murray et al., 2002; Camilo et al., 2002). The distance to 3C 58 was determined to be 3.2 kpc by Roberts et al. (1993). This distance has since been challenged by Kothes (2010) to be 2 kpc.

SN 1054 (The Crab SN) This event was primarily recorded by Chinese, Japanese, and Arab observers in AD 1054 (Stephenson & Green, 2002). However, there have been debates of possible reports from Europeans and even North American tribes. The guest star was described as being 'several inches' south-east of the Chinese asterism *Tianguan*. Stephenson & Green (2002) translate this to about 1 degree to the south-east of the known star ζ Tau. Similar to SN 1181, there is little information regarding the guest star's brightness. We know that it certainly wasn't as brilliant as the SN 1006, but Chinese records do describe SN 1054 as having daylight visibility. Stephenson & Green (2002) estimate an apparent magnitude of about -3.5. The Crab Nebula was discovered in AD 1731 (in the optical) by the English physician and amateur astronomer, John Bevis. It has been recognized as the remnant of SN 1054 since the 1940s (Duyvendak, 1942; Mayall & Oort, 1942). The Crab Nebula is the only known SNR within 5 degrees of the star ζ Tau and observations of the nebula support its young age. Therefore, astronomers are confident that the Crab Nebula is the only viable contender for being the remnant of SN 1054. A pulsar (PSR B0531+21) was discovered in the Crab Nebula in 1968 (Staelin & Reifenstein, 1968; Comella et al., 1969), indicating that SN 1054 was a core-collapse event. Like SN 1181, the Crab SN and the search for its light echoes is also a primary focus of this thesis. Therefore, further details about the Crab Nebula, its pulsar, and its distance will be discussed in later sections.

SN 1006 In terms of apparent magnitude, this stellar event was the brightest ever recorded, with an estimated visual magnitude of -7.5 (Winkler et al., 2003). It was recorded by Chinese, Japanese, European, and Arab observers in AD 1006 and first appeared in the constellation Lupus (Stephenson & Green, 2002). Its Galactic latitude of $\sim +12$ degrees is an unusual location for a SN - SNe are rare in this region of the MW as the majority of stars, both massive and old, are concentrated close to the Galactic plane. Gardner & Milne (1965) and later Milne & Dickel (1971) searched radio catalogues for objects in the Lupus region with the hopes of finding the remnant of SN 1006. Two SNR candidates were revealed: the radio source PKS 1459-51 (a limb-brightened shell with two bright arcs of emission) and the ‘Lupus Loop’ (G330.0+15.0). The Lupus Loop was found to be too large and faint to be the associated remnant of SN 1006. Since then, the connection has been confirmed with observations in the X-ray, optical and resurveying the remnant in the radio. The distance to the SNR has been estimated from various observations to be ~ 2 kpc (Winkler et al., 2003). Although it is not completely certain, SN 1006 is thought to have been a Type Ia event because: (1) no associated neutron star or black hole has been discovered in the SNR; (2) the environment in which the SNR is found (high Galactic latitude) is most consistent with a progenitor star that was low-mass, indicating a SN Ia.

The Cassiopeia A SNR Cas A is a young, relatively nearby SNR located in the constellation Cassiopeia. It is one of the brightest radio sources in the sky and was detected in the 1940s (Brown & Hazard (1953), during the dawn of radio astronomy). It wasn’t until Minkowski (1959), however, that it was recognized as a SNR after his observations of optical circular nebulosity associated with the radio source - expansion velocities of the optical filaments (from radial velocity measurements) were observed to be typical of a SN event (~ 7000 km s⁻¹). It was estimated that the expansion had to have begun near the end of the seventeenth century (Minkowski, 1959). Since then, the expansion of Cas A has been measured at radio, X-ray and optical wavelengths (Fesen, 2001). Assuming that the remnant has undergone a *constant* expansion, most of the observations agree with Cas A being produced by a SN in ~ 1670 AD. By the late 1600s, the field of astronomy and the technology available should have been advanced enough to easily detect an event at the position and distance of Cas A (~ 3.4 kpc; Fesen et al. (2006)) and therefore it is rather surprising that the SN wasn’t

recorded. The question remains - *why* did this SN escape detection? Although no associated pulsar has been discovered for Cas A, there have been observations using the *Chandra X-ray Observatory* of a compact X-ray source near the centre of the remnant (Chakrabarty et al., 2001). Whether or not this X-ray source is the compact remnant of a CCSN is still under debate (Stephenson & Green, 2002). In 2008, observations and spectral analysis of infrared light echoes discovered from the original Cas A outburst determined that the SN was a Type I Ib event (Krause et al., 2008a). Recall that Type I Ib SNe are rare core-collapse events. They begin with spectra like Type II, but evolve to display He lines while the H lines fade and eventually disappear. It is thought that the progenitor was a giant star, whose hydrogen envelope had been mostly stripped through binary interactions or winds. The transition between the H and He lines are thought to represent the expansion of the star's ejecta, as the deeper layers are revealed (Nomoto et al., 1993).

The five historical SNe and Cas A represent a complete list of known Galactic SN events that have occurred over the past ~ 1000 yrs. Unfortunately, these SNe occurred before modern astronomy and the invention of the telescope. Therefore, the spectra and detailed light curves of the original outbursts were thought to have been lost forever. A newly emerging field of astronomy however, has allowed us to overcome these astronomical timescales using spectroscopy of *supernova light echoes* (SN LEs). SN LEs allow astronomers to simultaneously observe the outburst of an object with its remnant, separated by intervals of hundreds of years. This can be achieved due to the extra distance light must travel as it scatters off interstellar dust surrounding the SN and is redirected into our line of sight. The details regarding finding, interpreting, and analyzing scattered LEs will be discussed further in the next chapter. Our research group (Doug Welch, Brendan Sinnott, Armin Rest and the SuperMACHO collaboration) has a campaign to search for scattered LEs from historical SNe. The list of historical SNe however is limited, particularly when you focus on those younger than ~ 1000 yrs. In terms of recorded motionless guest stars *predating* AD 1000, a few notable examples do exist: AD 837, 393, 386, 369, 185, and 70. With the growth of Galactic SNR catalogues, many of the above events have been connected with known remnants in the MW (Stephenson & Green, 2002). It is likely that these SNe are *too old* for their respective LEs to be detected (the light would simply be too faint). Thus, our group is concentrating

its efforts on the six younger events for the time-being.

CHAPTER 2

INTRODUCTION TO LIGHT ECHOES

A light echo (LE) is a pulse of light generated by a transient event that encounters interstellar dust grains and is scattered as it expands into the surrounding medium. The light is scattered off dust and a small fraction is re-directed in Earth's direction. If this portion of scattered light is bright enough, we observe it as a LE. Due to the extra distance the light travels when it reflects off the dust, we are able to observe the *original* light from an event at a later time than the light that took the direct path. For historical SNe, this is *key*, as we can observe the light from the original outburst during modern times (hundreds of years later) while simultaneously observing its expanding, gaseous SN remnant. LE investigations present a valuable perspective and unique set of observables for investigating the SN explosion mechanism (Section 2.2.5) as well as properties of the scattering dust surrounding the SN (Section 2.2.2). It is important to note that the SN light discussed herein has been simply *scattered*, preserving the fine spectral energy distribution (SED) of the source event. *Infrared echoes*, on the other hand, result from light absorbed by the dust and re-radiated at longer wavelengths. In this chapter we discuss: (1) the search for LEs from transient events and the history of LE discovery; (2) the analysis of LEs including spectroscopic follow-up and pinpointing the location of the original outburst (if unknown). We focus primarily on LEs found and investigated by our own research group, who have originated and led the development in this research area as well as pioneered the analysis of observed LE profiles and spectra.

2.1 Finding Light Echoes

Light echos have now been found and investigated around a variety of variable objects: novae, eruptive variables, Cepheids, extragalactic SNe, and historical Galactic SNe. In this section, we summarize the history of LE detection and discuss recent advances made in LE discovery surveys with a specific focus on the technique of *difference-imaging*.

2.1.1 The First Light Echo Discoveries

Nova Persei 1901 The first set of LE discoveries were made unexpectedly while observing still-luminous source events. In 1901, Thomas Anderson observed the famous nova explosion from GK Persei - the nova reached a maximum magnitude of 0.2. LEs from the outburst were discovered when Flammarion & Antoniadis (1901) photographed a “luminous shell surrounding the nova” - at first the bright knots were considered debris from the outburst and were not recognized as LEs. The bright knots of light were observed to be travelling at a rate of 11 arc min yr⁻¹ or ten times the speed of light at the estimated nova distance (Perrine, 1901)! This *superluminal motion* puzzled astronomers until Kapteyn (1901) proposed that the shell did not represent moving “clouds”, but *light* from the nova illuminating surrounding stationary dust (LEs). In 1939, Paul Courdec refined this theory and fully explained the phenomena of superluminal motion using scattered LEs (see Figure 2.1) (Courdec, 1939). The phenomenon occurs due to light reaching the dust sheet *off the line of sight* and being deflected to Earth a short time after the *direct* forward-scattering light reached us - the difference in position on the sky between the direct ray and deflected ray represent what we observe as the apparent “superluminal” motion. Today Nova Persei 1901, which is now considered a *cataclysmic variable star*, is still a subject of investigation due to the regular periodic outbursts that occur about every three to four years (Bianchini et al., 1982; Brat et al., 2006).

SN 1987A A famous case of LE discovery is surely the iconic LE ring system around SN 1987A in the Large Magellanic Cloud. They were first detected by Crotts (1988) using coronagraphic observations of SN 1987A. SN 1987A has been an object of intense investigation

as it was the SN with the greatest apparent brightness observed in the sky since Kepler's SN in 1604. The outburst led to the confirmation of our standard model for core-collapse SNe as it was the first time neutrinos were detected from a SN event (Hirata et al., 1987). Since Crotts (1988), the evolution of SN 1987A's LE system has been followed continuously and has revealed valuable information about: (1) the circumstellar environment and dust structures surrounding SN 1987A (Sugerman et al., 2005a,b); (2) the interstellar medium of the LMC (Xu et al., 1994; Xu & Crotts, 1999); (3) and the asymmetry of the actual outburst itself (Sinnott et al., in prep).

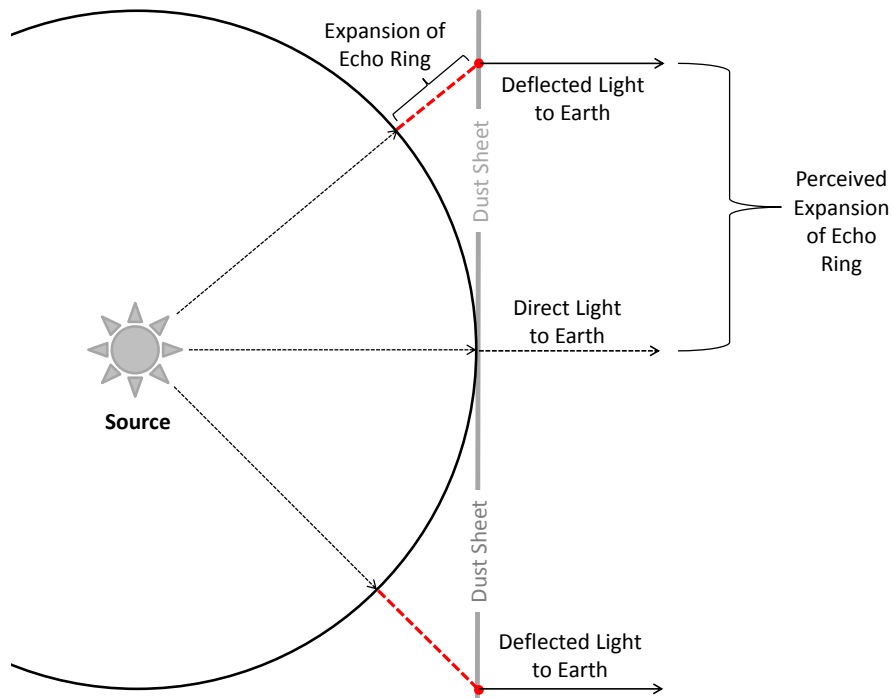


Figure 2.1 This diagram explains the *superluminal* LEs observed from the Nova Persei 1901 outburst. The black circle represents the pulse of light from the outburst, which expands over time, and the grey line represents an interstellar dust sheet. Light from a dust deflected ray reaches Earth a short time after the direct ray reaches us due to the extra distance it travelled (shown in red). However, it appears to us that the rays are expanding faster than the speed of light. This figure is adapted from Felton (1991).

2.1.2 Discovering Light Echoes using Difference Imaging

Before LEs can be investigated, they must be found. For LEs to exist: (1) there must be a rapidly varying (in brightness) source; (2) the source must be intrinsically luminous and; (3) interstellar dust must lie at the appropriate position around the source such that the re-directed light can be observed today. LEs are *notorious* for being extended, faint objects ($V > 22.5$ mag/arcsec²) that are difficult to detect against stellar and galactic backgrounds. Therefore, scattered LEs (particularly those from historic events) have been very difficult to find and many searches led to disappointing results (van den Bergh, 1965a,b, 1966; Boffi et al., 1999).

Since the detection of LEs from both Nova Persei in 1901 and SN 1987A, there have been advances in the search and discovery of LEs with both the technique of digital image subtraction and the advent of CCDs and telescopes with large field-of-views. The former is usually deemed *difference-imaging* and has recently helped overcome some of the hurdles associated with locating LEs. Difference-imaging was originally developed to help handle the flood of data coming in from new wide-field ground-based optical and infrared surveys - particularly those focused on the detection of transients (e.g. microlensing surveys, SN surveys, Cepheid variable surveys). For such surveys (especially the time-domain ones), it is important to detect and classify real transient objects *quickly* for follow-up observations. Difference-imaging helped reduce false detections due to instrument or reduction artifacts. In general, difference-imaging involves the digital image subtraction of two or more epochs of the same fields. For the most part, the stellar and galactic background is removed in the resulting difference image and any moving objects have been left *highlighted*. Although the concept of difference-imaging is simple, the implementation is actually quite difficult and it has taken years to develop a reliable method. The difficulty lies in the alignment and PSF-matching of the images *before* they can be subtracted. Nonetheless, there now exist many sophisticated difference-imaging techniques, including: Tomaney & Crotts (1996), Alard & Lupton (1998), Alard (2000), Sugerman (2005) and Rest et al. (2005a).

Since LEs propagate across the sky with time, they can be detected via difference-imaging (Figure 2.2). The separation of imaging epochs must be large enough that the LEs don't subtract themselves. Specifically, the technique developed by Rest et al. (2005a) is the one that has been employed for all targeted LE searches by our research group and was the process used for this research. This technique and the details involved in the image reduction process will be described in the *Observations, Reductions and Searching* chapter of this thesis (see Chapter 4). In the rest of this subsection, we continue to discuss the detection of LEs in the current era of difference-imaging and wide-field time-domain surveys.



Figure 2.2 Example of image subtraction using LEs from the Tycho SN found during my project.

SuperMACHO and LMC SN LEs The first LEs of *ancient* SNe (i.e. centuries old) were serendipitously discovered in the LMC during the SuperMACHO Project (Rest et al., 2005a). The SuperMACHO Project was a five-year survey of the Large Magellanic Cloud (LMC) that searched for distinctive brightenings of stars, some of which bore the signature of gravitational microlensing. The project implemented a difference-imaging technique to highlight any flux changes of stars. Through this process, the SuperMACHO team unexpectedly discovered faint, extended objects that propagated on the sky with time. They determined that these objects *were not* associated with microlensing, but were in fact the optical LE complexes from three different historical SNe in the LMC (Rest et al., 2005b). Based on their apparent motions, the LEs allowed the source event (now apparent as a SNR) to be identified (SNRs 0509-675, 0519-69.0, and N103B). The apparent motions and locations of the LEs indicated that the ages of the SNRs were between 400-800 years old.

Historical SNe The unexpected discovery of the LEs from ancient LMC SNe motivated *targeted searches* (via difference-imaging) for LEs from the Milky Way’s historical SNe. The search for LEs from such ancient events is a specific focus for our research group and is the topic of this thesis. So far, LEs have been successfully discovered and investigated from both Tycho’s SN (Rest et al., 2007; Rest et al., 2008) and the Cas A SN (Rest et al., 2007; Rest et al., 2008; Krause et al., 2008a). Given the known age and approximate distance to these historical events, the search strategies by Rest et al. (2008) were developed based on regions of significant dust along the line-of-sight the SNRs. Specifically, re-processed 100- μm IRAS images (Miville-Deschênes & Lagache, 2005) were used to select fields with lines of sight which contained such dust.

Extragalactic SN LEs In addition to the LEs discovered by the SuperMACHO Project in the LMC, LEs have been observed from the following extragalactic SNe: 1980K (Sugerman et al., 2012), 1991T (Schmidt et al., 1994; Sparks et al., 1999), 1993J (Sugerman & Crofts, 2002; Liu et al., 2003), 1995E (Quinn et al., 2006), 1998bu (Garnavich et al., 2001; Cappellaro et al., 2001), 2002hh (Welch et al., 2007), 2003gd (Sugerman, 2005; Van Dyk et al., 2006; Otsuka et al., 2012), 2004et (Otsuka et al., 2012), 2006X (Wang et al., 2008; Crofts & Yourdon, 2008), 2006bc (Gallagher et al., 2011; Otsuka et al., 2012), 2006gy (Miller et al., 2010), and 2007it (Andrews et al., 2011). It should be mentioned that the LEs from all of these extragalactic SNe were discovered unintentionally through observations of the still-luminous source event or remnant.

LEs from Novae and Eruptive Variables After Nova Persei 1901, LEs have also been discovered to be associated with other local novae and eruptive or large amplitude variable stars. These include the Galactic Nova Sagittarii 1936 (Swope 1940), the eruptive variable V838 Monocerotis (Bond et al., 2003), the Cepheid RS Puppis (Westerlund, 1961; Havlen, 1972), the T Tauri star S CrA (Ortiz et al., 2010), the Herbig Ae/Be star R CrA (Ortiz et al., 2010) and the eruptive supergiant η Carinae (Rest et al., 2012). The discovery of LEs from the 19th-century “Great Eruption” of η Carinae was the result of a targeted search by our research group and collaborators. With the exception of η Carinae, the novae/variable star LE discoveries listed above were serendipitous. After the discovery of η Carinae’s LEs

using difference-imaging, subsequent follow-up spectroscopy was performed and details about its spectral type and the symmetry of the outburst were revealed (Rest et al. (2011a), see Section 2.2).

The Future of LE Searching There are a few next generation wide-field, time-domain surveys that hold promise for the future of LE discovery. The surveys include: the *Panoramic Survey Telescope and Rapid Response System* (Pan-STARRS) (Kaiser et al., 2010), the *Palomar Transient Factory* (PTF) (Rau et al., 2009), *Skymapper* (Keller et al., 2007), and *The Large Synoptic Survey Telescope* (LSST) (Ivezic et al., 2008). Overall, the flood of future imaging data will be enormous, with a few of these surveys predicting nightly data yields in the hundreds of terabytes and total accumulated data in petabytes! For most LE searches, finding LEs have depended on the *visual inspection* of difference images - an automated system that searches for LEs has yet to be developed. There are many “artifacts” which appear in difference images that software can easily confuse for a LE (Rest et al., 2012): (1) scattered/reflected light from bright stars falling in the focal plane beyond the edges of the detectors; (2) pointing offsets between image epochs that can produce features in the resulting difference image (diffraction pattern differences); (3) artifacts due to charge traps in CCDs; (4) “dust doughnuts” in one epoch but not another. Overall, these objects can *mimic* the shape and surface brightness of LEs - unfortunately the most reliable and effective way to search for LEs at the moment requires visual inspection. Needless to say, this is a very time-consuming process and given the prospect of the above surveys and the expected quantity of incoming data, the development of a new automated system must be a high-priority for future LE searches.

2.2 Light Echo Formalism and Analysis

2.2.1 Geometry

A schematic of the geometry of a light echo system is provided in Figure 2.3. An *imaginary ellipsoidal surface* represents all possible pulse reflections from a source event associated with constant arrival time at Earth, where Earth and the source are each at a focus. For the light

pulse to be scattered, dust must lie on this imaginary surface. If the distance to the SN event and time since explosion are known, then the geometry of the ellipsoid can easily be quantified.

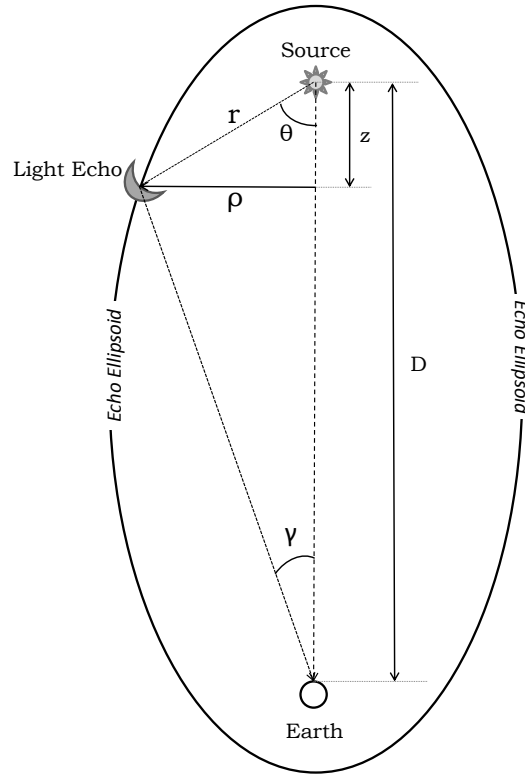


Figure 2.3 Light echo geometry. Figure adapted from Sugerman (2007)

Assuming the distance to the event (D) is much greater than r , the echo depth z along the line of sight can be approximated by Equation (2.1) which describes a parabola (Couderc, 1939).

$$z = \frac{\rho^2}{2ct} - \frac{ct}{2} \quad (2.1)$$

where ρ is the projected distance perpendicular to the line of sight, t is the time a light echo is observed as measured from when direct light first reached Earth, and c is the speed of light.

The distance r is $r^2 = \rho^2 + z^2$, and ρ is

$$\rho = (D - z) \tan \gamma \quad (2.2)$$

where γ is the angular separation on the sky between the source event and the scattering dust and can be measured through imaging. Through the apparent motion of LEs or the observation of multiple echoes, the three-dimensional dust distribution surrounding the event can be mapped out.

2.2.2 Dust Scattering

The surface brightness of a LE can constrain the composition, density, and grain-size distribution of dust in both the circumstellar (CSM) and interstellar medium (ISM) surrounding the source. Different frequencies of light will scatter with different efficiencies based on grain size distribution and composition - the different *types* of dust grains include: (1) silicate dust grains; (2) carbonaceous dust grains with a neutral Polycyclic Aromatic Hydrocarbon (PAH) component; (3) or carbonaceous dust grains with an ionized (PAH) component (Weingartner & Draine, 2001). The integrated scattering function $S(\lambda, \theta)$ describes the wavelength-dependent *efficiency* of light scattering off dust grains (Sugerman et al., 2005b). The integrated scattering function S_X for a particular dust grain type X is:

$$S_X(\lambda, \theta) = \int Q_{SC,X}(\lambda, a) \sigma_g \phi_X(\theta, \lambda, a) f_X(a) da \quad (2.3)$$

where $Q_{SC,X}$ is the dust grain scattering efficiency, $f_X(a)$ is the dust grain density distribution, a is the radius of the individual dust grains, and σ_g is the grain cross section (πa^2). The scattering function also incorporates the *Henye-Greenstien* phase function (Henyey & Greenstein, 1941):

$$\phi_X(\theta, \lambda) = \frac{1 - g_X^2(\lambda, a)}{(1 + g_X^2(\lambda, a) - 2g_X(\lambda, a)\cos\theta)^{3/2}} \quad (2.4)$$

where $g_X^2(\lambda, a)$ represents the amount of forward scattering for a given grain. The angle θ is called the *scattering angle* and can be seen in Figure 2.3. Rest et al. (2012) have illustrated the behaviour of $S(\lambda, \theta)$ by plotting the results that one obtains using the Milky Way dust mixtures modelled by Weingartner & Draine (2001). Rest et al. (2012) have determined that for scattering angles $\theta \lesssim 60^\circ$, the efficiency of blueward scattering is *greater*. Therefore, it appears to be beneficial to concentrate our targeted optical searches to regions representative of $\theta \lesssim 60^\circ$.

2.2.3 Apparent Proper Motion

The observations of LEs at various epochs automatically provides us with their *apparent proper motion* on the sky. Due to the geometry of the situation, LEs often have superluminal apparent proper motions (see Section 2.1.1). Given multiple LEs, the location of the original outburst can be determined quite accurately. A good example is shown in Rest et al. (2008) - the motion of LEs found from both Tycho's SN and Cas A trace back to their respective remnant locations within one standard deviation.

Apparent proper motion depends on the distance to the source event (D), the time since explosion (t), and the angular separation on the sky (γ). Recently, it has been shown that the apparent proper motion can be highly dependent on the *inclination angle* (α) of the scattering dust sheet (Rest et al., 2011b,a; Rest et al., 2012). When the dust filament is in the plane of the sky then $\alpha = 0^\circ$. When the dust filament is tilted away from the observer (towards the negative z axis), it has a positive α . By watching the apparent motion of a LE move on a dust sheet and knowing the expansion of the LE ellipsoid $f(t)$, the precise dust filament inclination can be determined.

The apparent motion of LEs can be predicted given t and an estimate of the average dust inclination. Through statistical arguments described in Rest et al. (in prep), a good approximation of the average dust inclination is $\alpha = 90$ degrees to the LE ellipsoid (perpendicular). Therefore, an *expectation value* of the apparent motion can be obtained, which can be used to space out observations of epochs when searching for LEs for a particular

event. The effects of dust inclination on the apparent motion had been previously neglected resulting in incorrect assumptions (Krause et al., 2005). The dust inclination also affects the LE flux profile (Section 2.2.4) and the LE spectral analysis (Section 2.2.5).

2.2.4 Light Echo Profile

LE profiles are defined as the flux of the LE versus the projected distance perpendicular to the line of sight (ρ). The LE profile is essentially the original light curve of the source event - *but* the light curve's shape and size can be heavily influenced by the thickness of the dust filament (σ_d), its inclination (α) and the seeing. The inclination simply stretches or compresses the light curve. The light curve's *shape* and whether or not it is distinguishable depends on the dust width and seeing. The light curve *shape* is distinguishable if: (1) the dust width is sufficiently thin ($\sigma_d = 0.008$ ly) and; (2) the PSF FWHM is small (*HST*-like PSF size of $0.05''$) (Rest et al., 2011b). In order to resolve the true light curve and spectrum of the event, it is crucial to correctly model or determine the dust filament thickness, inclination and seeing leading to the observed LE profile.

2.2.5 Light Echo Spectroscopy

The ability to extract the original spectrum of the outburst is one of the most valuable applications of SN LEs, particularly if the SN was not recorded in historical documents. Unlike imaging, a spectroscopic LE analysis will unveil more detailed information about the actual outburst event. Using LE spectroscopy, the original outburst can be classified. With two or more LEs, the degree of *spectroscopic symmetry* of the outburst can be revealed (exposing clues about the explosion mechanism).

The Model

The process of analyzing an observed LE spectrum to obtain clues about the true spectral energy distribution (SED) of the outburst is not a trivial task. The observed LE spectrum *will not* be identical to the original due to both astrophysical (dust inclination, scattering

and reddening) and observational effects (seeing and slit width) (Rest et al., 2011b).

A dust sheet reflecting the light has a finite size, which may result in a limited part of the source’s light curve actually being observed via the LE (a *window function*). The LE spectrum will not be the full lightcurve-integrated spectrum of the source. Therefore, it is crucial to obtain the detailed properties of the dust sheet through imaging before any spectral analysis can take place. A specific window function for each LE can be determined by modelling its profile (taking dust inclination and width as well as seeing and slit width into account - see Section 2.2.4). When multiplied by the original lightcurve, the window function will create an *effective* lightcurve. The observed LE spectrum represents an integration-weighted spectrum with this *effective* lightcurve (Rest et al., 2011b).

SN 1987A

Our group successfully tested the LE spectroscopy process using SN 1987A which already has well-observed photometry and spectroscopy as well as a well-determined LE system. Rest et al. (2011b) determined the *effective* lightcurve by multiplying the true SN 1987A lightcurve by the appropriately modelled LE window function. They then compared the model spectra to the observed LE spectrum - it was clear that the model spectra using the full lightcurve did not fit with the observed LE spectra while the model spectra using the effective lightcurve agreed well.

Cas A

For situations where we do not have observations of the original outburst (all of the historical SNe), the LE window function can be used in concert with well-observed lightcurves from various types of past supernovae which have well-defined spectra in order to correctly type the LE spectra. The SNe spectra are then weighted with their corresponding *effective* lightcurves. The result is a library of spectral templates for different types of SNe that can be compared with the LE spectra or spectrum. With this process, we can accurately classify historical SNe using LEs as well as inter-compare LE spectra of the same event.

Our group has successfully applied the above method to the Cas A SN event (~ 330 years old). After discovering scattered LEs from Cas A (Rest et al., 2008), LE spectra were subsequently obtained via follow-up observations by Rest et al. (2011a). The LE spectra were compared with a library of spectra from various SNe that has been modelled using the appropriate LE window function. Rest et al. (2011a) confirmed that the modelled Type IIb SN 1993J spectra was in *excellent* agreement with the Cas A LE spectra. A previous investigation by Krause et al. (2008a) came to the same conclusion also using spectroscopy of Cas A LEs. However, Krause et al. (2008a) simply assumed that the observed LE spectrum represented the full lightcurve-weighted integration of the SN spectra. The outcome of the Krause et al. (2008a) analysis could have been skewed by an unfavourable combination of astrophysical (dust inclination, scattering and reddening) and observational effects (seeing and slit width) and could have led to an incorrect conclusion concerning the classification. Overall, it is important to carefully consider the scattering dust and observational effects when correctly interpreting LE spectrum and determining the true classification.

η Carinae

After Rest et al. (2012) discovered LEs from the Great Eruption of η Carinae, subsequent follow-up LE spectroscopy revealed that the spectra resembled those of G2-to-G5 supergiant stars. η Carinae was originally thought to be associated with an observed class of F-type stars or luminous blue variables (LBV) - in fact, η Carinae was considered the *prototype* for this class. The LE observations from Rest et al. (2012) have challenged the traditional models and interpretations of these outbursts.

Three-Dimensional LE Spectroscopy

Our team furthered the investigation of Cas A by pioneering the method of 3D LE spectroscopy (Rest et al., 2011a). Observing LEs at *multiple* position angles on the sky is equivalent to observing the SN outburst from multiple perspectives. Three observed Cas A LEs were geometrically chosen to represent three different viewpoints of the Cas A SN. Three-dimensional spectroscopy was then performed by placing spectroscopic slits on the LEs, and comparing their spectra. 3D spectroscopy represents a rare occasion in astronomy

when one astronomical source can be viewed from multiple viewing angles, allowing for a wholly-observation-based method of probing for *asymmetries* in the outburst.

After comparing all three LEs, Rest et al. (2011a) found that, while two of three directions have spectra which are indistinguishable from each other (and that of SN 1993J), one direction has spectral features that are significantly blueshifted by 4000 km s^{-1} . The blueshift indicates that there was higher ejecta velocity in that particular direction, revealing a significant asymmetry of the explosion. An outflow in the SE direction (tilted slightly towards us and at a position angle of 115 degrees) has been observed by recent optical and X-ray studies of the Cas A SNR (Wheeler et al., 2008; Burrows et al., 2005; DeLaney et al., 2010). This outflow also has a *counterpart* outflow on the opposite side (NW). The asymmetric observations of Cas A LEs from Rest et al. (2011a) agrees well with this scenario - their blueshifted detection looks into the counter-outflow in the NW corner. The detection is also in agreement with the apparent motion of the proposed central compact object, which has been observed to move at a position angle of $169^\circ \pm 8.4^\circ$ away from the center of the SNR (Tananbaum 1999; Fesen et al. 2006a).

SN 1987A provides an ideal opportunity to test our methods of using 3D LE spectroscopy to gauge the symmetry of a SN outburst and this is something our group is currently investigating (Sinnott et al. in prep).

Overall, there is growing evidence from simulations that the breaking of spherical symmetry is the key ingredient in the explosion mechanism for SNe (Fryer et al., 2005) (see Section 1.1.2). Particularly in the case of CCSNe, the central engine of the outburst is still largely under debate and a central focus in the field at this time. With observations of 3D LE spectra, we can *directly* measure the symmetry of a SN and compare it to the structure of the remnant - this analysis will provide valuable information for CCSN theory and hopefully settle the issues at hand.

CHAPTER 3

THE ANCIENT SNE OF 1054 AD (CRAB) & 1181 AD

This thesis involves my observing efforts to discover scattered light echoes (LEs) from the historical Crab SN and SN 1181. Although the Crab and 1181 SNe have both already been introduced (Section 1.2), we will discuss the Crab SN and SN 1181 in more detail here and describe our motivation to search for LEs from these particular outbursts.

3.1 The Crab Supernova

Since its discovery in 1731 AD by the English physician and amateur astronomer, John Bevis, the Crab Nebula has been a subject of intense and detailed investigation (Mitton, 1978). In 1758, Charles Messier observed the Crab Nebula and it became the first object in his famous catalog of nebulous objects (Mitton, 1978). It is the most famous SN remnant in the Milky Way and was the first object to be identified with a historical SN explosion (SN 1054 AD) (Hester, 2008). The connection between SN 1054 AD and the Crab Nebula wasn't confirmed until 1942 with modern observations of the expanding nebula (Duyvendak, 1942; Mayall & Oort, 1942). Today, the Crab Nebula is among the most heavily investigated objects outside our own solar system (Hester, 2008). The nebula has been recently observed by many facilities that include (but are not limited to): (1) *Hubble Space Telescope* (HST) (Hester et al., 1995, 1996; Blair et al., 1997; Sankrit & Hester, 1997; Sankrit et al., 1998; Loll et al., 2007; Hester, 2007); (2) *Chandra X-ray Observatory* (*Chandra*) (Weisskopf et al., 2000;

Hester et al., 2002; Mori et al., 2004; Seward et al., 2006a,b); (3) *Spitzer Space Telescope* (*Spitzer*) (Temim et al., 2006); (4) Very Large Array (VLA) (Frail et al., 1995; Bietenholz et al., 2001, 2004). The Crab SN and its SNR have become an important astrophysical example of connecting theory with observations.

The Crab pulsar (PSR B0531+21) is a relatively young neutron star located at the centre of the Crab Nebula. It was first discovered in 1968 in the radio (Staelin & Reifenstein, 1968; Comella et al., 1969) and is the compact remnant associated with SN 1054, indicating that the outburst was a core-collapse SN. The Crab pulsar has been observed in all wavelengths and has become the *prototypical* neutron star. The Crab pulsar has a period of 33 *ms*, a spin-down rate of $\dot{P} = 4.21 \times 10^{-13}$ (Hester, 2008) and has been estimated to have lost $\sim 3.6 \times 10^{49}$ ergs since its birth (Bejger & Haensel, 2003). This energy is efficiently being converted into *synchrotron emission* due to the rapidly rotating magnetic field of the spinning pulsar accelerating electrons and positrons to high energies. Therefore, the Crab has a ellipsoidal synchrotron nebula with strong radio emission that fills a volume of ~ 30 pc³ and is the defining member of a class of pulsar-powered SNRs deemed *plerions* or *Pulsar Wind Nebulae* (PWN). In terms of the 3-D structure of the Crab, the nebula is asymmetrical. Although the Crab Nebula seems to be somewhat symmetric about the pulsar spin axis, there seems to be a pronounced southeast-northwest asymmetry. The Crab pulsar also has a known proper motion relative to the remnant, supporting the suggestion that the explosion was asymmetrical - a phenomenon called a *pulsar kick* (i.e. momentum kick given to the pulsar at birth). Ng & Romani (2006) found a best-fit proper motion of 14.9 ± 0.8 mas year⁻¹ based on archival HST data taken over seven years. This proper motion has a position angle of $278^\circ \pm 3^\circ$ which aligns with the axis of greatest symmetry observed in the Crab Nebula.

Although it is clear that SN 1054 was a CCSNe, the specific sub-type has remained a mystery as well as its lightcurve shape. Discovering LEs from the original Crab outburst would represent a remarkable opportunity for astronomers - it would allow us to *type* the Crab explosion by taking an optical spectrum of its LE. With the discovery of multiple LEs, we would be able to obtain a three-dimensional spectroscopic view of the original explosion and allow a comparison with the currently observed asymmetrical remnant. Such

an analysis could also provide clues for the *origin* of the observed nebula asymmetry. Is the dominant influence the SN explosion itself or the pulsar wind? Finding LEs from the Crab would represent the first LE discovery from a pulsar-producing SN. The Crab’s location also facilitated our decision to prioritize a search for Crab LEs. Unlike many of the other historical SNe (i.e. Kepler’s SN), the Crab happens to lie slightly out of the galactic plane ($b = -5.8^\circ$), limiting foreground dust and therefore potentially increasing our chances of observing LEs. However, the high latitude could also potentially be a drawback, as ISM dust needs to exist in order to scatter the light from the outburst in the first place. Given the above arguments and its scientific importance to the community, searching for LEs from the Crab was a natural next target for our group.

3.2 Supernova 1181 AD & Radio Source 3C 58

According to eight different historical Chinese and Japanese accounts, a guest star appeared in the night sky in the year 1181 AD. The records describe the star as lasting 185 days before its disappearance (Stephenson & Green, 2002). The long duration of naked-eye visibility is a clear indication that the guest star was most likely a SN event, since deemed *Supernova (SN) 1181*, and one of the half dozen, well-recorded historical SNe in the Milky Way. From the historical records, the SN was determined to be located in the present-day constellation of Cassiopeia (Stephenson & Green, 2002).

Stephenson (1971) were the first to suggest that the bright radio source 3C 58 could be the remnant counterpart of SN 1181 based on their positional agreement. Since then, 3C 58 has been classified as a pulsar wind nebula (PWN; Weiler & Panagia (1978)) and more recently, a pulsar was detected in X-rays (Murray et al., 2002) and then in the radio (Camilo et al., 2002). The presence of a pulsar indicates that 3C 58 is the remnant of a core-collapse SN event. Over the past decade, however, there have been a number of arguments against a connection between SN 1181 and 3C 58 (Fesen et al. (2008), Table 3). The primary reasoning has been based on the PWN’s expansion rate, evolution, and energy. A variety of observations indicated that 3C 58 is likely a remnant of a considerably older supernova event ($\gtrsim 4000$ yrs) and therefore has *no association* with SN 1181 (~ 830 yrs).

An obvious counterargument is that 3C 58 is the only known supernova remnant with a position that can be so closely connected to SN 1181 based on historical records. More recently, Kothes (2010) has suggested that many of these arguments are based on the assumption that the distance to 3C 58 is 3.2 kpc, a distance calculated using HI absorption radial velocity and assuming the galaxy’s flat rotation curve (Roberts et al., 1993). Kothes (2010) proposed a new distance of 2 kpc based on dynamical arguments associated with its Perseus Arm location. Kothes (2010) suggested a 2 kpc distance would imply a much younger age for 3C 58 (~ 1000 yrs), renewing the possibility of a connection between SN 1181 and 3C 58. Of the handful of certain historical supernovae in the Milky Way, SN 1181 and its association with the PWN, pulsar, and radio source 3C 58 remains the most disputed.

Overall, SN 1181 has remained unclassified and surrounded in controversy. Imaging detection of SN 1181 LEs *alone* would settle the SNR identification dispute and spectroscopy would provide the class and sub-class of the CCSN. The location of the radio source 3C 58 also encouraged us to prioritize this particular historical SN for our next search - it happens to lie at an angular distance $\sim 20^\circ$ and $\sim 11^\circ$ from the Cas A and Tycho remnants, respectively. With the discovery of LEs from both Tycho and Cas A, the region seems to be well-suited for LE discovery in terms of dust distribution. Furthermore, searching for 1181 LEs would also increase our chances of finding additional LEs from Tycho and Cas A due to the close proximity of all three.

CHAPTER 4

OBSERVATIONS, REDUCTIONS AND SEARCHING

4.1 Reduction and Difference-Imaging Technique

Difference-imaging involves the digital image subtraction of two or more epochs of the same field (Section 2.1.2). The constant stellar and galactic background is removed in the resulting difference image and any variable objects appear as significant positive or negative deviations. Since LEs are extended astrophysical features that are moving, searching for these objects using difference-imaging is ideal.

As part of the SuperMACHO microlensing survey, Rest et al. (2005a) created a near real-time software pipeline in order to *reduce* and *difference* the survey’s images. The difference-imaging technique used by Rest et al. (2005a) is the process that our group has utilized for *all* of our targeted LE searches (the historical SNe and η Carinae). The pipeline combines existing astronomical software packages, such as IRAF (Tody, 1993), and custom software in order to reduce and subtract the raw images. A brief description of the steps implemented by the image pipeline are described below:

1. **“Cross-Talk Correction”** - electronic artifacts are subtracted (“ghosts” of bright objects appear in images due to low-level cross-talk between the signals from different CCD chips).

2. **Astrometric Calibration** - mathematical transformation from pixel to celestial coordinates on the sky.
3. **Separation into Amplifier Images** - the single field is broken down into independent units called the *amplifier images*, which correspond to each used CCD amplifier. For example, the MOSAIC-1.1 imager at the KPNO 4m has eight CCDs - each half of each CCD is read out by its own amplifier.
4. **Flatfielding & Bias Subtraction** - the standard reduction steps of bias subtraction and flattening are applied to the individual amplifier-images.
5. **Deprojection** - each image must be resampled to the same geometry as the template image (earlier epoch image) so that it can be properly subtracted (i.e. the images are photometrically aligned). To do this, the *SWarp* software package was employed (Bertin et al., 2002).
6. **Aperture Photometry** - reduced and resampled images are photometrically calibrated using the *DoPHOT* photometry package to identify and measure sources (Schechter et al., 1993). The aperture photometry process determines a photometric zero point for the image.
7. **Pixel Masking** - saturated pixels must be properly masked because the true brightness value isn't known when the measurement is saturated (i.e. for saturated stars, both the star and its spikes are masked).
8. **Image Subtraction** - before subtraction can take place, the images also need to be *PSF-matched*. Once they are matched, the images are subtracted and a clean difference-image is produced. The software implemented for this part is the "*High Order Transform of PSF and Template Subtraction*" (HOTPANTS) package.

The *fifth* and *eighth* steps above (alignment and PSF-matching) are certainly the most difficult part of the process - in general, the images one wants to subtract are taken under different conditions, including atmospheric transparency, atmospheric seeing, or exposure times. These factors result in each image having a different PSF. The crux is to find a *convolution kernel* that matches the PSFs of two astronomical images - the convolution

of an image means that the output pixel is a weighted sum of the input pixels within a kernel of a certain size. Also, since the PSF varies spatially in all astronomical images, the kernel must be modelled as a spatially varying function (Alard & Lupton, 1998; Alard, 2000).

The image pipeline has been adapted and modified for the specific instrument used. For this thesis, two instruments have been used: KPNO MOSAIC-1.1 and CFHT MegaCam. It is important to note that the CFHT MegaCam data was *already* reduced when it was distributed to us, allowing us to skip directly to the difference-imaging process in the pipeline.

4.2 Imaging at KPNO

Since the beginning of our group's search for SN LEs, the two telescopes that we have utilized most for our searching is the *Cerro Tololo Inter-American Observatory's* (CTIO) 4-meter Blanco telescope and the *Kitt Peak National Observatory's* (KPNO) Mayall 4-meter telescope. Both telescopes are managed by the National Optical Astronomy Observatory (NOAO). This section will focus on the KPNO Mayall 4-m, as this was the telescope used for my thesis work. Our motivation for selecting these telescopes derives from the following qualities: (1) they are both equipped with a wide-field imager camera (large field-of-view); (2) both telescopes contain atmospheric dispersion correctors (ADCs); (3) ability to search for SN LEs in the northern hemisphere (KPNO) and southern hemisphere (CTIO). The four northern SNe for which we have used the KPNO 4m are: Tycho, Cas A, SN 1181, and the Crab. The wide-field CCD imager at KPNO is currently MOSAIC-1.1 (MOSA) (8192×8192 pixels in the focal plane covering just over a quarter of a square degree on the sky). A few general parameters of the MOSAIC-1.1 instrument and the KPNO 4-m are summarized in Table 4.1. In Table 4.2, we summarize our group's KPNO programs over the past six years - in each program we have obtained first and second epoch images in the north in the search for scattered LEs from historical SNe.

An observing program was established for the 2010/2011 year with the goal of discovering the first LEs associated with SN 1054 (Crab) and to locate additional LE complexes around Cas A and SN 1572 (Tycho) (see the 2010B-0529 proposal in Table 4.2). At this point in

Arrays	Eight 2048×4096 pixel e2v CCDs (4×2)
Image Size	8192×8192 pixels
FOV	$36' \times 36'$
Pixel Size	$15 \mu\text{m}$ ($0.26''$ /pixel at the 4 m)
Filters	34 filters available at KPNO

Table 4.1 General MOSAIC-1.1 characteristics at the KPNO 4-meter

Approved Program	PI	Details
2006B-0301	N. Suntzeff	4 nights in Sept. and 4 nights in Dec.
2007B-0332	A. Rest	4 nights in Sept. and 1.5 nights in Dec.
2009B-0493	A. Rest	4 nights in Oct. and 4 nights in Dec.
2010B-0529	A. Rest	4 nights in Nov. and Jan.
2011B-0130	A. Rest	2 nights in Sept., Oct., Dec., and Jan.

Table 4.2 Summary of our group’s LE programs at KPNO

time, LEs had already been discovered from both Tycho’s SN and Cas A using the KPNO 4m. In November 2010, I took part in the observing run at the KPNO 4-m. Our observing strategy for this program was organized as follows:

- **Targets:** Fields were chosen based on higher-intensity areas of $100\text{-}\mu\text{m}$ IRIS (re-processed IRAS) maps of the Galactic plane (Miville-Deschênes & Lagache, 2005).
- **Filter:** We observed using the broadband *VR Bernstein* (k1040) custom filter, which has a central wavelength of 5944.95 \AA and a FWHM of 2119.56 \AA . This unusually broad bandpass allows us to record more photons per unit time than traditional filters.
- **Exposure Times:** For the Crab fields, we used exposure times of 200 seconds and for Tycho/Cas A fields we used 160 seconds. Using the KPNO 4m in the past, we had identified many LEs from Tycho and Cas A in 160-second exposure VR images. The Crab exposure time was increased based on its older age and the fact that it was a CCSNe (intrinsically fainter than SNe Ia).
- **Field Names:** The naming convention used for Crab and Tycho/Cas A fields were

“crab####” and “tyc####”, respectively. The #’s represent the x vs. y coordinates on an angular grid of fields placed over the region we wish to observe (i.e. tyc2345 represents the field with $x = 23$ and $y = 45$ on the grid). Due to the fact that Tycho and Cas A are spatially close to each other (their search annuli overlap), we used one grid for both and thus the naming convention for both was “tyc”.

Overall, the best seeing during this run was 0.65 arcsec - but typically the seeing was around 0.8-1.2 arcsec. Each night, the raw data was transferred from the observatory to our McMaster machine, *Tera*. For the reduction and differencing process, the data was transferred to the *Odyssey* cluster supported by the *FAS Science Division Research Computing Group* at Harvard University to make use of multiple CPUs. Recall that the image reduction pipeline divides each single MOSA field into sixteen $1k \times 4k$ pixel images corresponding to each CCD amplifier. Using first epoch images taken in the previous semester (2009B-0493), approximately **990** Crab difference images were created from the 2010B-0529 KPNO program.

I also had the opportunity of participating in two observing runs for our 2011B-0130 KPNO program. The goal and strategy of this program was the same as 2010B-0529: discovering LEs from the Crab and searching for additional LEs from Tycho and Cas A. We also took some time to image a few SN 1181 fields during this program.

4.3 Imaging at CFHT

In 2010, our team decided to expand our searching by using the *Canada-France-Hawaii Telescope* (CFHT) on Mauna Kea and its wide-field optical imaging facility, *MegaPrime*. The properties of the wide-field imager, MegaCam (built by CEA, France) are summarized in Table 4.3. MegaCam’s large field-of-view and routinely excellent image quality make it the ideal instrument for detecting SN LEs. The observations were carried out through *Queued Service Observing* (QSO) and the data was preprocessed and calibrated before being distributed to the *Principal Investigator* (PI) of the program. CFHT prepared data distributions in batches throughout the semester that were downloaded by the PI. The distribution schedule depended on when CFHT performed their bulk data reduction runs. The distribu-

tion remained online for three months, but can further be accessed through the *Canadian Astronomy Data Centre* (CADC) archive.

Arrays	Thirty-six 2048×4612 pixel CCDs (9×4)
Image Size	$18,432 \times 18,448$ pixel
FOV	$60' \times 60'$
Pixel Size	$13.5 \mu\text{m}$ ($0.187''$ /pixel)
Filters	u^*, g', r', i', z'

Table 4.3 General MegaPrime/MegaCam Characteristics at CFHT

4.3.1 CFHT & the Crab SN

In September 2010, our team submitted a proposal for observing time with CFHT MegaCam specifically geared towards searching for Crab LEs (proposal ID = 11AC033). Brendan Sinnott was the *Principal Investigator*. Our proposal ranked 3/33 from CanTAC and we were allocated the full 40 hours that we requested. Based on the expected apparent motion of Crab LEs, detection should be possible via difference-imaging with pairs of epochs in the same observing semester - therefore it was emphasized to the observer that 1st and 2nd epochs of the same fields *must* be separated by at least a month during this program. Our observing strategy and target selection for this program is displayed in Figure 4.1 and summarized below:

- **Exposure Times and Filter:** Exposure times of 200 seconds for each field in the SDSS g' filter (central wavelength 4825 \AA and a FWHM of 1380 \AA). The expected low foreground reddening encouraged us to observe towards the blue.
- **Priority 1 Targets:** Fields were selected to represent forward-scattering from dust located $z=0-500$ ly in front of the SN event. Our groups previous experience detecting galactic LEs from Tycho and Cas A revealed that most LEs are detected in this scattering angle regime. This observing region is shown inside the red circles in Figure 4.1. We requested to observe 30% of this area which corresponded to 150 fields - each field is observed *twice*, totalling 16.6 hours.

- **Priority 2 Targets:** Priority 2 targets were fields for which a potential LE could be observed due to back-scattering 100 ly behind the SN, or forward-scattering 2000 ly in front of the SN. The observing region is shown inside the yellow circles in Figure 4.1. We requested to observe 10% of this area which corresponded to 185 fields - each field is observed *twice*, totalling 20.6 hours.
- **Naming Convention:** The field names were chosen in the same way the KPNO fields were created (based a grid of fields with xy coordinates), except instead of using “crab2337”, we used “ccrab2337” to identify the field with CFHT observations.

In Appendix A we have listed the coordinates of the observed target fields for this program. The observations were carried out between February and July 2011. We began receiving the data in March 2011. The pipeline was adapted by A. Rest to suit CFHT MegaCam images - as mentioned in Section 4.1, the MegaCam data was received *already* reduced and therefore only the image subtraction process was required. Overall, **13,880** difference images were produced from this program to search for Crab LEs. The difference images from CFHT MegaCam were of the highest quality we had seen to date on a 4m-class telescope with a much lower level of artifacts (main contaminants when searching for LEs).

4.3.2 CFHT & SN 1181 AD

In March 2011, I submitted a proposal (as Principal Investigator) for observing time with CFHT MegaCam specifically geared towards searching for multiple LEs from another of the Milky Way’s historical supernova, SN 1181 (proposal ID = 11BC021). Like the Crab, LEs from this outburst have yet to be discovered. Our CFHT proposal for 1181 was a success. We were given a QSO grade of “B”, which means our program was “Prioritized” (this is the second best grade a program can obtain in terms of global priority for CFHT) - therefore, we were awarded the full 21.3 hours that we requested. Our observing strategy and target selection for this program is displayed in Figure 4.2 and summarized below:

- **Exposure Times and Filter:** Exposure times of 150 seconds for each field in the SDSS r' filter (central wavelength 6261 Å and a FWHM of 1382 Å). The r' band

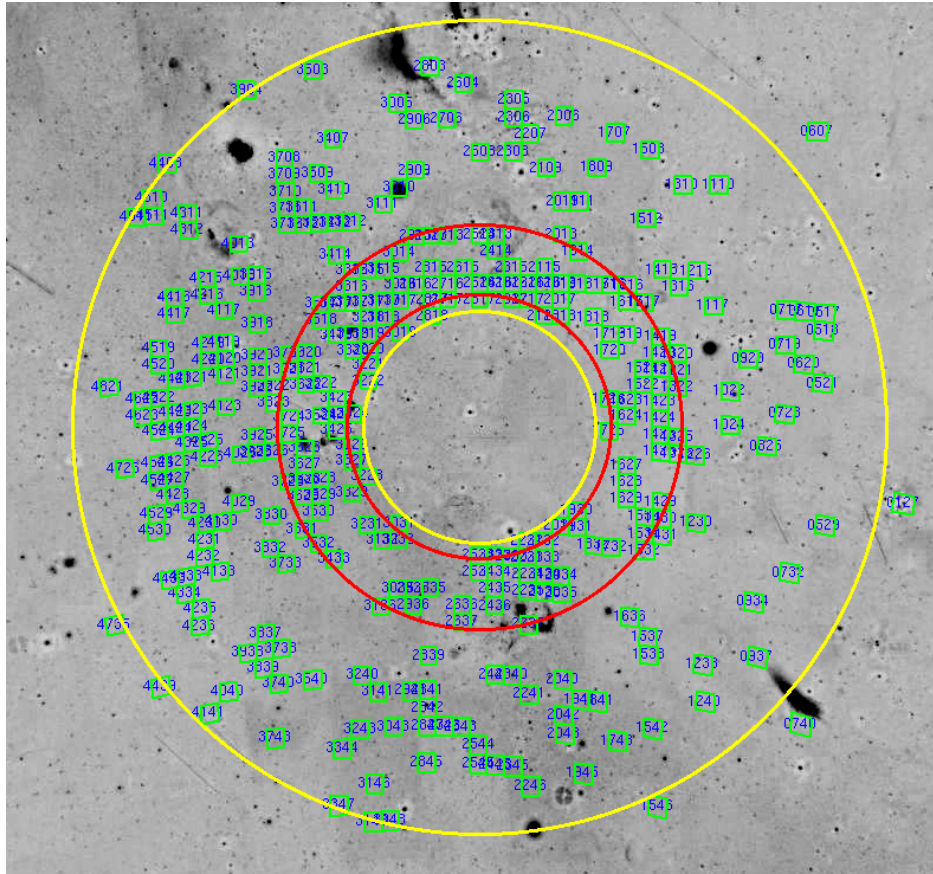


Figure 4.1 The region inside the two red circles indicates our high-priority observing region representing forward scattering dust locations 0 ly and 500 ly in front of the SN event. The region between the large yellow circles indicates our second-priority region representing scattering dust locations 100 ly *behind* and 2000 ly in front of the SN. The green fields ($1^\circ \times 1^\circ$) represent our 335 pointings. The Crab Nebula is located in the centre of the circles.

was chosen as opposed to g' (used in 11AC033 program) because r' is closer to the peak sensitivity of the CCD and our potential LE observations will suffer less if the foreground absorption and reddening are greater (which was expected in this case).

- **Targets:** Fields were selected to represent forward-scattering from dust located $z=100$ -2000 ly in front of the SN event. Again, this is based on our groups previous experience detecting galactic LEs from Tycho and Cas A - most LEs are detected in this scattering angle regime. This observing region is shown as the green fields in Figure 4.2. We avoided obvious foreground dust in the north. Overall, there were 196 pointings in total that were evenly distributed around the radio source 3C 58. Our fields covered

23% of our chosen wedge of sky.

- **Naming Convention:** The field names were chosen in the same way the KPNO fields were created (based a grid of fields with xy coordinates), except we used “c3c” as the designation (i.e. c3c2337) to represent the CFHT observations and the remnant 3C58.

In Appendix B we have listed the coordinates of the observed target fields for this program. Observing took place from August 2011 to January 2012. We began receiving the data in September 2011. The pipeline had already been adapted to suit CFHT MegaCam images. Second epoch data was distributed from CFHT beginning in December 2011 - the images were immediately subtracted and visual searching could progress from there. In total, **11,052** difference images were produced from this program to search for SN 1181 LEs.

4.4 Inspecting the Difference Images for LEs

Difference images must be *visually inspected* for SN LEs - an automatic search technique simply does not yet exist due to difference image features that can resemble scattered LEs, which software cannot differentiate. Visually searching for LEs is a time-consuming task. In order to make our searching more efficient, we took advantage of the *Purr* machine run by the SHARCNET facility at McMaster. *Purr* has a *Toshiba P56QHD-4* display monitor that has a resolution of 3840×2160 and physical dimensions (width \times height) of 52.8×31.4 inches. Its high resolution and large monitor allow us to notice and record faint features more effectively than on our own monitors. Therefore, we were able to inspect difference images in a rapid fashion. The “*sniffing*” process involves these steps: (1) open 50-100 difference images at one time in ds9 using *Purr*; (2) make ds9 as large as possible and zoom out so that you should be able to see the full frame on the monitor; (4) tab through each frame (each image) and spend a few seconds on each searching for LEs - if a particular feature stands out and resembles a LE you stop and record it.

All possible LE candidates were recorded and sorted in log files that describe (1) the field I.D. and amplifier of the image in which the object was seen; (2) which approximate section of the image it lies in so that it can be found again easily (i.e. right side, left side, middle);

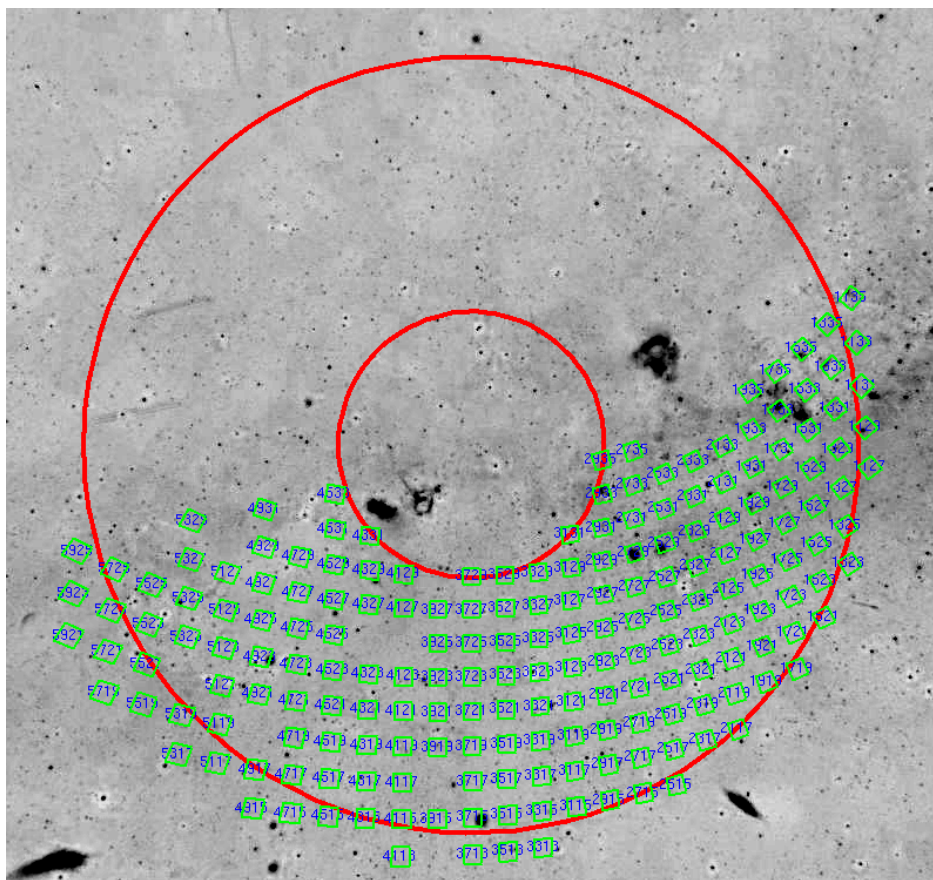


Figure 4.2 SN 1181 Light Echo Survey CFHT MegaCam Fields. The green fields ($1^\circ \times 1^\circ$) represent our 196 pointings. North is up and east is left. The two red circles with angular diameters 16.4 and 47.8 degrees represent scattering dust locations 100 ly and 2000 ly in front of the SN, respectively. The position of 3C 58 is located at the center of the concentric circles.

(3) description of the feature (i.e. faint, bright, extended); (4) and a ranking number (1,2,3) associated with how much the object resembles a possible LE - where 1 represents an object that looked very much like a LE and 3 represented a likely artifact, but was interesting enough to be investigated further. After the sniffing process was completed, the candidate objects were reviewed in more detail to determine if they were likely real and whether their apparent motion matched any of the locations of our known SNRs.

KPNO Results I inspected the 987 difference images from the 2010B-0529 program for Crab LEs. No Crab LEs were found. Crab LEs were also not detected in the 2011B-0130

program. Although Tycho and Cas A LEs have been discovered using the 4-m at KPNO in the past, LEs from the Crab and SN 1181 have not been detected.

CFHT Results I inspected 13,880 difference images for the Crab CFHT program and 11,052 difference images for the 1181 CFHT program. No LE candidates were found for the Crab SN or SN 1181. In the 1181 data, however, we *did* discover *new* LE complexes from Tycho and Cas A - not surprising due to the proximity of all three of these historical SNe on the sky. The positions of the brightest 20 LEs found in the MegaCam data are shown in Figure 4.3 and Figure 4.4 with respect to the three SNRs on the sky. A summary of their coordinates is in Table 4.4. Six examples of these LEs are shown in Figure 4.5. It was satisfying to confirm that high-quality LEs *can* be observed using CFHT MegaCam. These LEs add to our growing list of Cas A and Tycho LEs. The more LEs we have, the more *viewing angles* we have for an outburst, adding valuable information about the explosion symmetry.

Overall, we have had *no* success thus far in finding LEs from the Crab or 1181 SNe or any other unknown and unexpected sources. In Chapter 5, we discuss the implications of the non-detections, what we can conclude from these studies, and what might be achieved by future observations.

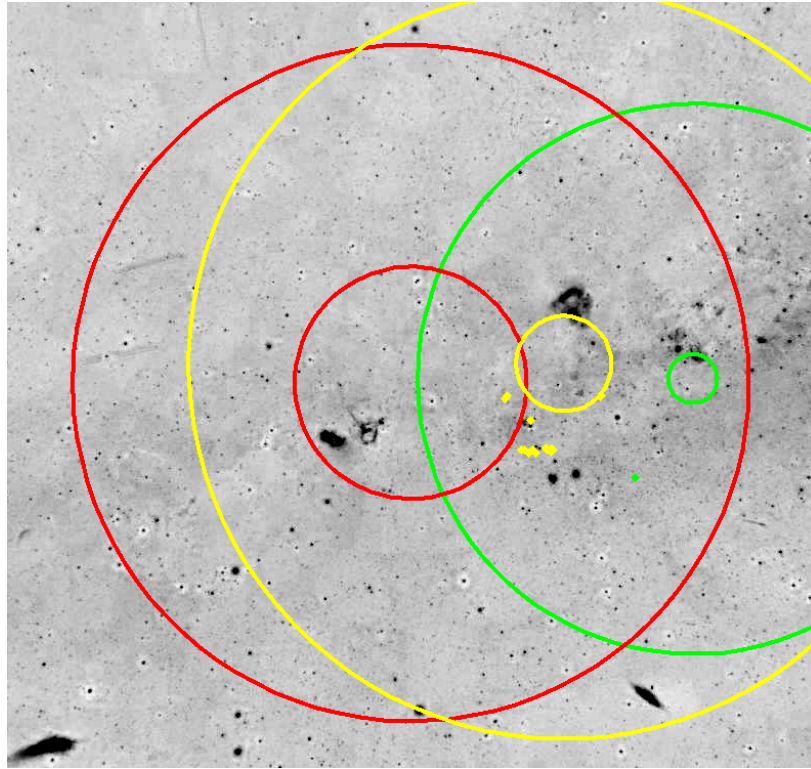


Figure 4.3 Positions of the brightest Tycho (yellow diamonds) and Cas A (green diamond) LEs found in the 2011B MegaCam data. Our SN 1181 observing strategy is represented by the red circles. The yellow and green circles represent Tycho and Cas A observing areas with $z = 0$ to $z = D/2$.

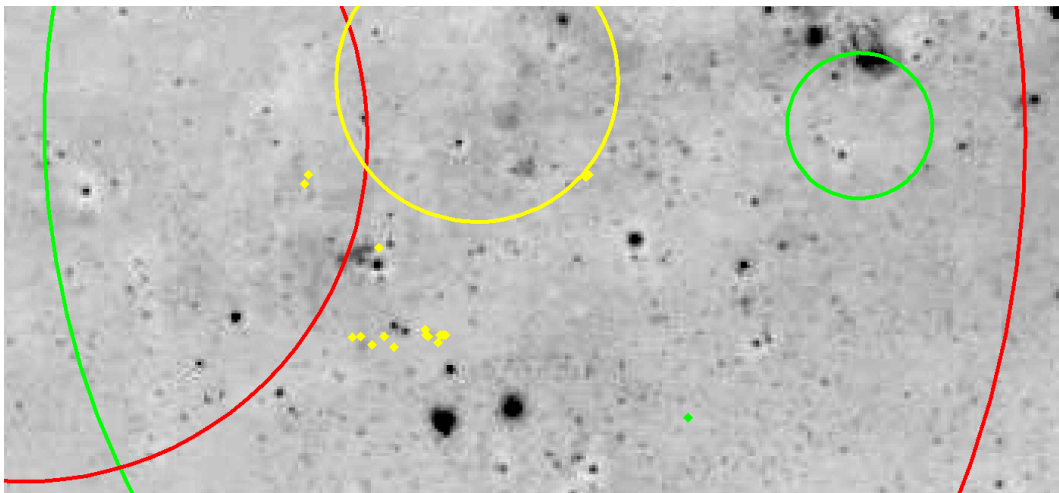


Figure 4.4 Close-up of region in Figure 4.3 with Tycho and Cas A LE positions.

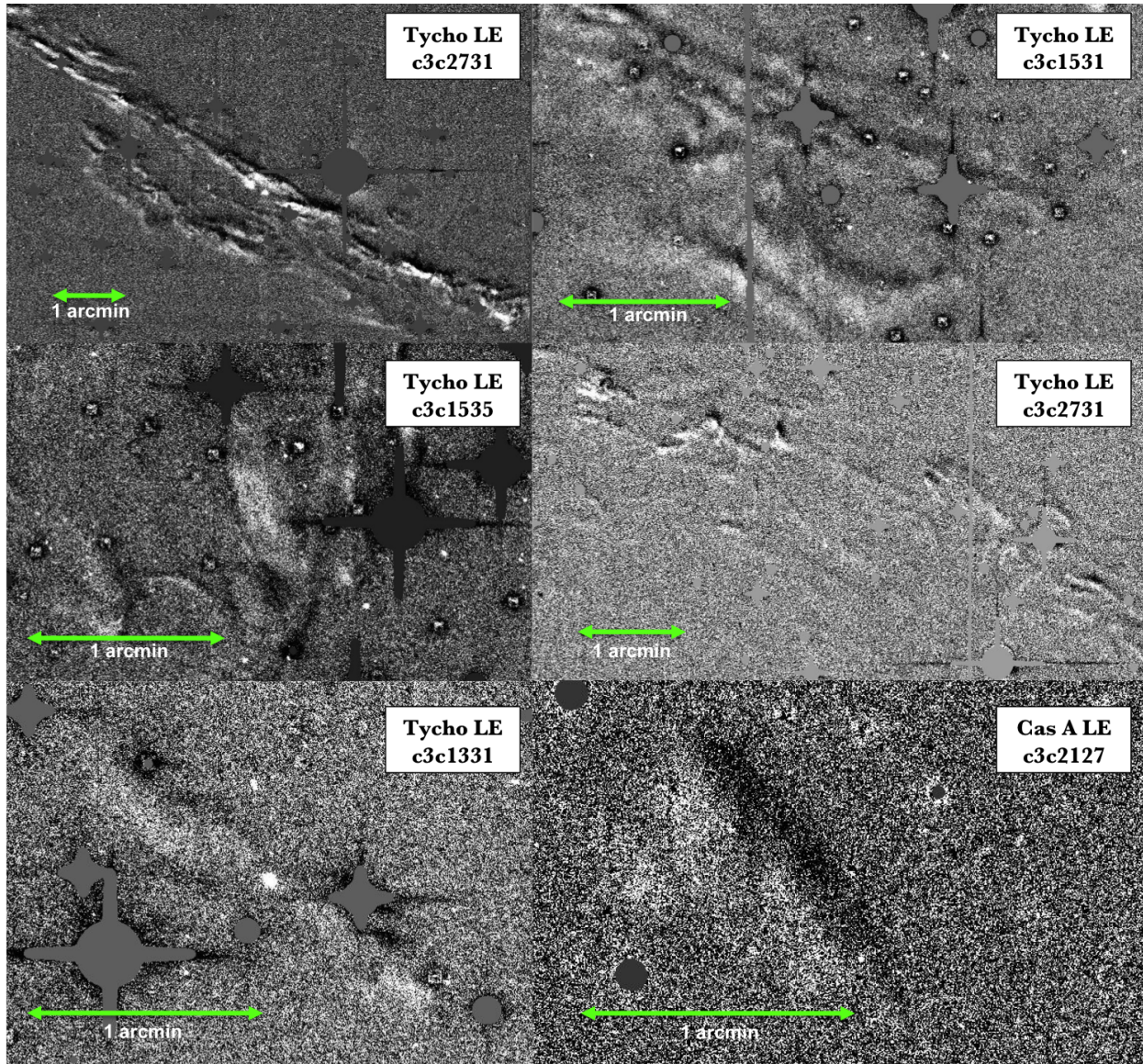


Figure 4.5 Difference images showing a few of the brightest LEs found in the 2011B MegaCam data.

Field ID_Amp	RA	Dec	SNR
c3c2731_22	00:48:57.358	+58:43:42.50	Tycho
c3c1531_19	00:48:01.854	+58:41:00.29	Tycho
c3c1535_6	01:05:59.307	+63:12:37.49	Tycho
c3c2731_23	00:48:25.677	+58:42:27.42	Tycho
c3c1331_1	01:03:12.802	+59:11:43.18	Tycho
c3c2731_10	00:51:23.951	+58:56:55.69	Tycho
c3c2731_30	00:49:47.958	+58:33:49.59	Tycho
c3c1331_15	00:59:05.053	+59:02:42.05	Tycho
c3c1533_4	00:55:40.039	+61:07:39.34	Tycho
c3c1331_12	01:01:35.266	+58:55:48.00	Tycho
c3c1331_25	00:57:46.316,	+58:44:59.76	Tycho
c3c1535_14	01:07:10.133	+63:02:00.04	Tycho
c3c1727_22	00:13:49.055	+54:49:07.51	Tycho
c3c2931_4	01:04:52.119	+59:13:03.98	Tycho
c3c2931_6	01:02:58.188	+59:09:10.44	Tycho
c3c2731_19	00:51:29.855	+58:49:03.74	Tycho
c3c2731_20	00:51:13.125	+58:46:44.67	Tycho
c3c2333_12	00:12:37.826	+61:00:30.67	Tycho
c3c2333_30	00:11:51.207	+61:01:11.47	Tycho
c3c2127_24	00:13:48.858	+54:49:04.34	Cas A

Table 4.4 New Tycho and Cas A LEs found in the MegaCam 11BC021 data.

CHAPTER 5

IMPLICATIONS OF NON-DETECTION

It has now been over seven years since our group began the search for LEs from the Milky Way's historical supernovae. It is important to review our results up to this point and discuss the implications of our non-detections. We must reassess our observations and compare the properties of the various historical supernovae to determine what constraints our non-detections have provided.

In the following sections I examine the various factors that would contribute to a non-detection of SN LEs: (1) dust distribution in the SNR regions; (2) the ages and distances of the SNRs in terms of both their measurement reliability and their effect on LE flux; (3) the luminosity of the original outburst event (a function of SN type) which also has an effect on the LE flux. In the last section, I combine the contributing factors to estimate the surface brightness (SB) of SN 1181 and Crab LEs *relative* to Tycho's SN and the maximum flux of its LEs.

5.1 Dust

Foreground dust is detrimental to the light from LEs reaching us, but dust also needs to exist along our LE ellipsoid surface for scattering to occur. The dust distributions in our search regions could potentially be a defining factor in our non-detections. Interstellar dust

can be mapped in many ways. One can measure the optical, near-infrared or microwave light from background stars that have been absorbed or re-emitted by the dust in the line of sight. Another way of tracing dust is to use *molecular gas* in the Milky Way as a proxy.

CO as a Proxy for Dust Molecular clouds in galaxies are comprised of interstellar dust and gas. The most abundant gas molecule associated with molecular clouds is molecular hydrogen gas (H_2) followed by carbon monoxide gas (CO) (Combes, 1991). Unfortunately, H_2 is difficult to detect directly - no transitions can be excited under the typical conditions of molecular clouds. On the other hand, CO has a dipole moment with rotational transitions that are *easily* excited at typical molecular cloud temperatures and densities (Combes, 1991). Therefore, extensive work has been done to assess the reliability of CO as a tracer of both H_2 and dust in molecular clouds. Specifically in the case of dust, column density maps derived from ^{12}CO and ^{13}CO observations have been compared with dust extinction maps. These studies show that a linear relationship *does* exist between the column of CO and dust for observed visual extinctions up to some maximum value (Lada et al., 1994; Alves et al., 1999; Hayakawa et al., 1999; Pineda et al., 2010). Overall, the Milky Way’s average gas-to-dust ratio has been determined to be ~ 150 (Draine et al., 2007).

Given the fact that CO correlates with dust, it would be ideal to establish a correlation between CO emission and our known LE locations so that we can selectively search for LEs in the future using Galactic CO maps. Therefore, it is worth our while to investigate and compare CO emission in our search fields versus CO emission in the fields where LEs have been detected. I focus on the SN 1181 MegaCam fields, as we did detect LEs in some of these fields. We refer to a Galactic CO survey by Dame et al. (2001). Dame et al. (2001) combined a large-scale CO survey obtained using the CfA 1.2 m telescope with 31 other CO surveys over the past two decades to produce a composite CO survey of the Milky Way. The CO data for this survey is available online in the form of moment masked whole galaxy data cubes (all l , b , and v). The moment-masked data cube was obtained and then collapsed with the help of Christine Wilson by integrating over velocity to obtain the W_{CO} map in [K km/s]. W_{CO} is the integrated brightness temperature or the observed CO intensity. I obtained the W_{CO} values for: (1) known bright Cas A and Tycho LE positions (total of 33

used) and; (2) all of the observing field locations for which we *didn't* find LEs in the 11BC021 MegaCam program. The W_{CO} distribution for LE fields and non-LE fields are plotted in Figure 5.1 and Figure 5.2, respectively. Table C.1 gives a list of the LE positions used and the corresponding W_{CO} values.

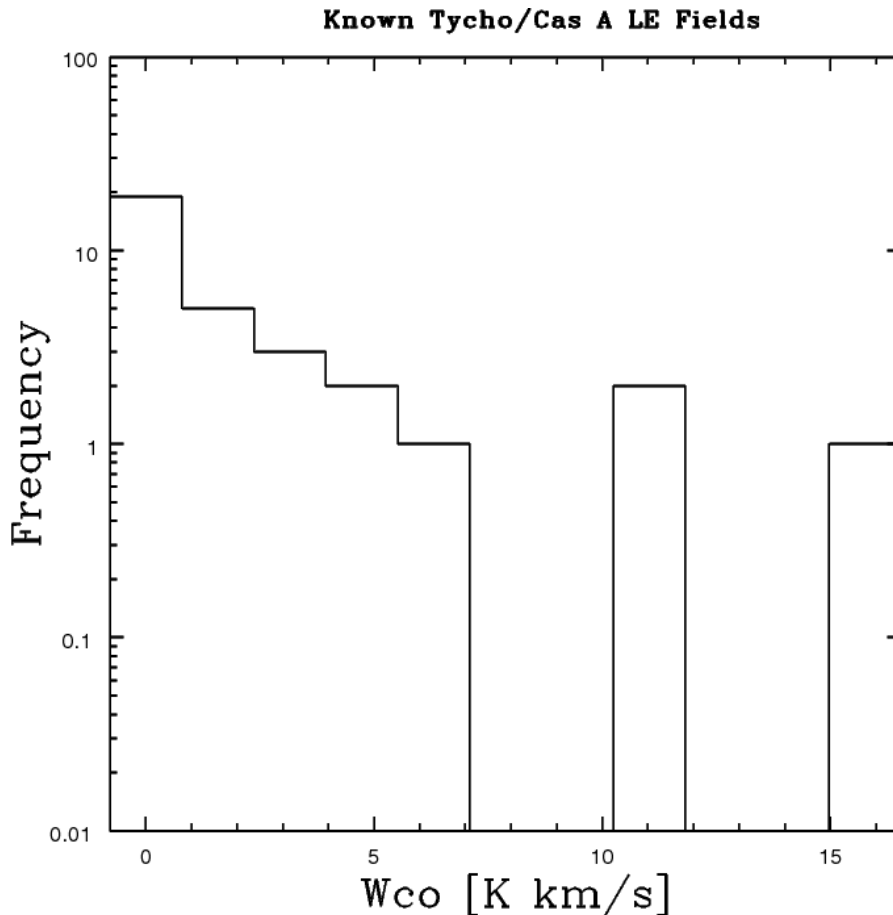


Figure 5.1 Distribution of W_{CO} for fields with known Tycho and Cas A LEs.

The W_{CO} values for the LE locations are listed in Appendix C. The measurements have an angular resolution of $7.5'$. A Kolmogorov-Smirnov test (KS-test) was performed and it was found that $D = 0.3576$ and the P-value = 0.001903 for the two data sets, which indicates that they are *distinct* with a high degree of significance. However, it is important to be cautious against the acceptance of this statistical result due to: (1) the fact that the Dame et al. (2001) survey was mostly concentrated on mapping the full extent of the Galactic

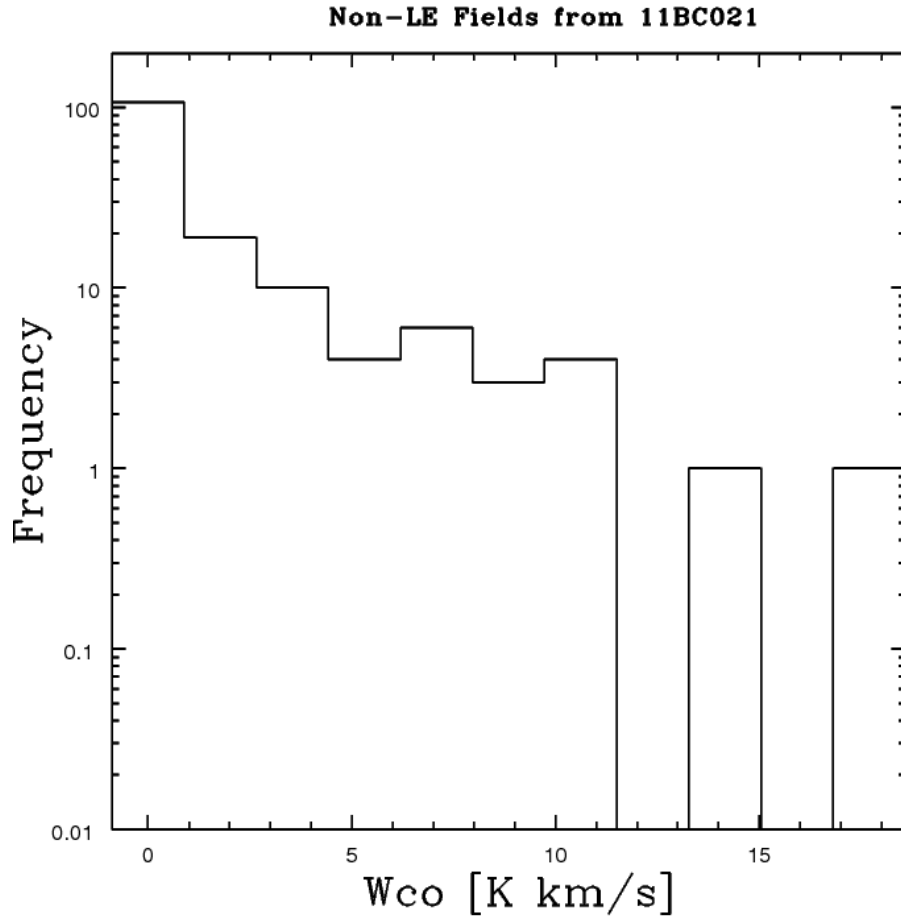


Figure 5.2 Distribution of W_{CO} for the fields from the 11BC021 MegaCam program (SN 1181 LE search) that we *did not* detect LEs in.

plane, leaving large areas of the sky unobserved - interpolated pixels and gaps increased the further you got from the Galactic plane and unfortunately our observing fields cover a significant portion of this section (Figure 5.3); (2) the difference between the angular resolution of the survey and the typical angular size scale of light echo features (~ 1 arcmin) is large.

For the 11BC021 MegaCam program, we did not observe the region of sky for which $z < 100$ - a significant portion of this region is located on the Galactic plane (See Figure 5.3). If future observations are carried out with the focus of finding SN 1181 LEs, observing in the $z < 100$ region (where more dust likely exists) may be worthwhile.

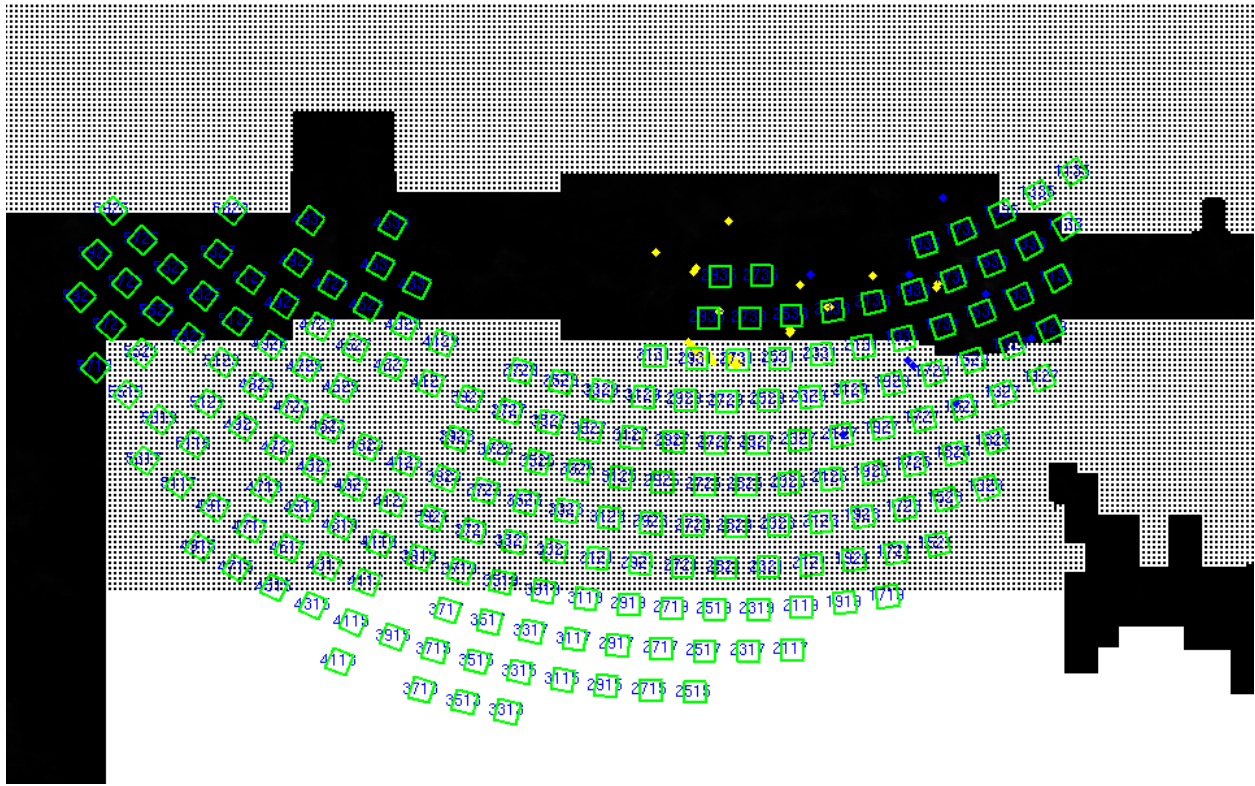


Figure 5.3 MegaCam 11BC021 observing field locations ($1^\circ \times 1^\circ$ green boxes) and positions of known bright Cas A (yellow) and Tycho (blue) LEs on Dame et al. (2001) W_{CO} map (black boxes).

Our selection of fields has been largely dominated by scattering angle consideration. Prior to this research, our group *had* tested various field selection strategies that have incorporated dust arguments:

- We have observed fields based on higher-intensity areas of $100\text{-}\mu\text{m}$ IRIS (re-processed IRAS) maps of the Galactic plane (Miville-Deschênes & Lagache, 2005). Based on the location of the LEs we have discovered from Tycho and Cas A, the IRIS-based strategy has a detection rate of only around 5%.
- As part of Lindsay Oaster’s MSc. thesis (2008), she developed a *relative probability model* for the detection of SN LEs based on the physical characteristics of interstellar dust and absorption near the Galactic plane. The model included a dust scattering function, distribution of dust in the Galaxy (scale height), the dilution of echo flux with

distance, and the absorption along the SN-dust-Earth travel paths. Unfortunately, our 10 detected Tycho and Cas A SN LEs at the time were all located in the model's low-probability fields.

- Lindsay Oaster *also* checked for a possible correlation between CO emission and the locations of the 10 known LEs at the time (2008) using the *Canadian Galactic Plane Survey* (CGPS). Using CO cubes, she generated velocity line profiles for the LE locations - all the profiles were empty, indicating no detectable excess CO at those LE coordinates.

We have yet to find a reliable singular trend connecting the known LEs with available survey data, making it difficult to develop an efficient strategy which would be an improvement over random field selection. It would be useful to re-examine this with future, more encompassing dust or CO surveys - for example, the *Planck* team is in the process of producing the first all-sky map of CO ever compiled.

5.2 Distance Reliability

Calculations of the observable characteristics of supernova remnants (SNRs) are often highly dependent on distance estimates. Unfortunately, distances to SNRs cannot usually be measured directly and rarely do nearby, associated stars exist from which you can infer distances (a process possible for H_{II} regions). Therefore, the distance to SNRs are *notoriously* difficult to estimate and most existing estimates rely in some way on kinematics.

In the past, distances have been kinematically determined using the interaction with the SNR and its surrounding medium and/or HI absorption measurements if the SNR is a radio-bright source (observations of the 21 cm line of neutral hydrogen). For the latter case, the systematic velocity is normally obtained from the HI absorption profile, assuming a flat rotation curve with pure circular motion (assuming the 1985 IAU standard Galactocentric radius of 8.5 kpc and a rotation speed of 220 km s^{-1}). The uncertainties in deriving distances from observing velocities are largely due to deviations from circular motion - as will be described further on, this is especially an issue for remnants residing in the spiral arms of

the Galaxy (Kothes, 2010). Therefore, the precise distance to any SNR remains an evasive quarry. Our observing strategy for SN LEs depends on both the distance and age of the SN outburst. It is worth examining the uncertainty of distance measurements to the Crab SNR and radio source 3C 58.

5.2.1 The Distance to the Crab Nebula

Trimble (1973) estimated a range of distances to the Crab SNR between 1.4 and 2.7 kpc based on 12 lines of evidence. Some of these depended on the remnant’s dynamical expansion (1500 km s^{-1} at the edge of the nebula, Clark et al. (1983)), the interpretation of its physical characteristics, and absorption measurements. The unweighted mean of the values determined from the 12 methods was 1930 ± 110 pc (Trimble, 1973). Since then, expansion studies together with observed proper motions of the SNR have more-or-less concurred with Trimble (1973) and the consensus in the literature is a distance of 2.0 ± 0.5 kpc (Hester, 2008; Kaplan et al., 2008). A distance of 1.7 kpc has also been determined using the observed pulsar dispersion measurement and a model of the Galactic electron density distribution (Cordes & Lazio, 2002). Given the Crab’s prominent place in our understanding of SNRs and neutron stars, the fact that its distance still remains this uncertain is surprising.

5.2.2 The Distance to the Radio Source 3C 58

The controversy surrounding the distance estimate to the SN remnant 3C 58 was introduced in Section 3.2. The distance towards 3C 58 was estimated first using 21-cm absorption measurements by Goss et al. (1973) and Williams (1973) to be 8.2 and > 8 kpc, respectively. Later on, Green & Gull (1982) determined a distance of 2.6 kpc using the same method. Given the inconsistency of distance estimates at the time, Roberts et al. (1993) was motivated to re-examine the distance using better velocity sampling. They used HI absorption measurements from observations at the *Westerbork Synthesis Radio Telescope* (WSRT) and the *Effelsberg* 100 m telescope to obtain a systematic velocity of -38 km/s in the direction of 3C 58. Using the kinematic model of Fich et al. (1989) (flat rotation curve for outer Galaxy $\Theta = 220$ km s^{-1} assuming the 1985 IAU standard values of $R_0 = 8.5$ kpc and $\Theta_0 = 220$ km s^{-1} as rotational constants), this velocity corresponded to a distance of 3.2 kpc from the

Sun. This has been the distance estimate used for most investigations of 3C 58 over the past ~ 20 years. Unfortunately, Roberts et al. (1993) *does not* quote an associated uncertainty with this distance determination. For the purpose of our investigations in this chapter, I have adopted a 25% uncertainty associated with the 3.2 kpc distance estimate - this was the approximate error quoted by Fich et al. (1989) for determining kinematic distances (the distance computed with a flat curve, best-fit linear curve, and best-fit power-law curve is less than 10% for the outer galaxy while distance uncertainties will likely be 25% from other sources of error).

A Better Kinematic Distance Tool The distance debate for 3C 58 was recently resurrected by Kothés (2010). Before delving into the details of Kothés (2010), we first discuss the growing awareness in the field of Galactic kinematics surrounding the reliability of assuming circular gas orbits to determine kinematic distances to objects in the Milky Way (Gómez, 2006; Foster & MacWilliams, 2006; Russeil et al., 2007; Vallée, 2008; Baba et al., 2009). In particular, deviations from circular motion have been found to be significant at positions associated with the spiral arms. Due to these non-circular motions, it is estimated that a kinematically-determined gas map of our Galaxy has large systematic errors of ~ 2 -3 kpc in distance from the Sun (for distances of up to 20 kpc) (Baba et al., 2009). There have been a few investigations attempting to solve the issue at hand by introducing a *new* distance-velocity relationship that incorporates non-circular motions as opposed to relying on a purely circular rotation model described by standard Galactic kinematics - one apparently successful example is the work of Foster & MacWilliams (2006). They developed a three-dimensional model for Galactic neutral hydrogen that incorporates spiral shocks in order to accurately determine distances for objects in the second- and third- quadrant directions (where the Perseus arm is the first major arm encountered). The velocity field of the gas is modelled using both circular rotation and non-circular motions from a two-armed density wave pattern. By fitting this model to HI observations, it is expected that the distance estimate will be improved. The model was tested using 22 HII regions and SNRs with well-known, kinematically-independent distances (primarily photometric distances to exciting stars). The distances calculated by the fitted velocity field were in excellent agreement with the photometric distances. The contribution of all sources of uncertainty produced a

total fractional uncertainty in distance of 20%-30% when using this model. It is also important to note that Foster & MacWilliams (2006) had assumed $R_0 = 7.6 \pm 0.3$ kpc and $v_0 = 210$ km s⁻¹ - these were the latest measurements of the Sun's Galactocentric distance and velocity, respectively at the time.

Kothes (2010) and A New Distance to 3C 58 One aspect of Kothes' field of work involves using HI and CO observations from the *Canadian Galactic Plane Survey* (CGPS) to deduce more reliable distances to SNRs and HII regions. Specifically, their collaboration employs the distance-velocity relationship obtained from the Foster & MacWilliams (2006) model (see above) to determine their distances. Kothes also specializes in attempting to associate the SNRs with neighbouring sources to determine their distances more accurately. In Table 5.1, I have summarized the work of Kothes and his collaborators over the last ~ 10 years, with specific focus on their campaign to determine more reliable distances to SNRs associated with spiral arms. All of the studies in Table 5.1 have utilized either the Foster & MacWilliams (2006) model or the similar but older model Foster & Routledge (2003) for their distance estimates.

Kothes (2010) specifically focuses on the remnant 3C 58. The distance to 3C 58 is re-examined not only using new HI data but also the new distance-velocity relationship developed by Foster & MacWilliams (2006). Kothes (2010) determined a systematic velocity of -36 km/s for 3C 58 using HI absorption measurements obtained as part of the CGPS. Applying the Foster & MacWilliams (2006) model, two possible distances corresponding with -36 km/s exist for the direction of 3C 58: (1) 2 kpc (in the Perseus arm shock); (2) 2.5 - 2.8 kpc (beyond the Perseus arm shock). Kothes (2010) described the 2 kpc distance as being the most reliable choice because young objects like SNRs, whose progenitor most likely formed in the Perseus arm, are not likely to have migrated beyond that region since their formation. Although Kothes (2010) did not quote an uncertainty associated with this distance measurement, I have adopted a 30% error for the purpose of our work (this was the maximum error quoted by Foster & MacWilliams (2006) for distance determinations using their model).

Reference	SNR	Distance (kpc)
Kothes & Foster (2012)	CTB109	3.2 ± 0.2
Kothes (2010)	3C 58	2
Kothes et al. (2008)	DA 495	1.0 ± 0.4
Jackson et al. (2008)	G85.4+0.7	3.5 ± 1.0
	G85.9-0.6	3.5 ± 1.0
Kothes et al. (2005)	G96.0+2.0	4.0
	G113.0+0.2	3.1
Foster et al. (2004)	3C 434.1	5.2 ± 1.1
Kothes (2003)	G107.5-1.5	1.1 ± 0.4
Kothes et al. (2003)	CTB 87	6.1 ± 0.9

Table 5.1 A summary of recent studies that have determined distances to Galactic SNRs associated with spiral arms. The studies have used new distance-velocity relationships that incorporate non-circular motions due to spiral shocks in Galactic spiral arms - the models used were Foster & MacWilliams (2006) and Foster & Routledge (2003).

Dependence of SN 1181 Detection Success on Distance Our group decided to adopt the new distance to 3C 58 of 2 kpc by Kothes (2010) for our 11BC021 MegaCam observing strategy as this distance is based on a fitted line-of-sight model of the kinematics and shock HI distribution in the direction of the remnant as opposed to a blind assumption of circular motion. However, it is in our interest to compare the observing strategies for a 2 and 3.2 kpc distance, to see how large of an effect this difference would have on our search area. Figure 5.4 shows the difference between the two search areas. We have assumed the same z range that was used in our true observing strategy, which translates to the same *scattering angle* (θ) range - recall that z represents the distance in front of the SN and the *scattering angle* (θ) represents the angle between Earth and the scattering dust such that $\rho = z \tan \theta$ (ρ is the projected distance perpendicular to the line-of-sight). The two circles represent scattering dust locations $z = 100$ ly to $z = 2000$ ly in front of the SN which correspond to $\theta = 83^\circ$ and 45° respectively - these were the angles decided upon based on efficiency of dust

scattering and our previous experiences with finding SN LEs. For a distance of 2 kpc, the red circles in Figure 5.4 represent angular radii (γ) of 8.2 and 23.8 degrees on the sky. For a distance of 3.2 kpc, the yellow circles represent angular radii (γ) of 5.1 and 13.4 degrees on the sky. The 2 kpc observing strategy has a 1568.28 deg² area and the 3.2 kpc observing strategy has a 482.39 deg² area. The amount of area that *doesn't* overlap with our 2 kpc strategy is 129.53 deg². Overall, the difference in area is not substantial and we ended up covering a lot more sky using the 2 kpc distance. For future SN 1181 LE searches, it would be worthwhile to cover the portion of sky inwards of $z = 100$ assuming a 2 kpc distance (i.e. $z < 100$) - we would be covering: (1) more of the ideal dust scattering area *if* the distance is truly higher than 2 kpc and; (2) an area closer to the Galactic Plane (more dust for scattering to occur).

5.3 Age Reliability

The outlook is much more positive when it comes to age reliability. Fortunately, we are investigating the Milky Way's historical SNe - outbursts that have been witnessed by eye over the last 1000 years. Therefore, in addition to current observations of the SNR, we have age estimates that come from *guest star* observations in historical literature. Although most of the historical sightings now have strongly confirmed SNR connections, some are still disputed - particularly the SN 1181 - 3C 58 connection as will be discussed later in this chapter. Overall, an age estimate for a SNR can be obtained from the following lines of evidence:

- Connection to historical guest star.
- Multi-wavelength expansion studies of the SNR.
- X-ray observations of pulsar location (if a pulsar has been observed in the SNR).
- PWN evolution and energy (if the SNR has been characterized as a PWN).
- Pulsar spin-down age (if a pulsar has been observed in the SNR).

In this section, I will explore how much weight should be assigned to the above processes and the reliability of age estimates for both the Crab Nebula and 3C 58.

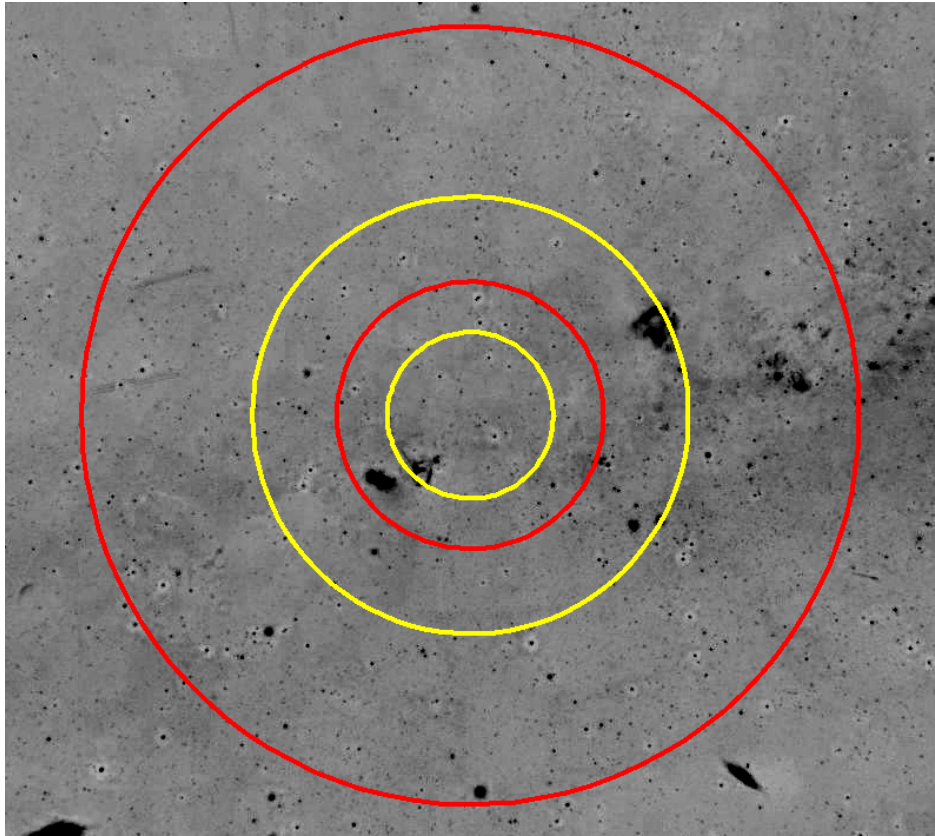


Figure 5.4 Comparing the observing strategy used for our SN 1181 LE MegaCam survey, which assumed a 2 kpc distance, to the area covered if we had assumed 3.2 kpc. Red and yellow circles represent 2 and 3.2 kpc distances to the outburst, respectively. The inner red and outer red circles represent angular radii (γ) of 8.2 and 23.8 degrees on the sky, respectively. The inner yellow and outer yellow circles represent angular radii (γ) of 5.1 and 13.4 degrees on the sky, respectively. North is up and east is left. The two circles for each distance correspond to scattering dust locations 100 ly and 2000 ly in front of the SN. The position of 3C 58 is located at the centre of the concentric circles.

5.3.1 The Age of the Crab SN

Although it is agreed upon within the community that the SN 1054-Crab Nebula connection is quite certain, I will review the most significant age estimates in the literature determined from observations of the Crab Nebula.

Expansion Age of the Crab Since Mayall & Oort (1942), it has been known that the expansion age of the Crab Nebula does not *quite* agree with the guest star of 1054 AD.

Studies of the nebula's expansion in the optical (Trimble, 1968; Wyckoff & Murray, 1977) and radio (Bietenholz et al., 1991) have reached a consensus on an age range of 1120 AD to 1233 AD - these ages are 60 to 180 years lower than the time since the 1054 AD outburst. The observations indicate that the ejecta must be moving $\sim 100\text{-}300$ km/s faster in the current epoch than if the nebula were freely expanding. Therefore, if the connection with SN 1054 exists, the expansion rate must have been accelerated. Trimble & Woltjer (1971) theorized that the acceleration is a result of pressure on the ejecta due to the confined synchrotron nebula associated with the Crab's pulsar.

The Crab Pulsar and the Concept of Spin-Down Age The Crab has been our archetypical pulsar wind nebula for four decades now. It is rather interesting that it remains the prototype, even though its spectral and physical properties are rather unique when compared to our growing list of known plerions. The Crab's pulsar (PSR J0534+220) is one of the most energetic pulsars known - it has a spin down power of $\dot{E} = 4.6 \times 10^{38}$ erg s^{-1} (assuming a distance of 2 kpc). When the period of a pulsar is measured over time, it is found to be increasing - usually this is occurring at a very consistent rate (Lorimer & Kramer, 2004). The slowing of its rotation is thought to be attributed to the braking caused by the pulsar's magnetic field. Observations of its spin-down rate can be used to determine a distance-independent *age* estimate for the pulsar - this is deemed the *spin-down age* of the pulsar. The pulsar age is given by:

$$\tau = \frac{P}{(n-1)\dot{P}} \left[1 - \left(\frac{P_0}{P} \right)^{n-1} \right] \quad (5.1)$$

Where P_0 is the initial period and n is the braking index. The braking index measures the efficiency of braking and is usually assumed to be constant - it is a measure of the slope of the curve where the rotation speed of a pulsar is plotted as a function of time. A braking index of $n = 3$ corresponds to a pulsar whose energy is purely radiated away via magnetic dipole radiation. Equation 5.1 above can be approximated to the *characteristic age*, $\tau_c = P/(2\dot{P})$ (Lorimer & Kramer, 2004). This characteristic age equation assumes: (1) that the pulsar's initial spin period was much shorter than that observed today ($P_0 \ll P$) and; (2) that the

spin-down is due to magnetic dipole radiation (i.e. braking index $n = 3$). The Crab pulsar’s characteristic age (from its rotation period of 33 ms and derivative $\dot{P} = 4.21 \times 10^{-13}$) yields an age of 1240 yr - this age is certainly comparable to the observed age of 958 years but not exact (Lorimer & Kramer, 2004). However, discrepancies in many other cases have been much larger (Gaensler & Frail, 2000; Kaspi et al., 2001; Murray et al., 2002; Kramer et al., 2003). Therefore, evidence has been growing that characteristic ages are a very inaccurate measure of a pulsar’s true age due to the assumption of negligible initial spin period. If the true age of a pulsar is known independently (i.e. a guest star observation), the birth period can be estimated assuming that the braking index $n = 3$. In 1993, the birth period of the Crab pulsar was estimated to be $P_0 = 19$ ms (Lyne et al., 1993). Unfortunately, this *unusually* small initial period set the framework for the $P_0 \ll P$ assumption which was used over the next decade to determine characteristic ages of pulsars. Recent estimates suggest a wide variety of initial spin periods from 14 ms to 140 ms (Migliazzo et al., 2002; Kramer et al., 2003), indicating that SNR ages obtained from pulsar characteristic ages should be interpreted with great care.

5.3.2 The Age of 3C 58

Although most of the 5 historical SNe have been confidently assigned known Galactic SNRs, there is still debate surrounding SN 1181 and its proposed remnant 3C 58. The following Table 5.2 has been adapted from Table 3 in Fesen et al. (2008) - it is a summary over the last decade of age estimates for the remnant 3C 58 based on a wide variety of observations and arguments. Table 5.2 highlights the current controversy surrounding the progenitor explosion of 3C 58 and whether the outburst was in fact, much older than ~ 831 yr.

Kothes(2010) & the Age of 3C 58 Recently, a new 2 kpc distance to 3C 58 was proposed by Kothes (2010) (see Section 5.2.2). The new distance dramatically alters many of 3C 58’s characteristics described in Table 5.2 as many of the observations are distance dependent and have assumed the Roberts et al. (1993) distance of 3.2 kpc. Kothes (2010) argued that the new 2 kpc distance *lowers* the age estimates determined the PWN evolution and energy. These arguments and others supporting a much younger age for 3C 58 (closer to a SN 1181 connection) will be discussed below.

Observation/Argument/Method	Age (yr)	Reference
Connection to historical SN 1181	831	Stephenson & Green (2002)
PWN evolution	~ 2400	Chevalier (2004, 2005)
PWN energy	~ 2500	Chevalier (2004, 2005)
Optical knot radial velocities	~ 3000	Fesen et al. (2008)
Optical knot proper motions	~ 3500	Fesen et al. (2008)
Pulsar location in thermal X-ray shell	~ 3700	Gotthelf et al. (2007)
Neutron star cooling models	≥ 5000	Slane et al. (2002)
Pulsar spin-down age	~ 5380	Murray et al. (2002)
Synchrotron expansion (radio)	~ 7000	Bietenholz (2006)
New 2 kpc distance measurement	~ 1000	Kothes (2010)

Table 5.2 A summary of age estimates for 3C 58 based on various observed properties and arguments over the past ~ 10 years. Most of the observed characteristics are dependent on distance and have assumed a distance of 3.2 kpc to 3C 58 with the exception of Kothes (2010).

- Expansion Studies: Kothes (2010) weakens the case for a large age from optical expansion studies of 3C 58 by discussing the likelihood of deceleration/acceleration of material in SNRs. He argued that, because a SN is a one-time event, the features associated with the explosion can typically be decelerated but not accelerated. The one exception to this would be the synchrotron emitting filaments (radio structures), which potentially could have been accelerated by the PWN (continuous source of energy). In the case of 3C 58, however, the radio structures show significant deceleration (~ 7000 yr) (Bietenholz, 2006) when compared to the optical filaments (~ 3500 yr) (Fesen et al., 2008). Therefore, Kothes (2010) argued that the appropriate material to consider when it comes to age are the *fastest* optical filaments. Fesen et al. (2008) assumes the *average* expansion velocity of the individually observed optical filaments to determine the age quoted in Table 5.2. Overall, insignificant deceleration cannot be assumed when interpreting the expansion of 3C 58.
- PWN Evolution: The PWN swept up mass can be determined: (1) theoretically using $M_{sw} = \dot{E}R^{-2}t^3$ where \dot{E} is the rotational energy loss rate of the pulsar (Chevalier,

2004) and; (2) observationally using X-rays (Bocchino et al., 2001). *Both* of these estimates are dependent on distance. For 3C 58 (assuming a distance of 3.2 kpc and age of 831 yr), Chevalier (2004) theoretically determines the swept-up mass to be $M_{sw} = 0.005M_{\odot}$. However, this does not agree with the $M_{sw} = 0.1M_{\odot}$ that Bocchino et al. (2001) determined using X-ray observations (assuming a 3.2 kpc distance). In order to match theory with observations, the PWN has to be about $t \approx 2400$ yr (see Table 5.2). Changing the distance assumption to 2 kpc in both cases, one obtains an observationally determined $M_{sw} = 0.03M_{\odot}$ and a theoretically determined $M_{sw} = 0.013M_{\odot}$ (assuming $t \approx 831$ yr) - these values are in much closer agreement. To get complete agreement, the age must be 1100 yr or the distance must be 1.7 kpc (Kothes, 2010). Overall, the lower distance reduces the age of the PWN in terms of its evolution.

- **PWN Energy:** For 3C 58, the total theoretical energy released from the pulsar into the nebula was estimated to be $\dot{E}t = 0.7 \times 10^{48}$ erg - this value is distance *independent* and assumes an age of ~ 831 yr. The minimum energy required to produce the observed synchrotron nebula was measured to be 10^{48} erg (Chevalier, 2004) - this value is distance dependent (relies on radio luminosity observations) and assumes 3.2 kpc. In this case, theory (assuming the SN 1181 connection) and observations simply do not agree. For a distance of 2 kpc, however, the minimum energy required to produce the observed synchrotron nebula drops to $\dot{E}t = 0.4 \times 10^{48}$ erg - this value is now lower than the total energy released by the pulsar and therefore the 2 kpc distance estimate is favoured.
- **Pulsar Spin-Down Age:** The details for determining the characteristic age of a pulsar were described in the previous section during the discussion of the pulsar spin-down age for the Crab. The consensus was that, in many cases, the characteristic age equation cannot be trusted due to its inherent assumption that $P_0 \ll P$. Instead, growing evidence supports the idea that individual pulsar properties can be very diverse and can have a wide variety of initial spin periods and rates that do not necessarily follow the assumption $P_0 \ll P$. The characteristic age for the 3C 58 pulsar (PSR J0205+6449) was determined to be 5.38×10^3 yr by Murray et al. (2002) (see Table 5.2) - this value was determined from its rotation period of 65.68 ms and derivative $\dot{P} = 1.931 \times 10^{-13}$ s s^{-1} . Murray et al. (2002) concluded that if the historical age for the pulsar is correct,

then the initial spin period for this neutron star cannot be neglected. The initial spin rate was then calculated to be 60.57 ms using the original Equation 5.1 and $\tau = 831$ yrs (still assumed braking index $n = 3$). This initial spin rate is actually slower than the current spin rate of the Crab! Therefore, if the historical age is correct, the 3C 58 pulsar hasn't slowed much since birth and its luminosity has always been low in contrast to the Crab pulsar. Whether or not this is the correct interpretation is debatable and hopefully advances in pulsar observations and theory will shed more light in the future. However, for now it is important to recognize both the growing diversity of observed pulsar characteristics including the uniqueness of our "prototype" pulsar, the Crab.

5.4 Type

Core-collapse SNe are generally not as luminous as thermonuclear SNe. A non-detection of LEs from a CCSNe could be attributed to an unfortunate case where the intrinsic luminosity of the SN outburst was simply not bright enough for us to observe the accompanying LEs. In order to compare our LE detections with our non-detections, the *type* of SN *must* be considered. We have detected LEs from Tycho's SN (a confirmed SN Ia; Krause et al. (2008b)) and the Cas A SN (a CCSNe with a confirmed Type IIb sub-classification; Krause et al. (2008a); Rest et al. (2011b)). As was described in the introduction, the average absolute peak magnitude of SNe Ia have been well-constrained to the value $M_B \approx M_V \approx -19.30 \pm 0.03$. The distribution of CCSN luminosities, however, show much more diversity. There have been a few studies that have attempted to obtain average absolute magnitude distributions for the other types of SNe (SNe Ib, Ic, II-L, and IIc) - see Table 5.3 for a summary of the most recent investigations.

The most recent study in the literature that incorporates all SN types is Li et al. (2011b), who determines the observed luminosity functions (LF) and fractions in a complete local sample of SNe from the Lick Observatory Supernova Search (LOSS). They select a volume-limited sample of 175 SNe with a cut-off distance of 80 Mpc for SNe Ia and 60 Mpc for the CCSNe. Since our knowledge of SNe Ia absolute magnitudes is already well-constrained, we

Study	Type of CCSN Investigated
Richardson et al. (2002)	Ibc, II-L, II-P, IIn
Richardson et al. (2006)	Ibc, IIb
Drout et al. (2011)	Ibc, Ic-BL
Li et al. (2011b)	Ibc, II-P, II-L, IIb, IIn
Kiewe et al. (2012)	IIn

Table 5.3 A summary of recent studies that have surveyed CCSNe and determined average absolute peak magnitudes of core-collapse sub-types.

will focus only on their results for core-collapse types of SNe. Li et al. (2011b) collected photometry for every object and fit them with a family of light curves to constrain the sub-type, peak magnitude, and light curve shape for each object. Their results are summarized in Table 5.4.

Type of CCSNe	\overline{M}_B	σ_{SDOM}
Type Ic	-16.04	0.31
Type Ib	-17.01	0.17
Type II-P	-15.66	0.16
Type II-L	-17.44	0.22
Type IIb	-16.65	0.40
Type IIn	-16.86	0.59

Table 5.4 The average absolute magnitudes of CCSNe from Li et al. (2011b). σ_{SDOM} represents the standard deviation of the mean.

5.5 Expected Brightness

The older age of a SN could play a factor in a non-detection due to geometric dilution. Flux density is inversely proportional to the square of the distance from the source. As the outburst ages, the size of the LE ellipsoid grows resulting in fainter light echoes. Our searches for light echoes have been successful for both Tycho’s Supernova (440 years old) and

Cas A (~ 300 years old). SN 1181 (830 years old) and the Crab SN (958 years old) are both older outbursts. The distance to the outburst has a similar effect. The larger the distance, the greater the major axis of the ellipsoid. In this section, I include these factors as well as those summarized in the previous sections to calculate an expected surface brightness (SB) for Crab and 1181 LEs. A rough estimate of the flux for a LE is described by

$$F_{LE} \propto \left(\frac{1}{distance^2} \right) \left(\frac{1}{age^2} \right) L_{outburst} \quad (5.2)$$

In order to estimate the flux of 1181 and Crab LEs, I can scale with the Tycho SN - a historical SN for which we have discovered LEs. Tycho is a better anchor for scaling than Cas A since there is far less uncertainty associated with both its age (Cas A has an age inferred only from SNR observations - no historical records exist) and peak absolute magnitude (SNe IIb have much more scatter in peak absolute magnitude when compared with SNe Ia). At this point, I assume no difference in reddening in the direction of the 3 events. This is a reasonable assumption for SN 1181, as both remnants reside in the same part of the sky. The age, distance and peak absolute magnitude (assuming a SN Ia) for the Tycho SN event as well as the surface brightness of our brightest Tycho LE are summarized in Table 5.5. For both the Crab SN and SN 1181, I have estimated the surface brightness of a potential LE and its associated uncertainty assuming various scenarios that include all possible values in terms of peak absolute magnitude, distance, and age that have been described throughout the last few sections of this chapter. The cases include:

- For both the Crab SN and SN 1181, I estimate a LE SB given four different peak absolute magnitudes corresponding with four different subtypes of CCSNe: Type Ibc, Type II-L, Type II-P, Type IIc, and Type IIb (Section 5.4).
- For the SN 1181 event, I estimate a LE SB given both the 2 kpc and 3.2 kpc distance to the outburst (Section 5.2.2)
- For comparison purposes, I also estimate the LE SB assuming that the radio source 3C 58 and SN 1181 *do not* have a connection. Recalling Section 5.3.2, there have been several observational studies of 3C 58 that indicate it is likely a remnant of a considerably older SN event with an average age of ~ 4000 yr. Therefore, if this is the

case, we are dealing with a different, older core-collapse event at the same location in the sky.

The results are summarized in Table 5.6, Table 5.7, and Table 5.8.

Tycho SN and LE Properties	
Brightest LE SB ($mag/arcsec^2$)	21
Peak M_B for SNe Ia	-19.30 ± 0.03
Distance (kpc) to SNR	2.5-3.0
Age of SN (yrs)	440

Table 5.5 Tycho SN and LE Properties

Estimated Surface Brightness ($mag/arcsec^2$) for SN 1181 LE ($Age = 831yrs$)		
	For $D = 2.0$ kpc	For $D = 3.2$ kpc
Type Ib	25.0 ± 0.8	26.0 ± 0.7
Type Ic	24.0 ± 0.7	25.0 ± 0.6
Type II-L	23.6 ± 0.7	25 ± 2
Type II-P	25.3 ± 0.7	26 ± 2
Type IIb	24.3 ± 0.8	25 ± 2
Type IIIn	24.1 ± 0.9	25 ± 2

Table 5.6 Surface brightness estimates for a SN 1181 LE in MegaCam using scaling arguments with Tycho’s SN. I have estimated the SB for various peak absolute magnitudes of CCSNe based on Li et al. (2011b). I have also estimated the SB using both distance measurements to the radio source 3C 58 currently being disputed in the field (2 kpc vs. 3.2 kpc).

Estimated Surface Brightness ($mag/arcsec^2$) for 3C 58 SN LE assuming $Age = 4000yrs$		
	For $D = 2.0$ kpc	For $D = 3.2$ kpc
Type Ib	28.4 ± 0.8	29.4 ± 0.7
Type Ic	27.4 ± 0.7	28.4 ± 0.6
Type II-L	27.0 ± 0.7	28 ± 2
Type II-P	28.7 ± 0.7	30 ± 2
Type IIb	27.8 ± 0.8	29 ± 2
Type IIc	27.5 ± 0.9	29 ± 2

Table 5.7 Surface brightness estimates using the same process as Table 5.6, but this time I assume the SN that created 3C 58 *was not* SN 1181, but a much older event (4000 years old).

Estimated Surface Brightness ($mag/arcsec^2$) for Crab SN LE ($Age = 958yrs$)	
	For $D = 2.0$ kpc
Type Ib	25.3 ± 0.7
Type Ic	24.3 ± 0.6
Type II-L	23.9 ± 0.6
Type II-P	25.6 ± 0.6
Type IIb	24.7 ± 0.8
Type IIc	24.4 ± 0.8

Table 5.8 Surface brightness estimates for a Crab SN LE in MegaCam using scaling arguments with Tycho's SN. I have estimated the SB for various peak absolute magnitudes of CCSNe based on Li et al. (2011b).

CHAPTER 6

DISCUSSION AND CONCLUSIONS

6.1 Light Echo Visibility in our Survey

A source's distance, age, and luminosity are all factors that must be considered with the non-detection. We did discover 20 additional bright light echo complexes from Tycho and Cas A using the data from the SN 1181 search due to the proximity of all three of these historical SNe on the sky. In Section 5.5, I have estimated the surface brightness we should expect for a Crab LE and 3C 58 LE given various scenarios involving distance, age and luminosity of the SN event. In this section, I compare these surface brightnesses to our surface brightness detection limit in MegaCam data - should I have been able to find these LEs against the background noise of our difference images? In order to bring this into context, we adopt a *detection limit* in our MegaCam difference images. For our detection limit I use the *faintest* LE found in our searching during this project - this happens to be a Tycho LE found in the SN 1181 MegaCam data. This Tycho LE had a surface brightness of 24.1 mag arcsec² (r-band) in this data. From Table 5.6, Table 5.7, and Table 5.8 in the previous chapter, I calculated the number of standard deviations by which each predicted SB estimation differs from our detection limit given their uncertainties. The probability of LE detection for each SB scenario has therefore been determined. The probabilities are summarized in Table 6.1, Table 6.2, and Table 6.3. I adopt an acceptance boundary of 65%, a value above which I would have a reasonable probability of LE detection in MegaCam.

Percentage of SN 1181 LE Detection in MegaCam		
(Age = 831yrs)		
	For $D = 2.0$ kpc	For $D = 3.2$ kpc
Type Ib	13%	0.2%
Type Ic	57%	7%
Type II-L	78%	38%
Type II-P	4%	7%
Type IIb	38%	24%
Type IIc	49%	31%

Table 6.1 The probability of LE detection for the SN 1181 - each SB scenario is considered in terms of distance and type of outburst.

Percentage of 3C 58 SN LE Detection in MegaCam		
assuming Age ~ 4000yrs		
	For $D = 2.0$ kpc	For $D = 3.2$ kpc
Type Ib	0%	0%
Type Ic	0%	0%
Type II-L	0.003%	1%
Type II-P	0%	0.003%
Type IIb	0%	0.5%
Type IIc	0.003%	2%

Table 6.2 The probability of LE detection for the SN that created 3C 58 - here I assume a SN age of ~ 4000 yr. Each SB scenario is considered in terms of distance and type of outburst.

Percentage of Crab SN LE Detection in MegaCam	
	For $D = 2.0$ kpc
Type Ib	4%
Type Ic	38%
Type II-L	65%
Type II-P	1%
Type IIb	34%
Type IIn	26%

Table 6.3 The probability of LE detection for the SN 1054 (the Crab) - each SB scenario is considered in terms type of outburst.

From the above tables, it is clear that there is only one scenario for each outburst in which a reasonable probability of LE detection exists: (1) for SN 1181, the original outburst had to have been a Type II-L at a distance of 2 kpc for LEs to have been noticeable in our MegaCam data and; (2) for the Crab, the original outburst had to also have been a Type II-L at a distance of 2 kpc for LEs to have been noticeable in our MegaCam data. For the scenario in which a 4000 year old SN created radio source 3C 58 (not SN 1181), there was no reasonable probability of LE detection from our data. From the results above and our non-detections, I can constrain that it is unlikely that either event was a Type II-L SN but cannot provide constraints on other sub-types. For future observations, it would be beneficial to probe lower surface brightness LEs using longer exposure times - even if we fail to detect LEs in these cases, we can provide additional constraints on the specific SN sub-types using this non-detection analysis.

6.2 Conclusions

The results of this thesis can be summarized as follows:

1. We have obtained a *wealth* of data from CFHT MegaCam in the search for SN LEs from the historical Crab SN and SN 1181. Unfortunately, *no* LEs from these outbursts were discovered. The data could be beneficial for exploring future secondary science considerations. Overall, we have yet to discover LEs from the Crab and 1181 SNe using other instruments as well (i.e. KPNO 4m MOSAIC-1.1).
2. For SN 1181 LEs to have a reasonable probability of detection in MegaCam data, the SN would have had to have been a Type II-L outburst, located at a distance of 2 kpc from Earth.
3. If SN 1181 is not associated with the radio source 3C 58 and 3C 58 is the remnant of a considerably older SN event (~ 4000 yrs old), its LEs would not be detectable in MegaCam data.
4. For Crab SN LEs to have a reasonable probability of detection in MegaCam data, the SN would have had to have been a Type II-L outburst, located at a distance of 2 kpc from Earth.
5. Overall, given the respective distances, ages and possible intrinsic luminosities of the Crab SN and SN 1181, their LEs would likely have been *too faint* to detect in our MegaCam data with the exposure times we used. It is important to note that LEs fainter than $24.0 \text{ mag/arcsec}^2$ would not produce useful LE spectra, which is why we chose the exposures we did in the first place. However, it *would* be worthwhile in future searches at CFHT to increase exposures times to >200 s for the following reasons: (1) using imaging of LEs alone (i.e. no spectroscopic analysis), one can obtain the original light curve of the outburst if conditions are favourable (the dust width is sufficiently thin $\sigma_d = 0.008$ ly and the PSF FWHM is small) - the light curve shape depends on SN sub-type and would be able to provide constraints on the classification; (2) discovering and imaging LEs alone from SN 1181 (i.e. no spectroscopic analysis) still has scientific potential as you can pinpoint the original outburst location and

solve the on-going debate as to whether 3C 58 has any association; (3) another *non-detection* in future observations that probed lower surface brightnesses would provide additional constraints on the possible SN sub-types using the non-detection analysis in Chapter 6.1.

6. We found a statistically-significant correlation between CO brightness temperature and the presence of scattering dust by examining known light echo locations for Tycho and Cas A. However, the spacing of grid points in existing CO surveys is too sparse to be useful even a few degrees away from the galactic plane. We have yet to identify a search strategy based on survey data which is superior than random field placement.
7. If *lack* of scattering dust is the issue behind our non-detections, it would be worthwhile to search the SN 1181 region in which $z < 100$ assuming a distance of 2 kpc - this is an area on the Galactic plane (more dust) that we have yet to observe using CFHT MegaCam.

Appendices

APPENDIX A

CFHT MEGACAM PROGRAM 11AC033 OBSERVED FIELDS

Band	Field ID	RA	Dec
Band A			
	CFHTcrab2413	05:30:28.26	+10:00:52.1
	CFHTcrab2513	05:34:31.97	+10:00:52.1
	CFHTcrab2713	05:42:39.40	+10:00:52.1
	CFHTcrab2813	05:46:43.11	+10:00:52.1
	CFHTcrab2913	05:50:46.83	+10:00:52.1
	CFHTcrab1914	05:10:04.95	+11:00:52.1
	CFHTcrab2414	05:30:27.47	+11:00:52.1
	CFHTcrab3014	05:54:54.49	+11:00:52.1
	CFHTcrab2115	05:18:10.47	+12:00:52.1
	CFHTcrab2315	05:26:21.22	+12:00:52.1
	CFHTcrab2615	05:38:37.35	+12:00:52.1
	CFHTcrab2815	05:46:48.10	+12:00:52.1
	CFHTcrab3115	05:59:04.22	+12:00:52.1
	CFHTcrab3215	06:03:09.60	+12:00:52.1
	CFHTcrab3315	06:07:14.97	+12:00:52.1
	CFHTcrab1616	04:57:35.03	+13:00:52.1

CFHTcrab1716	05:01:41.35	+13:00:52.1
CFHTcrab1816	05:05:47.68	+13:00:52.1
CFHTcrab1916	05:09:54.01	+13:00:52.1
CFHTcrab2016	05:14:00.34	+13:00:52.1
CFHTcrab2116	05:18:06.66	+13:00:52.1
CFHTcrab2216	05:22:12.99	+13:00:52.1
CFHTcrab2316	05:26:19.32	+13:00:52.1
CFHTcrab2416	05:30:25.65	+13:00:52.1
CFHTcrab2516	05:34:31.97	+13:00:52.1
CFHTcrab2716	05:42:44.63	+13:00:52.1
CFHTcrab2916	05:50:57.28	+13:00:52.1
CFHTcrab3016	05:55:03.61	+13:00:52.1
CFHTcrab3316	06:07:22.59	+13:00:52.1
CFHTcrab1517	04:53:18.34	+14:00:52.1
CFHTcrab1617	04:57:25.71	+14:00:52.1
CFHTcrab2017	05:13:55.16	+14:00:52.1
CFHTcrab2217	05:22:09.88	+14:00:52.1
CFHTcrab2317	05:26:17.25	+14:00:52.1
CFHTcrab2517	05:34:31.97	+14:00:52.1
CFHTcrab2717	05:42:46.70	+14:00:52.1
CFHTcrab2817	05:46:54.06	+14:00:52.1
CFHTcrab3017	05:55:08.79	+14:00:52.1
CFHTcrab3117	05:59:16.15	+14:00:52.1
CFHTcrab3217	06:03:23.51	+14:00:52.1
CFHTcrab3317	06:07:30.88	+14:00:52.1
CFHTcrab3417	06:11:38.24	+14:00:52.1
CFHTcrab3517	06:15:45.60	+14:00:52.1
CFHTcrab1818	05:05:32.59	+15:00:52.1
CFHTcrab2018	05:13:49.56	+15:00:52.1
CFHTcrab2118	05:17:58.04	+15:00:52.1
CFHTcrab2818	05:46:57.42	+15:00:52.1

CFHTcrab3118	05:59:22.87	+15:00:52.1
CFHTcrab3218	06:03:31.35	+15:00:52.1
CFHTcrab3518	06:15:56.80	+15:00:52.1
CFHTcrab1419	04:48:45.38	+16:00:52.1
CFHTcrab1619	04:57:04.76	+16:00:52.1
CFHTcrab1719	05:01:14.45	+16:00:52.1
CFHTcrab3019	05:55:20.42	+16:00:52.1
CFHTcrab3219	06:03:39.80	+16:00:52.1
CFHTcrab3319	06:07:49.49	+16:00:52.1
CFHTcrab3419	06:11:59.18	+16:00:52.1
CFHTcrab1320	04:44:20.15	+17:00:52.1
CFHTcrab1420	04:48:31.13	+17:00:52.1
CFHTcrab1720	05:01:04.09	+17:00:52.1
CFHTcrab3220	06:03:48.87	+17:00:52.1
CFHTcrab3320	06:07:59.86	+17:00:52.1
CFHTcrab3620	06:20:32.81	+17:00:52.1
CFHTcrab3720	06:24:43.80	+17:00:52.1
CFHTcrab1321	04:44:03.51	+18:00:52.1
CFHTcrab1421	04:48:15.88	+18:00:52.1
CFHTcrab1521	04:52:28.26	+18:00:52.1
CFHTcrab3221	06:03:58.57	+18:00:52.1
CFHTcrab3621	06:20:48.06	+18:00:52.1
CFHTcrab3721	06:25:00.43	+18:00:52.1
CFHTcrab1322	04:43:45.76	+19:00:52.1
CFHTcrab1522	04:52:13.46	+19:00:52.1
CFHTcrab3222	06:04:08.93	+19:00:52.1
CFHTcrab3522	06:16:50.48	+19:00:52.1
CFHTcrab3622	06:21:04.33	+19:00:52.1
CFHTcrab1423	04:47:42.29	+20:00:52.1
CFHTcrab1623	04:56:13.14	+20:00:52.1
CFHTcrab1723	05:00:28.56	+20:00:52.1

CFHTcrab3423	06:12:50.81	+20:00:52.1
CFHTcrab1424	04:47:23.88	+21:00:52.1
CFHTcrab1624	04:55:58.08	+21:00:52.1
CFHTcrab3324	06:08:48.77	+21:00:52.1
CFHTcrab3424	06:13:05.87	+21:00:52.1
CFHTcrab3524	06:17:22.97	+21:00:52.1
CFHTcrab3724	06:25:57.17	+21:00:52.1
CFHTcrab1325	04:42:45.48	+22:00:52.1
CFHTcrab1425	04:47:04.35	+22:00:52.1
CFHTcrab1725	05:00:00.98	+22:00:52.1
CFHTcrab3425	06:13:21.85	+22:00:52.1
CFHTcrab3725	06:26:18.47	+22:00:52.1
CFHTcrab1326	04:42:22.92	+23:00:52.1
CFHTcrab1426	04:46:43.67	+23:00:52.1
CFHTcrab3326	06:09:18.01	+23:00:52.1
CFHTcrab3626	06:22:20.27	+23:00:52.1
CFHTcrab1627	04:55:07.29	+24:00:52.1
CFHTcrab3327	06:09:33.91	+24:00:52.1
CFHTcrab3627	06:22:42.14	+24:00:52.1
CFHTcrab1628	04:54:48.40	+25:00:52.1
CFHTcrab3228	06:05:25.87	+25:00:52.1
CFHTcrab3528	06:18:40.39	+25:00:52.1
CFHTcrab3628	06:23:05.23	+25:00:52.1
CFHTcrab3728	06:27:30.08	+25:00:52.1
CFHTcrab1429	04:45:34.34	+26:00:52.1
CFHTcrab1629	04:54:28.46	+26:00:52.1
CFHTcrab3329	06:10:08.43	+26:00:52.1
CFHTcrab3529	06:19:02.55	+26:00:52.1
CFHTcrab3629	06:23:29.60	+26:00:52.1
CFHTcrab1430	04:45:08.65	+27:00:52.1
CFHTcrab1530	04:49:38.04	+27:00:52.1

CFHTcrab1930	05:07:35.62	+27:00:52.1
CFHTcrab3530	06:19:25.90	+27:00:52.1
CFHTcrab1431	04:44:41.59	+28:00:52.1
CFHTcrab1531	04:49:13.44	+28:00:52.1
CFHTcrab1931	05:07:20.85	+28:00:52.1
CFHTcrab2031	05:11:52.71	+28:00:52.1
CFHTcrab3031	05:57:11.24	+28:00:52.1
CFHTcrab3231	06:06:14.95	+28:00:52.1
CFHTcrab3631	06:24:22.36	+28:00:52.1
CFHTcrab1532	04:48:47.54	+29:00:52.1
CFHTcrab1732	04:57:56.43	+29:00:52.1
CFHTcrab1832	05:02:30.87	+29:00:52.1
CFHTcrab2132	05:16:14.20	+29:00:52.1
CFHTcrab2232	05:20:48.64	+29:00:52.1
CFHTcrab3032	05:57:24.19	+29:00:52.1
CFHTcrab3132	06:01:58.63	+29:00:52.1
CFHTcrab3532	06:20:16.41	+29:00:52.1
CFHTcrab2133	05:16:03.30	+30:00:52.1
CFHTcrab2233	05:20:40.47	+30:00:52.1
CFHTcrab2333	05:25:17.64	+30:00:52.1
CFHTcrab2433	05:29:54.80	+30:00:52.1
CFHTcrab2533	05:34:31.97	+30:00:52.1
CFHTcrab3433	06:16:06.49	+30:00:52.1
CFHTcrab2034	05:11:11.80	+31:00:52.1
CFHTcrab2134	05:15:51.84	+31:00:52.1
CFHTcrab2234	05:20:31.87	+31:00:52.1
CFHTcrab2434	05:29:51.94	+31:00:52.1
CFHTcrab2534	05:34:31.97	+31:00:52.1
CFHTcrab2035	05:10:56.74	+32:00:52.1
CFHTcrab2135	05:15:39.78	+32:00:52.1
CFHTcrab2235	05:20:22.83	+32:00:52.1

CFHTcrab2435	05:29:48.93	+32:00:52.1
CFHTcrab2835	05:48:41.12	+32:00:52.1
CFHTcrab2935	05:53:24.16	+32:00:52.1
CFHTcrab3035	05:58:07.21	+32:00:52.1
CFHTcrab2436	05:29:45.76	+33:00:52.1
CFHTcrab2636	05:39:18.19	+33:00:52.1
CFHTcrab2936	05:53:36.83	+33:00:52.1
CFHTcrab3136	06:03:09.26	+33:00:52.1
CFHTcrab2237	05:20:03.35	+34:00:52.1
CFHTcrab2637	05:39:21.51	+34:00:52.1

Band B

CFHTcrab2803	05:46:31.97	+00:00:52.1
CFHTcrab3503	06:14:31.97	+00:00:52.1
CFHTcrab2604	05:38:32.01	+01:00:52.1
CFHTcrab3904	06:30:32.50	+01:00:52.1
CFHTcrab2305	05:26:31.68	+02:00:52.1
CFHTcrab3005	05:54:32.72	+02:00:52.1
CFHTcrab2006	05:14:30.31	+03:00:52.1
CFHTcrab2306	05:26:31.31	+03:00:52.1
CFHTcrab2706	05:42:32.64	+03:00:52.1
CFHTcrab2906	05:50:33.30	+03:00:52.1
CFHTcrab0607	04:18:20.76	+04:00:52.1
CFHTcrab1707	05:02:27.25	+04:00:52.1
CFHTcrab2207	05:22:30.20	+04:00:52.1
CFHTcrab3407	06:10:37.29	+04:00:52.1
CFHTcrab1508	04:54:22.75	+05:00:52.1
CFHTcrab2308	05:26:30.13	+05:00:52.1
CFHTcrab2508	05:34:31.97	+05:00:52.1
CFHTcrab3708	06:22:43.04	+05:00:52.1
CFHTcrab4408	06:50:49.49	+05:00:52.1

CFHTcrab1809	05:06:22.67	+06:00:52.1
CFHTcrab2109	05:18:26.66	+06:00:52.1
CFHTcrab2909	05:50:37.29	+06:00:52.1
CFHTcrab3509	06:14:45.26	+06:00:52.1
CFHTcrab3709	06:22:47.91	+06:00:52.1
CFHTcrab1110	04:38:06.63	+07:00:52.1
CFHTcrab1310	04:46:10.25	+07:00:52.1
CFHTcrab3010	05:54:41.02	+07:00:52.1
CFHTcrab3410	06:10:48.26	+07:00:52.1
CFHTcrab3710	06:22:53.69	+07:00:52.1
CFHTcrab4510	06:55:08.17	+07:00:52.1
CFHTcrab1911	05:10:17.77	+08:00:52.1
CFHTcrab2011	05:14:20.14	+08:00:52.1
CFHTcrab3111	05:58:46.18	+08:00:52.1
CFHTcrab3611	06:18:58.01	+08:00:52.1
CFHTcrab3711	06:23:00.38	+08:00:52.1
CFHTcrab4311	06:47:14.58	+08:00:52.1
CFHTcrab4511	06:55:19.32	+08:00:52.1
CFHTcrab4611	06:59:21.68	+08:00:52.1
CFHTcrab1512	04:54:01.96	+09:00:52.1
CFHTcrab3312	06:06:55.98	+09:00:52.1
CFHTcrab3412	06:10:58.99	+09:00:52.1
CFHTcrab3512	06:15:01.99	+09:00:52.1
CFHTcrab3612	06:19:04.99	+09:00:52.1
CFHTcrab3712	06:23:07.99	+09:00:52.1
CFHTcrab4312	06:47:26.00	+09:00:52.1
CFHTcrab2013	05:14:13.41	+10:00:52.1
CFHTcrab4013	06:35:27.67	+10:00:52.1
CFHTcrab3414	06:11:12.51	+11:00:52.1
CFHTcrab1215	04:41:22.10	+12:00:52.1
CFHTcrab1415	04:49:32.85	+12:00:52.1

CFHTcrab3915	06:31:47.22	+12:00:52.1
CFHTcrab4015	06:35:52.60	+12:00:52.1
CFHTcrab4215	06:44:03.35	+12:00:52.1
CFHTcrab1316	04:45:16.04	+13:00:52.1
CFHTcrab3916	06:32:00.56	+13:00:52.1
CFHTcrab4216	06:44:19.54	+13:00:52.1
CFHTcrab4416	06:52:32.19	+13:00:52.1
CFHTcrab0517	04:12:04.72	+14:00:52.1
CFHTcrab0617	04:16:12.08	+14:00:52.1
CFHTcrab0717	04:20:19.44	+14:00:52.1
CFHTcrab1117	04:36:48.89	+14:00:52.1
CFHTcrab4117	06:40:29.78	+14:00:52.1
CFHTcrab4417	06:52:51.87	+14:00:52.1
CFHTcrab0518	04:11:42.31	+15:00:52.1
CFHTcrab3918	06:32:30.74	+15:00:52.1
CFHTcrab0719	04:19:37.55	+16:00:52.1
CFHTcrab4119	06:41:07.01	+16:00:52.1
CFHTcrab4219	06:45:16.70	+16:00:52.1
CFHTcrab4519	06:57:45.77	+16:00:52.1
CFHTcrab0620	04:15:03.25	+17:00:52.1
CFHTcrab0920	04:27:36.21	+17:00:52.1
CFHTcrab3920	06:33:05.77	+17:00:52.1
CFHTcrab4120	06:41:27.74	+17:00:52.1
CFHTcrab4220	06:45:38.72	+17:00:52.1
CFHTcrab4520	06:58:11.68	+17:00:52.1
CFHTcrab0521	04:10:24.54	+18:00:52.1
CFHTcrab3921	06:33:25.18	+18:00:52.1
CFHTcrab4121	06:41:49.92	+18:00:52.1
CFHTcrab4321	06:50:14.66	+18:00:52.1
CFHTcrab4421	06:54:27.03	+18:00:52.1
CFHTcrab4821	07:11:16.52	+18:00:52.1

CFHTcrab1022	04:31:04.21	+19:00:52.1
CFHTcrab3822	06:29:32.04	+19:00:52.1
CFHTcrab3922	06:33:45.89	+19:00:52.1
CFHTcrab4522	06:59:08.99	+19:00:52.1
CFHTcrab4622	07:03:22.84	+19:00:52.1
CFHTcrab0723	04:17:54.30	+20:00:52.1
CFHTcrab3823	06:29:52.51	+20:00:52.1
CFHTcrab4123	06:42:38.79	+20:00:52.1
CFHTcrab4323	06:51:09.64	+20:00:52.1
CFHTcrab4423	06:55:25.07	+20:00:52.1
CFHTcrab4623	07:03:55.92	+20:00:52.1
CFHTcrab1024	04:30:15.48	+21:00:52.1
CFHTcrab4324	06:51:39.77	+21:00:52.1
CFHTcrab4424	06:55:56.87	+21:00:52.1
CFHTcrab4524	07:00:13.97	+21:00:52.1
CFHTcrab0825	04:21:11.10	+22:00:52.1
CFHTcrab3925	06:34:56.22	+22:00:52.1
CFHTcrab4225	06:47:52.84	+22:00:52.1
CFHTcrab4325	06:52:11.72	+22:00:52.1
CFHTcrab1226	04:38:02.17	+23:00:52.1
CFHTcrab3826	06:31:01.78	+23:00:52.1
CFHTcrab3926	06:35:22.54	+23:00:52.1
CFHTcrab4026	06:39:43.29	+23:00:52.1
CFHTcrab4226	06:48:24.80	+23:00:52.1
CFHTcrab4426	06:57:06.31	+23:00:52.1
CFHTcrab4526	07:01:27.06	+23:00:52.1
CFHTcrab4726	07:10:08.57	+23:00:52.1
CFHTcrab0127	03:49:26.16	+24:00:52.1
CFHTcrab4427	06:57:44.08	+24:00:52.1
CFHTcrab4527	07:02:06.82	+24:00:52.1
CFHTcrab4428	06:58:23.97	+25:00:52.1

CFHTcrab0529	04:05:30.83	+26:00:52.1
CFHTcrab4029	06:41:17.83	+26:00:52.1
CFHTcrab4329	06:54:39.01	+26:00:52.1
CFHTcrab4529	07:03:33.12	+26:00:52.1
CFHTcrab1230	04:36:09.86	+27:00:52.1
CFHTcrab3830	06:32:54.08	+27:00:52.1
CFHTcrab4130	06:46:22.26	+27:00:52.1
CFHTcrab4230	06:50:51.65	+27:00:52.1
CFHTcrab4530	07:04:19.83	+27:00:52.1
CFHTcrab4231	06:51:33.48	+28:00:52.1
CFHTcrab0732	04:12:11.99	+29:00:52.1
CFHTcrab3832	06:33:59.74	+29:00:52.1
CFHTcrab4232	06:52:17.51	+29:00:52.1
CFHTcrab3733	06:29:58.00	+30:00:52.1
CFHTcrab4133	06:48:26.67	+30:00:52.1
CFHTcrab4333	06:57:41.01	+30:00:52.1
CFHTcrab4433	07:02:18.18	+30:00:52.1
CFHTcrab0934	04:19:51.42	+31:00:52.1
CFHTcrab4334	06:58:32.59	+31:00:52.1
CFHTcrab4235	06:54:43.78	+32:00:52.1
CFHTcrab4735	07:18:19.02	+32:00:52.1
CFHTcrab1636	04:51:36.05	+33:00:52.1
CFHTcrab4236	06:55:37.61	+33:00:52.1
CFHTcrab0937	04:17:19.31	+34:00:52.1
CFHTcrab1537	04:46:16.56	+34:00:52.1
CFHTcrab3837	06:37:16.01	+34:00:52.1
CFHTcrab1238	04:31:02.48	+35:00:52.1
CFHTcrab1538	04:45:41.60	+35:00:52.1
CFHTcrab3738	06:33:08.43	+35:00:52.1
CFHTcrab3938	06:42:54.50	+35:00:52.1
CFHTcrab2839	05:49:22.11	+36:00:52.1

CFHTcrab3839	06:38:49.21	+36:00:52.1
CFHTcrab4439	07:08:29.48	+36:00:52.1
CFHTcrab0740	04:04:21.72	+37:00:52.1
CFHTcrab1240	04:29:24.57	+37:00:52.1
CFHTcrab2040	05:09:29.12	+37:00:52.1
CFHTcrab2340	05:24:30.83	+37:00:52.1
CFHTcrab2440	05:29:31.40	+37:00:52.1
CFHTcrab3240	06:09:35.96	+37:00:52.1
CFHTcrab3540	06:24:37.67	+37:00:52.1
CFHTcrab3740	06:34:38.81	+37:00:52.1
CFHTcrab4040	06:49:40.52	+37:00:52.1
CFHTcrab1841	04:58:59.60	+38:00:52.1
CFHTcrab1941	05:04:04.23	+38:00:52.1
CFHTcrab2241	05:19:18.10	+38:00:52.1
CFHTcrab2841	05:49:45.85	+38:00:52.1
CFHTcrab2941	05:54:50.47	+38:00:52.1
CFHTcrab3141	06:04:59.72	+38:00:52.1
CFHTcrab4141	06:55:45.96	+38:00:52.1
CFHTcrab1542	04:43:03.12	+39:00:52.1
CFHTcrab2042	05:08:47.55	+39:00:52.1
CFHTcrab2842	05:49:58.63	+39:00:52.1
CFHTcrab1743	04:52:45.06	+40:00:52.1
CFHTcrab2043	05:08:25.15	+40:00:52.1
CFHTcrab2643	05:39:45.34	+40:00:52.1
CFHTcrab2743	05:44:58.70	+40:00:52.1
CFHTcrab2843	05:50:12.07	+40:00:52.1
CFHTcrab3043	06:00:38.79	+40:00:52.1
CFHTcrab3243	06:11:05.52	+40:00:52.1
CFHTcrab3743	06:37:12.34	+40:00:52.1
CFHTcrab2544	05:34:31.97	+41:00:52.1
CFHTcrab3344	06:16:56.56	+41:00:52.1

CFHTcrab1945	05:02:13.82	+42:00:52.1
CFHTcrab2345	05:23:45.92	+42:00:52.1
CFHTcrab2445	05:29:08.95	+42:00:52.1
CFHTcrab2545	05:34:31.97	+42:00:52.1
CFHTcrab2845	05:50:41.05	+42:00:52.1
CFHTcrab1546	04:39:49.61	+43:00:52.1
CFHTcrab2246	05:18:07.27	+43:00:52.1
CFHTcrab3146	06:07:21.39	+43:00:52.1
CFHTcrab3347	06:19:01.74	+44:00:52.1
CFHTcrab3048	06:02:49.46	+45:00:52.1
CFHTcrab3148	06:08:28.95	+45:00:52.1

Extra Band A

CFHTcrab2613	05:38:35.69	+10:00:52.1
CFHTcrab2114	05:18:13.96	+11:00:52.1
CFHTcrab2614	05:38:36.48	+11:00:52.1
CFHTcrab2714	05:42:40.98	+11:00:52.1
CFHTcrab2814	05:46:45.49	+11:00:52.1
CFHTcrab1715	05:01:48.97	+12:00:52.1
CFHTcrab2215	05:22:15.85	+12:00:52.1
CFHTcrab2715	05:42:42.72	+12:00:52.1
CFHTcrab3015	05:54:58.85	+12:00:52.1
CFHTcrab3416	06:11:28.92	+13:00:52.1
CFHTcrab1717	05:01:33.07	+14:00:52.1
CFHTcrab1618	04:57:15.63	+15:00:52.1
CFHTcrab2918	05:51:05.91	+15:00:52.1
CFHTcrab3318	06:07:39.84	+15:00:52.1
CFHTcrab1819	05:05:24.14	+16:00:52.1
CFHTcrab2019	05:13:43.52	+16:00:52.1
CFHTcrab1620	04:56:53.10	+17:00:52.1
CFHTcrab3722	06:25:18.19	+19:00:52.1

CFHTcrab3523	06:17:06.23	+20:00:52.1
CFHTcrab3625	06:21:59.60	+22:00:52.1
CFHTcrab3726	06:26:41.03	+23:00:52.1
CFHTcrab1327	04:41:59.07	+24:00:52.1
CFHTcrab1427	04:46:21.81	+24:00:52.1
CFHTcrab1527	04:50:44.55	+24:00:52.1
CFHTcrab3527	06:18:19.40	+24:00:52.1
CFHTcrab3630	06:23:55.30	+27:00:52.1
CFHTcrab1731	04:58:17.15	+28:00:52.1
CFHTcrab2932	05:52:49.75	+29:00:52.1
CFHTcrab1633	04:52:57.46	+30:00:52.1
CFHTcrab1933	05:06:48.96	+30:00:52.1
CFHTcrab3034	05:57:52.15	+31:00:52.1
CFHTcrab2737	05:44:11.06	+34:00:52.1

Table A.1: CFHT MegaCam Program 11AC033 Observed Crab Fields

APPENDIX B

CFHT MEGACAM PROGRAM 11BC021 OBSERVED FIELDS

Field ID	RA	Dec
c3c1127	00:54:54.80	+54:49:42.0
c3c1129	01:04:26.56	+56:49:42.0
c3c1131	01:15:17.55	+58:49:42.0
c3c1133	01:27:43.89	+60:49:42.0
c3c1135	01:42:06.49	+62:49:42.0
c3c1323	00:26:21.03	+50:49:42.0
c3c1325	00:33:15.19	+52:49:42.0
c3c1327	00:41:01.51	+54:49:42.0
c3c1329	00:49:49.29	+56:49:42.0
c3c1331	00:59:50.20	+58:49:42.0
c3c1333	01:11:19.13	+60:49:42.0
c3c1335	01:24:35.38	+62:49:42.0
c3c1521	00:08:02.45	+48:49:42.0
c3c1523	00:13:41.11	+50:49:42.0
c3c1525	00:20:00.75	+52:49:42.0
c3c1527	00:27:08.22	+54:49:42.0
c3c1529	00:35:12.02	+56:49:42.0

c3c1531	00:44:22.85	+58:49:42.0
c3c1533	00:54:54.37	+60:49:42.0
c3c1535	01:07:04.26	+62:49:42.0
c3c1719	00:08:42.37	+46:49:42.0
c3c1721	00:04:06.68	+48:49:42.0
c3c1723	00:01:01.19	+50:49:42.0
c3c1725	00:06:46.32	+52:49:42.0
c3c1727	00:13:14.93	+54:49:42.0
c3c1729	00:20:34.74	+56:49:42.0
c3c1731	00:28:55.50	+58:49:42.0
c3c1733	00:38:29.61	+60:49:42.0
c3c1735	00:49:33.15	+62:49:42.0
c3c1919	00:20:23.93	+46:49:42.0
c3c1921	00:16:15.81	+48:49:42.0
c3c1923	00:11:38.73	+50:49:42.0
c3c1925	00:06:28.11	+52:49:42.0
c3c1927	00:00:38.37	+54:49:42.0
c3c1929	00:05:57.47	+56:49:42.0
c3c1931	00:13:28.15	+58:49:42.0
c3c1933	00:22:04.85	+60:49:42.0
c3c1935	00:32:02.03	+62:49:42.0
c3c2117	00:35:23.62	+44:49:42.0
c3c2119	00:32:05.50	+46:49:42.0
c3c2121	00:28:24.95	+48:49:42.0
c3c2123	00:24:18.65	+50:49:42.0
c3c2125	00:19:42.54	+52:49:42.0
c3c2127	00:14:31.66	+54:49:42.0
c3c2129	00:08:39.81	+56:49:42.0
c3c2131	00:01:59.20	+58:49:42.0
c3c2133	00:05:40.09	+60:49:42.0
c3c2317	00:46:40.42	+44:49:42.0

c3c2319	00:43:47.06	+46:49:42.0
c3c2321	00:40:34.08	+48:49:42.0
c3c2323	00:36:58.56	+50:49:42.0
c3c2325	00:32:56.97	+52:49:42.0
c3c2327	00:28:24.95	+54:49:42.0
c3c2329	00:23:17.08	+56:49:42.0
c3c2331	00:17:26.55	+58:49:42.0
c3c2333	00:10:44.67	+60:49:42.0
c3c2515	01:00:11.05	+42:49:42.0
c3c2517	00:57:57.21	+44:49:42.0
c3c2519	00:55:28.62	+46:49:42.0
c3c2521	00:52:43.21	+48:49:42.0
c3c2523	00:49:38.48	+50:49:42.0
c3c2525	00:46:11.41	+52:49:42.0
c3c2527	00:42:18.24	+54:49:42.0
c3c2529	00:37:54.36	+56:49:42.0
c3c2531	00:32:53.90	+58:49:42.0
c3c2533	00:27:09.43	+60:49:42.0
c3c2715	01:11:05.54	+42:49:42.0
c3c2717	01:09:14.01	+44:49:42.0
c3c2719	01:07:10.18	+46:49:42.0
c3c2721	01:04:52.34	+48:49:42.0
c3c2723	01:02:18.40	+50:49:42.0
c3c2725	00:59:25.84	+52:49:42.0
c3c2727	00:56:11.54	+54:49:42.0
c3c2729	00:52:31.63	+56:49:42.0
c3c2731	00:48:21.25	+58:49:42.0
c3c2733	00:43:34.20	+60:49:42.0
c3c2735	00:38:02.43	+62:49:42.0
c3c2915	01:22:00.03	+42:49:42.0
c3c2917	01:20:30.81	+44:49:42.0

c3c2919	01:18:51.75	+46:49:42.0
c3c2921	01:17:01.47	+48:49:42.0
c3c2923	01:14:58.32	+50:49:42.0
c3c2925	01:12:40.27	+52:49:42.0
c3c2927	01:10:04.83	+54:49:42.0
c3c2929	01:07:08.90	+56:49:42.0
c3c2931	01:03:48.60	+58:49:42.0
c3c2933	00:59:58.96	+60:49:42.0
c3c2935	00:55:33.54	+62:49:42.0
c3c3115	01:32:54.53	+42:49:42.0
c3c3117	01:31:47.61	+44:49:42.0
c3c3119	01:30:33.31	+46:49:42.0
c3c3121	01:29:10.60	+48:49:42.0
c3c3123	01:27:38.24	+50:49:42.0
c3c3125	01:25:54.70	+52:49:42.0
c3c3127	01:23:58.12	+54:49:42.0
c3c3129	01:21:46.18	+56:49:42.0
c3c3131	01:19:15.95	+58:49:42.0
c3c3313	01:44:29.29	+40:49:42.0
c3c3315	01:43:49.02	+42:49:42.0
c3c3317	01:43:04.40	+44:49:42.0
c3c3319	01:42:14.87	+46:49:42.0
c3c3321	01:41:19.74	+48:49:42.0
c3c3323	01:40:18.16	+50:49:42.0
c3c3325	01:39:09.14	+52:49:42.0
c3c3327	01:37:51.41	+54:49:42.0
c3c3329	01:36:23.45	+56:49:42.0
c3c3513	01:55:03.64	+40:49:42.0
c3c3515	01:54:43.51	+42:49:42.0
c3c3517	01:54:21.20	+44:49:42.0
c3c3519	01:53:56.44	+46:49:42.0

c3c3521	01:53:28.87	+48:49:42.0
c3c3523	01:52:58.08	+50:49:42.0
c3c3525	01:52:23.57	+52:49:42.0
c3c3527	01:51:44.71	+54:49:42.0
c3c3529	01:51:00.73	+56:49:42.0
c3c3713	02:05:38.00	+40:49:42.0
c3c3715	02:05:38.00	+42:49:42.0
c3c3717	02:05:38.00	+44:49:42.0
c3c3719	02:05:38.00	+46:49:42.0
c3c3721	02:05:38.00	+48:49:42.0
c3c3723	02:05:38.00	+50:49:42.0
c3c3725	02:05:38.00	+52:49:42.0
c3c3727	02:05:38.00	+54:49:42.0
c3c3913	02:16:12.36	+40:49:42.0
c3c3915	02:16:32.49	+42:49:42.0
c3c3917	02:16:54.80	+44:49:42.0
c3c3919	02:17:19.56	+46:49:42.0
c3c3921	02:17:47.13	+48:49:42.0
c3c3925	02:18:52.43	+52:49:42.0
c3c3929	02:20:15.27	+56:49:42.0
c3c4113	02:26:46.71	+40:49:42.0
c3c4115	02:27:26.98	+42:49:42.0
c3c4119	02:29:01.13	+46:49:42.0
c3c4121	02:29:56.26	+48:49:42.0
c3c4123	02:30:57.84	+50:49:42.0
c3c4129	02:34:52.55	+56:49:42.0
c3c4315	02:38:21.47	+42:49:42.0
c3c4317	02:39:28.39	+44:49:42.0
c3c4319	02:40:42.69	+46:49:42.0
c3c4321	02:42:05.40	+48:49:42.0
c3c4323	02:43:37.76	+50:49:42.0

c3c4325	02:45:21.30	+52:49:42.0
c3c4327	02:47:17.88	+54:49:42.0
c3c4329	02:49:29.82	+56:49:42.0
c3c4331	02:52:00.05	+58:49:42.0
c3c4515	02:49:15.97	+42:49:42.0
c3c4517	02:50:45.19	+44:49:42.0
c3c4519	02:52:24.25	+46:49:42.0
c3c4521	02:54:14.53	+48:49:42.0
c3c4523	02:56:17.68	+50:49:42.0
c3c4525	02:58:35.73	+52:49:42.0
c3c4527	03:01:11.17	+54:49:42.0
c3c4529	03:04:07.10	+56:49:42.0
c3c4531	03:07:27.40	+58:49:42.0
c3c4715	03:00:10.46	+42:49:42.0
c3c4717	03:02:01.99	+44:49:42.0
c3c4719	03:04:05.82	+46:49:42.0
c3c4721	03:06:23.66	+48:49:42.0
c3c4723	03:08:57.60	+50:49:42.0
c3c4725	03:11:50.16	+52:49:42.0
c3c4727	03:15:04.46	+54:49:42.0
c3c4729	03:18:44.37	+56:49:42.0
c3c4731	03:22:54.75	+58:49:42.0
c3c4915	03:11:04.95	+42:49:42.0
c3c4917	03:13:18.79	+44:49:42.0
c3c4919	03:15:47.38	+46:49:42.0
c3c4921	03:18:32.79	+48:49:42.0
c3c4923	03:21:37.52	+50:49:42.0
c3c4925	03:25:04.59	+52:49:42.0
c3c4927	03:28:57.76	+54:49:42.0
c3c4929	03:33:21.64	+56:49:42.0
c3c4931	03:38:22.10	+58:49:42.0

c3c5117	03:24:35.58	+44:49:42.0
c3c5121	03:30:41.92	+48:49:42.0
c3c5123	03:34:17.44	+50:49:42.0
c3c5125	03:38:19.03	+52:49:42.0
c3c5129	03:47:58.92	+56:49:42.0
c3c5317	03:35:52.38	+44:49:42.0
c3c5319	03:39:10.50	+46:49:42.0
c3c5321	03:42:51.05	+48:49:42.0
c3c5323	03:46:57.35	+50:49:42.0
c3c5325	03:51:33.46	+52:49:42.0
c3c5327	03:56:44.34	+54:49:42.0
c3c5329	04:02:36.19	+56:49:42.0
c3c5519	03:50:52.07	+46:49:42.0
c3c5521	03:55:00.19	+48:49:42.0
c3c5523	03:59:37.27	+50:49:42.0
c3c5525	04:04:47.89	+52:49:42.0
c3c5527	04:10:37.63	+54:49:42.0
c3c5719	04:02:33.63	+46:49:42.0
c3c5721	04:07:09.32	+48:49:42.0
c3c5723	04:12:17.19	+50:49:42.0
c3c5725	04:18:02.32	+52:49:42.0
c3c5921	04:19:18.45	+48:49:42.0
c3c5925	04:31:16.75	+52:49:42.0

Table B.1: CFHT MegaCam Program 11BC021 Observed SN 1181 Fields

APPENDIX C

W_{CO} VALUES FOR LIGHT ECHO FIELDS

Field ID	RA	DEC	SNR	W_{CO} [K km/s]
c3c2731_22	00:48:57.358	+58:43:42.50	Tycho	0
c3c1531_19	00:48:01.854	+58:41:00.29	Tycho	0
c3c1535_6	01:05:59.307	+63:12:37.49	Tycho	2.9
c3c2731_23	00:48:25.677	+58:42:27.42	Tycho	0
c3c1331_1	01:03:12.802	+59:11:43.18	Tycho	0.03
c3c2731_10	00:51:23.951	+58:56:55.69	Tycho	0.12
c3c1331_15	00:59:05.053	+59:02:42.05	Tycho	0
c3c1533_4	00:55:40.039	+61:07:39.34	Tycho	11
c3c1331_12	01:01:35.266	+58:55:48.00	Tycho	0
c3c1331_25	00:57:46.316,	+58:44:59.76	Tycho	0
c3c1535_14	01:07:10.133	+63:02:00.04	Tycho	2.7
c3c1727_22	00:13:49.055	+54:49:07.51	Tycho	0
c3c2731_19	00:51:29.855	+58:49:03.74	Tycho	0.12
c3c2731_20	00:51:13.125	+58:46:44.67	Tycho	0.12
c3c2333_12	00:12:37.826	+61:00:30.67	Tycho	2.3
c3c2333_30	00:11:51.207	+61:01:11.47	Tycho	1.1
c3c2127_24	00:13:48.858	+54:49:04.34	Cas A	0

tyc2116	23:02:42.9	+56:48:18	Cas A	0.93
tyc2729	23:13:36.6	+64:41:15	Cas A	2.4
tyc3024	23:37:53.6	+61:42:55	Cas A	0.64
tyc3826	00:17:39.7	+62:40:59	Cas A	0.09
tyc3325	23:52:04.4	+62:03:19	Tycho	1.7
tyc4022	00:28:25.6	+60:10:14	Tycho	0.0004
tyc4430	00:52:10.1	+65:28:54	Tycho	4.9
tyc4523	00:55:27.1	+61:10:13	Tycho	11

tyc2521	23:12:03.778	+59:34:59.10	Cas A	16
tyc2822	23:28:45.367	+60:41:12.50	Tycho	7
tyc2823	23:27:41.746	+60:52:32.94	Tycho	0.69
tyc3925	00:22:17.346	+62:15:13.65	Tycho	0.13
tyc4021_1	00:28:37.824	+59:59:42.93	Tycho	0.0004
tyc4022_4	00:28:01.637	+60:05:59.09	Tycho	0.0004
tyc5027_1	01:23:40.131	+63:47:02.34	Tycho	1.5
tyc4430_2	00:52:15.363	+65:29:07.96	Tycho	4.9

Table C.1: W_{CO} Values [K km/s] for Light Echo Fields

BIBLIOGRAPHY

Aharonian, F., Akhperjanian, A. G., Barres de Almeida, U., Bazer-Bachi, A. R., Behera, B., Beilicke, M., Benbow, W., Berge, D., Bernlöhner, K., Boisson, C., Bolz, O., Borrel, V., Braun, I., Brion, E., Brucker, J., Bühler, R., Bulik, T., Büsching, I., Boutelier, T., Carrigan, S., Chadwick, P. M., Chounet, L.-M., Clapson, A. C., Coignet, G., Cornils, R., Costamante, L., Dalton, M., Degrange, B., Dickinson, H. J., Djannati-Ataï, A., Domainko, W., O'C. Drury, L., Dubois, F., Dubus, G., Dyks, J., Egberts, K., Emmanoulopoulos, D., Espigat, P., Farnier, C., Feinstein, F., Fiasson, A., Förster, A., Fontaine, G., Füßling, M., Gallant, Y. A., Giebels, B., Glicenstein, J. F., Glück, B., Goret, P., Hadjichristidis, C., Hauser, D., Hauser, M., Heinzlmann, G., Henri, G., Hermann, G., Hinton, J. A., Hoffmann, A., Hofmann, W., Holleran, M., Hoppe, S., Horns, D., Jacholkowska, A., de Jager, O. C., Jung, I., Katarzyński, K., Kendziorra, E., Kerschhaggl, M., Khélifi, B., Keogh, D., Komin, N., Kosack, K., Lamanna, G., Latham, I. J., Lemoine-Goumard, M., Lenain, J.-P., Lohse, T., Martin, J. M., Martineau-Huynh, O., Marcowith, A., Masterson, C., Maurin, D., McComb, T. J. L., Moderski, R., Moulin, E., Naumann-Godo, M., de Naurois, M., Nedbal, D., Nekrassov, D., Nolan, S. J., Ohm, S., Olive, J.-P., de Oña Wilhelmi, E., Orford, K. J., Osborne, J. L., Ostrowski, M., Panter, M., Pedalletti, G., Pelletier, G., Petrucci, P.-O., Pita, S., Pühlhofer, G., Punch, M., Quirrenbach, A., Raubenheimer, B. C., Raue, M., Rayner, S. M., Renaud, M., Ripken, J., Rob, L., Rosier-Lees, S., Rowell, G., Rudak, B., Ruppel, J., Sahakian, V., Santangelo, A., Schlickeiser, R., Schöck, F. M., Schröder, R., Schwanke, U., Schwarzburg, S., Schwemmer, S., Shalchi, A., Sol, H., Spangler, D.,

- Stawarz, L., Steenkamp, R., Stegmann, C., Superina, G., Tam, P. H., Tavernet, J.-P., Terrier, R., van Eldik, C., Vasileiadis, G., Venter, C., Vialle, J. P., Vincent, P., Vivier, M., Völk, H. J., Volpe, F., Wagner, S. J., Ward, M., Zdziarski, A. A., & Zech, A. 2008, *A&A*, 488, 219
- Alard, C. 2000, *A&AS*, 144, 363
- Alard, C. & Lupton, R. H. 1998, *ApJ*, 503, 325
- Allen, S. W., Schmidt, R. W., & Fabian, A. C. 2002, *MNRAS*, 334, L11
- Alves, J., Lada, C. J., & Lada, E. A. 1999, *ApJ*, 515, 265
- Andrews, J. E., Sugerman, B. E. K., Clayton, G. C., Gallagher, J. S., Barlow, M. J., Clem, J., Ercolano, B., Fabbri, J., Meixner, M., Otsuka, M., Welch, D. L., & Wesson, R. 2011, *ApJ*, 731, 47
- Arnett, W. D. 1969, *AP&SS*, 5, 180
- Baade, W. 1943, *ApJ*, 97, 119
- Baba, J., Asaki, Y., Makino, J., Miyoshi, M., Saitoh, T. R., & Wada, K. 2009, *ApJ*, 706, 471
- Baldwin, J. E. & Edge, D. O. 1957, *The Observatory*, 77, 139
- Bejger, M. & Haensel, P. 2003, *A&A*, 405, 747
- Bertin, E., Mellier, Y., Radovich, M., Missonnier, G., Didelon, P., & Morin, B. 2002, in *Astronomical Society of the Pacific Conference Series*, Vol. 281, *Astronomical Data Analysis Software and Systems XI*, ed. D. A. Bohlender, D. Durand, & T. H. Handley, 228
- Bianchini, A., Sabbadin, F., & Hamzaoglu, E. 1982, *A&A*, 106, 176
- Bietenholz, M. F. 2006, *ApJ*, 645, 1180
- Bietenholz, M. F., Frail, D. A., & Hester, J. J. 2001, *ApJ*, 560, 254
- Bietenholz, M. F., Hester, J. J., Frail, D. A., & Bartel, N. 2004, *ApJ*, 615, 794

- Bietenholz, M. F., Kronberg, P. P., Hogg, D. E., & Wilson, A. S. 1991, *ApJL*, 373, L59
- Blair, W. P., Davidson, K., Fesen, R. A., Uomoto, A., MacAlpine, G. M., & Henry, R. B. C. 1997, *ApJS*, 109, 473
- Blondin, J. M., Mezzacappa, A., & DeMarino, C. 2003, *ApJ*, 584, 971
- Bocchino, F., Warwick, R. S., Marty, P., Lumb, D., Becker, W., & Pigot, C. 2001, *A&A*, 369, 1078
- Boffi, F. R., Sparks, W. B., & Macchetto, F. D. 1999, *A&AS*, 138, 253
- Bond, H. E., Henden, A., Levay, Z. G., Panagia, N., Sparks, W. B., Starrfield, S., Wagner, R. M., Corradi, R. L. M., & Munari, U. 2003, *Nature*, 422, 405
- Brat, L., Hudec, R., Simon, V., Strobl, J., Kubanek, P., Nekola, M., & Jelinek, M. 2006, *The Astronomer's Telegram*, 965, 1
- Brown, P. J., Dawson, K. S., Harris, D. W., Olmstead, M., Milne, P., & Roming, P. W. A. 2012, *ApJ*, 749, 18
- Brown, R. H. & Hazard, C. 1953, *MNRAS*, 113, 109
- Burrows, A., Walder, R., Ott, C. D., & Livne, E. 2005, in *Astronomical Society of the Pacific Conference Series*, Vol. 332, *The Fate of the Most Massive Stars*, ed. R. Humphreys & K. Stanek, 350
- Camilo, F., Stairs, I. H., Lorimer, D. R., Backer, D. C., Ransom, S. M., Klein, B., Wielebinski, R., Kramer, M., McLaughlin, M. A., Arzoumanian, Z., & Müller, P. 2002, *ApJL*, 571, L41
- Cappellaro, E., Evans, R., & Turatto, M. 1999, *A&A*, 351, 459
- Cappellaro, E., Patat, F., Mazzali, P. A., Benetti, S., Danziger, J. I., Pastorello, A., Rizzi, L., Salvo, M., & Turatto, M. 2001, *ApJL*, 549, L215
- Chakrabarty, D., Pivovarov, M. J., Hernquist, L. E., Heyl, J. S., & Narayan, R. 2001, *ApJ*, 548, 800

- Chevalier, R. A. 2004, *Advances in Space Research*, 33, 456
- . 2005, *ApJ*, 619, 839
- Chomiuk, L., Chornock, R., Soderberg, A. M., Berger, E., Chevalier, R. A., Foley, R. J., Huber, M. E., Narayan, G., Rest, A., Gezari, S., Kirshner, R. P., Riess, A., Rodney, S. A., Smartt, S. J., Stubbs, C. W., Tonry, J. L., Wood-Vasey, W. M., Burgett, W. S., Chambers, K. C., Czekala, I., Flewelling, H., Forster, K., Kaiser, N., Kudritzki, R.-P., Magnier, E. A., Martin, D. C., Morgan, J. S., Neill, J. D., Price, P. A., Roth, K. C., Sanders, N. E., & Wainscoat, R. J. 2011, *ApJ*, 743, 114
- Chomiuk, L., Soderberg, A. M., Moe, M., Chevalier, R. A., Rupen, M. P., Badenes, C., Margutti, R., Fransson, C., Fong, W.-f., & Dittmann, J. A. 2012, *ApJ*, 750, 164
- Clark, D. H., Murdin, P., Wood, R., Gilmozzi, R., Danziger, J., & Furr, A. W. 1983, *MNRAS*, 204, 415
- Clark, D. H. & Stephenson, F. R. 1977, *The historical supernovae* (Oxford [Eng.] ; New York : Pergamon Press, 1977. 1st ed.)
- Combes, F. 1991, *ARA&A*, 29, 195
- Comella, J. M., Craft, H. D., Lovelace, R. V. E., & Sutton, J. M. 1969, *Nature*, 221, 453
- Conley, A., Carlberg, R. G., Guy, J., Howell, D. A., Jha, S., Riess, A. G., & Sullivan, M. 2007, *The Astrophysical Journal Letters*, 664, L13
- Cordes, J. M. & Lazio, T. J. W. 2002, *ArXiv Astrophysics e-prints*
- Couderc, P. 1939, *Annales d'Astrophysique*, 2, 271
- Crotts, A. P. S. 1988, *ApJL*, 333, L51
- Crotts, A. P. S. & Yourdon, D. 2008, *ApJ*, 689, 1186
- da Silva, L. A. L. 1993, *AP&SS*, 202, 215
- Dame, T. M., Hartmann, D., & Thaddeus, P. 2001, *ApJ*, 547, 792

- DeLaney, T., Rudnick, L., Stage, M. D., Smith, J. D., Isensee, K., Rho, J., Allen, G. E., Gomez, H., Kozasa, T., Reach, W. T., Davis, J. E., & Houck, J. C. 2010, *ApJ*, 725, 2038
- Di Stefano, R. 2010, *ApJ*, 712, 728
- Doggett, J. B. & Branch, D. 1985, *AJ*, 90, 2303
- Draine, B. T., Dale, D. A., Bendo, G., Gordon, K. D., Smith, J. D. T., Armus, L., Engelbracht, C. W., Helou, G., Kennicutt, Jr., R. C., Li, A., Roussel, H., Walter, F., Calzetti, D., Moustakas, J., Murphy, E. J., Rieke, G. H., Bot, C., Hollenbach, D. J., Sheth, K., & Teplitz, H. I. 2007, *ApJ*, 663, 866
- Drout, M. R., Soderberg, A. M., Gal-Yam, A., Cenko, S. B., Fox, D. B., Leonard, D. C., Sand, D. J., Moon, D.-S., Arcavi, I., & Green, Y. 2011, *ApJ*, 741, 97
- Duyvendak, J. J. L. 1942, *PASP*, 54, 91
- Felton, J. E. 1991, *Sky & Telescope*, 153
- Fesen, R., Rudie, G., Hurford, A., & Soto, A. 2008, *ApJS*, 174, 379
- Fesen, R. A. 2001, in *Bulletin of the American Astronomical Society*, Vol. 33, American Astronomical Society Meeting Abstracts, 1364
- Fesen, R. A., Hammell, M. C., Morse, J., Chevalier, R. A., Borkowski, K. J., Dopita, M. A., Gerardy, C. L., Lawrence, S. S., Raymond, J. C., & van den Bergh, S. 2006, *ApJ*, 645, 283
- Fewell, M. P. 1995, *American Journal of Physics*, 63, 653
- Fich, M., Blitz, L., & Stark, A. A. 1989, *ApJ*, 342, 272
- Flammarion, C. & Antoniadis, E. M. 1901, *Astronomische Nachrichten*, 156, 253
- Foglizzo, T., Galletti, P., Scheck, L., & Janka, H.-T. 2007, *ApJ*, 654, 1006
- Fontaine, G., Brassard, P., & Bergeron, P. 2001, *PASP*, 113, 409
- Foster, T. & MacWilliams, J. 2006, *ApJ*, 644, 214

- Foster, T. & Routledge, D. 2003, *ApJ*, 598, 1005
- Foster, T., Routledge, D., & Kothes, R. 2004, *A&A*, 417, 79
- Frail, D. A., Kassim, N. E., Cornwell, T. J., & Goss, W. M. 1995, *ApJL*, 454, L129
- Fryer, C. L., Rockefeller, G., Timmes, F. X., Hungerford, A. L., & Belle, K. E. 2005, in *Open Issues in Core Collapse Supernova Theory*, ed. A. Mezzacappa & G. M. Fuller, 136–155
- Fuhrmann, K. 2005, *MNRAS*, 359, L35
- Gaensler, B. M. & Frail, D. A. 2000, *Nature*, 406, 158
- Gallagher, J. S., Clayton, G., Andrews, J., Sugerman, B., Clem, J., Barlow, M., Ercolano, B., Fabbri, J., Wesson, R., Otsuka, M., & Meixner, M. 2011, in *Bulletin of the American Astronomical Society*, Vol. 43, American Astronomical Society Meeting Abstracts, 337.22
- Gamezo, V. N., Khokhlov, A. M., & Oran, E. S. 2005, *ApJ*, 623, 337
- Gardner, F. F. & Milne, D. K. 1965, *AJ*, 70, 754
- Garnavich, P. M., Kirshner, R. P., Challis, P., Jha, S., Branch, D., Chevalier, R., Filippenko, A. V., Li, W., Fransson, C., Lundqvist, P., McCray, R., Panagia, N., Phillips, M. M., Pun, C. S. J., Sonneborn, G., Schmidt, B. P., Suntzeff, N. B., Wheeler, J. C., & Supernova INTensive Study SINS Collaboration. 2001, in *Bulletin of the American Astronomical Society*, Vol. 33, American Astronomical Society Meeting Abstracts, 1370
- Gaskell, C. M., Cappellaro, E., Dinerstein, H. L., Garnett, D. R., Harkness, R. P., & Wheeler, J. C. 1986, *ApJL*, 306, L77
- Gilfanov, M. & Bogdán, Á. 2010, *Nature*, 463, 924
- Gómez, G. C. 2006, *AJ*, 132, 2376
- González Hernández, J. I., Ruiz-Lapuente, P., Filippenko, A. V., Foley, R. J., Gal-Yam, A., & Simon, J. D. 2009, *ApJ*, 691, 1
- Goss, W. M., Schwarz, U. J., & Wesselius, P. R. 1973, *A&A*, 28, 305

- Gotthelf, E. V., Helfand, D. J., & Newburgh, L. 2007, *ApJ*, 654, 267
- Green, D. A. & Gull, S. F. 1982, *Nature*, 299, 606
- Guy, J., Astier, P., Baumont, S., Hardin, D., Pain, R., Regnault, N., Basa, S., Carlberg, R. G., Conley, A., Fabbro, S., Fouchez, D., Hook, I. M., Howell, D. A., Perrett, K., Pritchett, C. J., Rich, J., Sullivan, M., Antilogus, P., Aubourg, E., Bazin, G., Bronder, J., Filiol, M., Palanque-Delabrouille, N., Ripoche, P., & Ruhlmann-Kleider, V. 2007, *A&A*, 466, 11
- Hamuy, M., Phillips, M. M., Suntzeff, N. B., Schommer, R. A., Maza, J., & Aviles, R. 1996a, *AJ*, 112, 2398
- Hamuy, M., Phillips, M. M., Suntzeff, N. B., Schommer, R. A., Maza, J., Smith, R. C., Lira, P., & Aviles, R. 1996b, *AJ*, 112, 2438
- Hanbury Brown, R. & Hazard, C. 1952, *Nature*, 170, 364
- Havlen, R. J. 1972, *A&A*, 16, 252
- Hayakawa, T., Mizuno, A., Onishi, T., Yonekura, Y., Hara, A., Yamaguchi, R., & Fukui, Y. 1999, *PASJ*, 51, 919
- Heger, A., Fryer, C. L., Woosley, S. E., Langer, N., & Hartmann, D. H. 2003, *ApJ*, 591, 288
- Heney, L. G. & Greenstein, J. L. 1941, *ApJ*, 93, 70
- Hester, J. J. 2007, in *Bulletin of the American Astronomical Society*, Vol. 39, American Astronomical Society Meeting Abstracts, 100.26
- Hester, J. J. 2008, *Annual Review of Astronomy and Astrophysics*, 46, 127
- Hester, J. J., Mori, K., Burrows, D., Gallagher, J. S., Graham, J. R., Halverson, M., Kader, A., Michel, F. C., & Scowen, P. 2002, *ApJL*, 577, L49
- Hester, J. J., Scowen, P. A., Sankrit, R., Burrows, C. J., Gallagher, III, J. S., Holtzman, J. A., Watson, A., Trauger, J. T., Ballester, G. E., Casertano, S., Clarke, J. T., Crisp, D.,

- Evans, R. W., Griffiths, R. E., Hoessel, J. G., Krist, J., Lynds, R., Mould, J. R., O'Neil, Jr., E. J., Stapelfeldt, K. R., & Westphal, J. A. 1995, *ApJ*, 448, 240
- Hester, J. J., Stone, J. M., Scowen, P. A., Jun, B.-I., Gallagher, III, J. S., Norman, M. L., Ballester, G. E., Burrows, C. J., Casertano, S., Clarke, J. T., Crisp, D., Griffiths, R. E., Hoessel, J. G., Holtzman, J. A., Krist, J., Mould, J. R., Sankrit, R., Stapelfeldt, K. R., Trauger, J. T., Watson, A., & Westphal, J. A. 1996, *ApJ*, 456, 225
- Hillebrandt, W. & Niemeyer, J. C. 2000, *Annual Review of Astronomy and Astrophysics*, 38, 191
- Hirata, K., Kajita, T., Koshiba, M., Nakahata, M., Oyama, Y., Sato, N., Suzuki, A., Takita, M., Totsuka, Y., Kifune, T., Suda, T., Takahashi, K., Tanimori, T., Miyano, K., Yamada, M., Beier, E. W., Feldscher, L. R., Kim, S. B., Mann, A. K., Newcomer, F. M., Van, R., Zhang, W., & Cortez, B. G. 1987, *Phys. Rev. Lett.*, 58, 1490
- Iben, Jr., I. & Tutukov, A. V. 1984, *ApJS*, 54, 335
- Ivezic, Z., Tyson, J. A., Acosta, E., Allsman, R., Anderson, S. F., Andrew, J., Angel, R., Axelrod, T., Barr, J. D., Becker, A. C., Becla, J., Beldica, C., Blandford, R. D., Bloom, J. S., Borne, K., Brandt, W. N., Brown, M. E., Bullock, J. S., Burke, D. L., Chandrasekharan, S., Chesley, S., Claver, C. F., Connolly, A., Cook, K. H., Cooray, A., Covey, K. R., Cribbs, C., Cutri, R., Daues, G., Delgado, F., Ferguson, H., Gawiser, E., Geary, J. C., Gee, P., Geha, M., Gibson, R. R., Gilmore, D. K., Gressler, W. J., Hogan, C., Huffer, M. E., Jacoby, S. H., Jain, B., Jernigan, J. G., Jones, R. L., Juric, M., Kahn, S. M., Kalirai, J. S., Kantor, J. P., Kessler, R., Kirkby, D., Knox, L., Krabbendam, V. L., Krughoff, S., Kulkarni, S., Lambert, R., Levine, D., Liang, M., Lim, K., Lupton, R. H., Marshall, P., Marshall, S., May, M., Miller, M., Mills, D. J., Monet, D. G., Neill, D. R., Nordby, M., O'Connor, P., Oliver, J., Olivier, S. S., Olsen, K., Owen, R. E., Peterson, J. R., Petry, C. E., Pierfederici, F., Pietrowicz, S., Pike, R., Pinto, P. A., Plante, R., Radeka, V., Rasmussen, A., Ridgway, S. T., Rosing, W., Saha, A., Schalk, T. L., Schindler, R. H., Schneider, D. P., Schumacher, G., Seabag, J., Seppala, L. G., Shipsey, I., Silvestri, N., Smith, J. A., Smith, R. C., Strauss, M. A., Stubbs, C. W., Sweeney, D., Szalay, A., Thaler, J. J., Vanden Berk, D., Walkowicz, L., Warner, M., Willman, B., Wittman, D.,

- Wolff, S. C., Wood-Vasey, W. M., Yoachim, P., Zhan, H., & for the LSST Collaboration. 2008, ArXiv e-prints
- Jackson, M. S., Safi-Harb, S., Kothes, R., & Foster, T. 2008, *ApJ*, 674, 936
- Jacoby, G. H., Branch, D., Ciardullo, R., Davies, R. L., Harris, W. E., Pierce, M. J., Pritchett, C. J., Tonry, J. L., & Welch, D. L. 1992, *PASP*, 104, 599
- Janka, H.-T., Langanke, K., Marek, A., Martínez-Pinedo, G., & Müller, B. 2007, *Physics Reports*, 442, 38
- Jha, S., Riess, A. G., & Kirshner, R. P. 2007, *ApJ*, 659, 122
- Kaiser, N., Burgett, W., Chambers, K., Denneau, L., Heasley, J., Jedicke, R., Magnier, E., Morgan, J., Onaka, P., & Tonry, J. 2010, in *Society of Photo-Optical Instrumentation Engineers (SPIE) Conference Series*, Vol. 7733, Society of Photo-Optical Instrumentation Engineers (SPIE) Conference Series
- Kaplan, D. L., Chatterjee, S., Gaensler, B. M., & Anderson, J. 2008, *ApJ*, 677, 1201
- Kapteyn, J. C. 1901, *Astronomische Nachrichten*, 157, 201
- Kasen, D., Röpke, F. K., & Woosley, S. E. 2009, *Nature*, 460, 869
- Kaspi, V. M., Roberts, M. E., Vasisht, G., Gotthelf, E. V., Pivovarov, M., & Kawai, N. 2001, *ApJ*, 560, 371
- Keller, S. C., Schmidt, B. P., Bessell, M. S., Conroy, P. G., Francis, P., Granlund, A., Kowald, E., Oates, A. P., Martin-Jones, T., Preston, T., Tisserand, P., Vaccarella, A., & Waterson, M. F. 2007, *PASA*, 24, 1
- Kerzendorf, W. E., Schmidt, B. P., Asplund, M., Nomoto, K., Podsiadlowski, P., Frebel, A., Fesen, R. A., & Yong, D. 2009, *ApJ*, 701, 1665
- Khokhlov, A. M. 1991, *A&A*, 245, 114
- Kiewe, M., Gal-Yam, A., Arcavi, I., Leonard, D. C., Emilio Enriquez, J., Cenko, S. B., Fox, D. B., Moon, D.-S., Sand, D. J., Soderberg, A. M., & CCCP, T. 2012, *ApJ*, 744, 10

- Knop, R. A., Aldering, G., Amanullah, R., Astier, P., Blanc, G., Burns, M. S., Conley, A., Deustua, S. E., Doi, M., Ellis, R., Fabbro, S., Folatelli, G., Fruchter, A. S., Garavini, G., Garmond, S., Garton, K., Gibbons, R., Goldhaber, G., Goobar, A., Groom, D. E., Hardin, D., Hook, I., Howell, D. A., Kim, A. G., Lee, B. C., Lidman, C., Mendez, J., Nobili, S., Nugent, P. E., Pain, R., Panagia, N., Pennypacker, C. R., Perlmutter, S., Quimby, R., Raux, J., Regnault, N., Ruiz-Lapuente, P., Sainton, G., Schaefer, B., Schahmaneche, K., Smith, E., Spadafora, A. L., Stanishev, V., Sullivan, M., Walton, N. A., Wang, L., Wood-Vasey, W. M., & Yasuda, N. 2003, *ApJ*, 598, 102
- Kothes, R. 2003, *A&A*, 408, 187
- Kothes, R. 2010, Arxiv preprint arXiv:1010.4586
- Kothes, R. & Foster, T. 2012, *ApJL*, 746, L4
- Kothes, R., Landecker, T. L., Reich, W., Safi-Harb, S., & Arzoumanian, Z. 2008, *ApJ*, 687, 516
- Kothes, R., Reich, W., Foster, T., & Byun, D.-Y. 2003, *ApJ*, 588, 852
- Kothes, R., Uyaniker, B., & Reid, R. I. 2005, *A&A*, 444, 871
- Kramer, M., Lyne, A. G., Hobbs, G., Löhmer, O., Carr, P., Jordan, C., & Wolszczan, A. 2003, *ApJL*, 593, L31
- Krause, O., Birkmann, S. M., Usuda, T., Hattori, T., Goto, M., Rieke, G. H., & Misselt, K. A. 2008a, *Science*, 320, 1195
- Krause, O., Rieke, G. H., Birkmann, S. M., Le Floc'h, E., Gordon, K. D., Egami, E., Bieging, J., Hughes, J. P., Young, E. T., Hinz, J. L., Quanz, S. P., & Hines, D. C. 2005, *Science*, 308, 1604
- Krause, O., Tanaka, M., Usuda, T., Hattori, T., Goto, M., Birkmann, S., & Nomoto, K. 2008b, *Nature*, 456, 617
- Lada, C. J., Lada, E. A., Clemens, D. P., & Bally, J. 1994, *ApJ*, 429, 694

- Leibundgut, B. 2008, *General Relativity and Gravitation*, 40, 221
- Leonard, D. C. 2007, *ApJ*, 670, 1275
- Li, W., Bloom, J. S., Podsiadlowski, P., Miller, A. A., Cenko, S. B., Jha, S. W., Sullivan, M., Howell, D. A., Nugent, P. E., Butler, N. R., Ofek, E. O., Kasliwal, M. M., Richards, J. W., Stockton, A., Shih, H.-Y., Bildsten, L., Shara, M. M., Bibby, J., Filippenko, A. V., Ganeshalingam, M., Silverman, J. M., Kulkarni, S. R., Law, N. M., Poznanski, D., Quimby, R. M., McCully, C., Patel, B., Maguire, K., & Shen, K. J. 2011a, *Nature*, 480, 348
- Li, W., Leaman, J., Chornock, R., Filippenko, A. V., Poznanski, D., Ganeshalingam, M., Wang, X., Modjaz, M., Jha, S., Foley, R. J., & Smith, N. 2011b, *MNRAS*, 412, 1441
- Liu, J.-F., Bregman, J. N., & Seitzer, P. 2003, *ApJ*, 582, 919
- Loll, A. M., Hester, J. J., Blair, W. P., & Sankrit, R. 2007, in *Bulletin of the American Astronomical Society*, Vol. 39, American Astronomical Society Meeting Abstracts, 100.25
- Lorimer, D. R. & Kramer, M. 2004, *Handbook of Pulsar Astronomy* (Handbook of pulsar astronomy, by D.R. Lorimer and M. Kramer. Cambridge observing handbooks for research astronomers, Vol. 4. Cambridge, UK: Cambridge University Press, 2004)
- Lyne, A. G., Pritchard, R. S., & Graham-Smith, F. 1993, *MNRAS*, 265, 1003
- Maoz, D. & Mannucci, F. 2008, *MNRAS*, 388, 421
- . 2011, ArXiv e-prints
- Mayall, N. U. & Oort, J. H. 1942, *PASP*, 54, 95
- Mazzali, P. A., Benetti, S., Altavilla, G., Blanc, G., Cappellaro, E., Elias-Rosa, N., Garavini, G., Goobar, A., Harutyunyan, A., Kotak, R., Leibundgut, B., Lundqvist, P., Mattila, S., Mendez, J., Nobili, S., Pain, R., Pastorello, A., Patat, F., Pignata, G., Podsiadlowski, P., Ruiz-Lapuente, P., Salvo, M., Schmidt, B. P., Sollerman, J., Stanishev, V., Stehle, M., Tout, C., Turatto, M., & Hillebrandt, W. 2005, *The Astrophysical Journal Letters*, 623, L37

- Migliazzo, J. M., Gaensler, B. M., Backer, D. C., Stappers, B. W., van der Swaluw, E., & Strom, R. G. 2002, *ApJL*, 567, L141
- Miller, A. A., Smith, N., Li, W., Bloom, J. S., Chornock, R., Filippenko, A. V., & Prochaska, J. X. 2010, *AJ*, 139, 2218
- Milne, D. K. & Dickel, J. R. 1971, *Nature Physical Science*, 231, 33
- Minkowski, R. 1941, *PASP*, 53, 224
- Minkowski, R. 1959, in *IAU Symposium, Vol. 9, URSI Symp. 1: Paris Symposium on Radio Astronomy*, ed. R. N. Bracewell, 315
- Mitton, S. 1978, *The Crab Nebula* (New York : Scribner, 1979, c1978. 1st U.S. ed.)
- Miville-Deschênes, M.-A. & Lagache, G. 2005, *ApJS*, 157, 302
- Mori, K., Burrows, D. N., Hester, J. J., Pavlov, G. G., Shibata, S., & Tsunemi, H. 2004, *ApJ*, 609, 186
- Murray, S. S., Slane, P. O., Seward, F. D., Ransom, S. M., & Gaensler, B. M. 2002, *ApJ*, 568, 226
- Ng, C.-Y. & Romani, R. W. 2006, *ApJ*, 644, 445
- Nomoto, K. 1982, *ApJ*, 253, 798
- Nomoto, K., Suzuki, T., Shigeyama, T., Kumagai, S., Yamaoka, H., & Saio, H. 1993, *Nature*, 364, 507
- Nomoto, K., Thielemann, F.-K., & Yokoi, K. 1984, *ApJ*, 286, 644
- Nugent, P. E., Sullivan, M., Cenko, S. B., Thomas, R. C., Kasen, D., Howell, D. A., Bersier, D., Bloom, J. S., Kulkarni, S. R., Kandrashoff, M. T., Filippenko, A. V., Silverman, J. M., Marcy, G. W., Howard, A. W., Isaacson, H. T., Maguire, K., Suzuki, N., Tarlton, J. E., Pan, Y.-C., Bildsten, L., Fulton, B. J., Parrent, J. T., Sand, D., Podsiadlowski, P., Bianco, F. B., Dilday, B., Graham, M. L., Lyman, J., James, P., Kasliwal, M. M., Law, N. M.,

- Quimby, R. M., Hook, I. M., Walker, E. S., Mazzali, P., Pian, E., Ofek, E. O., Gal-Yam, A., & Poznanski, D. 2011, *Nature*, 480, 344
- Ortiz, J. L., Sugerman, B. E. K., de La Cueva, I., Santos-Sanz, P., Duffard, R., Gil-Hutton, R., Melita, M., & Morales, N. 2010, *A&A*, 519, A7
- Otsuka, M., Meixner, M., Panagia, N., Fabbri, J., Barlow, M. J., Clayton, G. C., Gallagher, J. S., Sugerman, B. E. K., Wesson, R., Andrews, J. E., Ercolano, B., & Welch, D. 2012, *ApJ*, 744, 26
- Pakmor, R., Kromer, M., Röpke, F. K., Sim, S. A., Ruiter, A. J., & Hillebrandt, W. 2010, *Nature*, 463, 61
- Perlmutter, S., Aldering, G., Goldhaber, G., Knop, R. A., Nugent, P., Castro, P. G., Deustua, S., Fabbro, S., Goobar, A., Groom, D. E., Hook, I. M., Kim, A. G., Kim, M. Y., Lee, J. C., Nunes, N. J., Pain, R., Pennypacker, C. R., Quimby, R., Lidman, C., Ellis, R. S., Irwin, M., McMahon, R. G., Ruiz-Lapuente, P., Walton, N., Schaefer, B., Boyle, B. J., Filippenko, A. V., Matheson, T., Fruchter, A. S., Panagia, N., Newberg, H. J. M., Couch, W. J., & Supernova Cosmology Project. 1999, *ApJ*, 517, 565
- Perrine, C. D. 1901, *ApJ*, 14, 359
- Phillips, M. M. 1993, *ApJL*, 413, L105
- Pineda, J. L., Goldsmith, P. F., Chapman, N., Snell, R. L., Li, D., Cambrésy, L., & Brunt, C. 2010, *ApJ*, 721, 686
- Podsiadlowski, P., Hsu, J. J. L., Joss, P. C., & Ross, R. R. 1993, *Nature*, 364, 509
- Quimby, R. M., Kulkarni, S. R., Kasliwal, M. M., Gal-Yam, A., Arcavi, I., Sullivan, M., Nugent, P., Thomas, R., Howell, D. A., Nakar, E., Bildsten, L., Theissen, C., Law, N. M., Dekany, R., Rahmer, G., Hale, D., Smith, R., Ofek, E. O., Zolkower, J., Velur, V., Walters, R., Henning, J., Bui, K., McKenna, D., Poznanski, D., Cenko, S. B., & Levitan, D. 2011, *Nature*, 474, 487
- Quinn, J. L., Garnavich, P. M., Li, W., Panagia, N., Riess, A., Schmidt, B. P., & Della Valle, M. 2006, *ApJ*, 652, 512

- Rau, A., Kulkarni, S. R., Law, N. M., Bloom, J. S., Ciardi, D., Djorgovski, G. S., Fox, D. B., Gal-Yam, A., Grillmair, C. C., Kasliwal, M. M., Nugent, P. E., Ofek, E. O., Quimby, R. M., Reach, W. T., Shara, M., Bildsten, L., Cenko, S. B., Drake, A. J., Filippenko, A. V., Helfand, D. J., Helou, G., Howell, D. A., Poznanski, D., & Sullivan, M. 2009, *PASP*, 121, 1334
- Rest, A., Becker, A. C., Bergmann, M., Blondin, S., Challis, P., Clocchiatti, A., Cook, K. H., Damke, G., Garg, A., Huber, M. E., Lanning, H., Matheson, T., Minniti, D., Morelli, L., Nikolaev, S., Olsen, K., Oosterle, L., Pignata, G., Prieto, J., Smith, R. C., Stubbs, C., Suntzeff, N. B., Welch, D. L., Wood-Vasey, W. M., & Zenteno, A. 2007, in *Bulletin of the American Astronomical Society*, Vol. 39, American Astronomical Society Meeting Abstracts, 107.02
- Rest, a., Foley, R. J., Sinnott, B., Welch, D. L., Badenes, C., Filippenko, a. V., Bergmann, M., Bhatti, W. a., Blondin, S., Challis, P., Damke, G., Finley, H., Huber, M. E., Kasen, D., Kirshner, R. P., Matheson, T., Mazzali, P., Minniti, D., Nakajima, R., Narayan, G., Olsen, K., Sauer, D., Smith, R. C., & Suntzeff, N. B. 2011a, *The Astrophysical Journal*, 732, 3
- Rest, a., Prieto, J. L., Walborn, N. R., Smith, N., Bianco, F. B., Chornock, R., Welch, D. L., Howell, D. a., Huber, M. E., Foley, R. J., Fong, W., Sinnott, B., Bond, H. E., Smith, R. C., Toledo, I., Minniti, D., & Mandel, K. 2012, *Nature*, 482, 375
- Rest, A., Sinnott, B., & Welch, D. L. 2012, *ArXiv e-prints*
- Rest, a., Sinnott, B., Welch, D. L., Narayan, G., Mandel, K., Huber, M. E., & Blondin, S. 2011b, *The Astrophysical Journal*, 732, 2
- Rest, A., Stubbs, C., Becker, A. C., Miknaitis, G. A., Miceli, A., Covarrubias, R., Hawley, S. L., Smith, R. C., Suntzeff, N. B., Olsen, K., Prieto, J. L., Hiriart, R., Welch, D. L., Cook, K. H., Nikolaev, S., Huber, M., Proctor, G., Clocchiatti, A., Minniti, D., Garg, A., Challis, P., Keller, S. C., & Schmidt, B. P. 2005a, *ApJ*, 634, 1103
- Rest, A., Suntzeff, N. B., Olsen, K., Prieto, J. L., Smith, R. C., Welch, D. L., Becker, A.,

- Bergmann, M., Clocchiatti, A., Cook, K., Garg, A., Huber, M., Miknaitis, G., Minniti, D., Nikolaev, S., & Stubbs, C. 2005b, *Nature*, 438, 1132
- Rest, A., Welch, D., & Suntzeff, N. 2008, *The Astrophysical Journal*, 2006
- Reynolds, S. P., Borkowski, K. J., Hwang, U., Hughes, J. P., Badenes, C., Laming, J. M., & Blondin, J. M. 2007, *ApJL*, 668, L135
- Reynoso, E. M. & Goss, W. M. 1999, *AJ*, 118, 926
- Richardson, D., Branch, D., & Baron, E. 2006, *The Astronomical Journal*, 131, 2233
- Richardson, D., Branch, D., Casebeer, D., Millard, J., Thomas, R. C., & Baron, E. 2002, *The Astronomical Journal*, 123, 745
- Riess, A. G., Filippenko, A. V., Li, W., Treffers, R. R., Schmidt, B. P., Qiu, Y., Hu, J., Armstrong, M., Faranda, C., Thouvenot, E., & Buil, C. 1999, *AJ*, 118, 2675
- Riess, A. G., Press, W. H., & Kirshner, R. P. 1996, *ApJ*, 473, 88
- Roberts, D. A., Goss, W. M., Kalberla, P. M. W., Herbstmeier, U., & Schwarz, U. J. 1993, *A&A*, 274, 427
- Röpke, F. K. & Hillebrandt, W. 2005, *A&A*, 431, 635
- Ruiz-Lapuente, P. 2004, *The Astrophysical Journal*, 612, 357
- Russeil, D., Adami, C., & Georgelin, Y. M. 2007, *A&A*, 470, 161
- Sankrit, R., Blair, W. P., Delaney, T., Rudnick, L., Harrus, I. M., & Ennis, J. A. 2005, *Advances in Space Research*, 35, 1027
- Sankrit, R. & Hester, J. J. 1997, *ApJ*, 491, 796
- Sankrit, R., Hester, J. J., Scowen, P. A., Ballester, G. E., Burrows, C. J., Clarke, J. T., Crisp, D., Evans, R. W., Gallagher, III, J. S., Griffiths, R. E., Hoessel, J. G., Holtzman, J. A., Krist, J., Mould, J. R., Stapelfeldt, K. R., Trauger, J. T., Watson, A., & Westphal, J. A. 1998, *ApJ*, 504, 344

- Schaefer, B. E. 1996, *ApJ*, 459, 438
- Schechter, P. L., Mateo, M., & Saha, A. 1993, *PASP*, 105, 1342
- Schmidt, B., Kirshner, R., Peters, J., & Bernstein, G. 1994, *IAUC*, 5962, 2
- Schmidt, B. P., Suntzeff, N. B., Phillips, M. M., Schommer, R. A., Clocchiatti, A., Kirshner, R. P., Garnavich, P., Challis, P., Leibundgut, B., Spyromilio, J., Riess, A. G., Filippenko, A. V., Hamuy, M., Smith, R. C., Hogan, C., Stubbs, C., Diercks, A., Reiss, D., Gilliland, R., Tonry, J., Maza, J., Dressler, A., Walsh, J., & Ciardullo, R. 1998, *ApJ*, 507, 46
- Seward, F. D., Gorenstein, P., & Smith, R. K. 2006a, *ApJ*, 636, 873
- Seward, F. D., Tucker, W. H., & Fesen, R. A. 2006b, *ApJ*, 652, 1277
- Slane, P. O., Helfand, D. J., & Murray, S. S. 2002, *ApJL*, 571, L45
- Smartt, S. J. 2009, *Annual Review of Astronomy and Astrophysics*, 47, 63
- Smartt, S. J., Maund, J. R., Hendry, M. A., Tout, C. A., Gilmore, G. F., Mattila, S., & Benn, C. R. 2004, *Science*, 303, 499
- Sparks, W. B., Macchetto, F., Panagia, N., Boffi, F. R., Branch, D., Hazen, M. L., & della Valle, M. 1999, *ApJ*, 523, 585
- Spergel, D. N., Verde, L., Peiris, H. V., Komatsu, E., Nolta, M. R., Bennett, C. L., Halpern, M., Hinshaw, G., Jarosik, N., Kogut, A., Limon, M., Meyer, S. S., Page, L., Tucker, G. S., Weiland, J. L., Wollack, E., & Wright, E. L. 2003, *ApJS*, 148, 175
- Staelin, D. H. & Reifenstein, III, E. C. 1968, *Science*, 162, 1481
- Stephenson, F. & Green, D. 2002, *Historical Supernovae and their Remnants* (Clarendon Press)
- Stephenson, F. R. 1971, *QJRAS*, 12, 10
- Sugerman, B. E. K. 2005, *ApJL*, 632, L17

- Sugerman, B. E. K. 2007, in *Astronomical Society of the Pacific Conference Series*, Vol. 363, *The Nature of V838 Mon and its Light Echo*, ed. R. L. M. Corradi & U. Munari, 121–+
- Sugerman, B. E. K., Andrews, J. E., Barlow, M. J., Clayton, G. C., Ercolano, B., Ghavamian, P., Kennicutt, Jr., R. C., Krause, O., Meixner, M., & Otsuka, M. 2012, *ApJ*, 749, 170
- Sugerman, B. E. K. & Crotts, A. P. S. 2002, *ApJL*, 581, L97
- Sugerman, B. E. K., Crotts, A. P. S., Kunkel, W. E., Heathcote, S. R., & Lawrence, S. S. 2005a, *ApJ*, 627, 888
- . 2005b, *ApJS*, 159, 60
- Temim, T., Gehrz, R. D., Woodward, C. E., Roellig, T. L., Smith, N., Rudnick, L., Polomski, E. F., Davidson, K., Yuen, L., & Onaka, T. 2006, *AJ*, 132, 1610
- Tian, W. W. & Leahy, D. A. 2011, *ApJL*, 729, L15
- Tody, D. 1993, in *Astronomical Society of the Pacific Conference Series*, Vol. 52, *Astronomical Data Analysis Software and Systems II*, ed. R. J. Hanisch, R. J. V. Brissenden, & J. Barnes, 173
- Tomaney, A. B. & Crotts, A. P. S. 1996, *AJ*, 112, 2872
- Trimble, V. 1968, *AJ*, 73, 535
- . 1973, *PASP*, 85, 579
- Trimble, V. & Woltjer, L. 1971, *ApJL*, 163, L97
- Turner, M. S. & Tyson, J. A. 1999, *Reviews of Modern Physics Supplement*, 71, 145
- Vallée, J. P. 2008, *AJ*, 135, 1301
- van den Bergh, S. 1965a, *AJ*, 70, 667
- . 1965b, *PASP*, 77, 269
- . 1966, *PASP*, 78, 74

- van den Heuvel, E. P. J., Bhattacharya, D., Nomoto, K., & Rappaport, S. A. 1992, *A&A*, 262, 97
- Van Dyk, S. D., Li, W., & Filippenko, A. V. 2003, *PASP*, 115, 1289
- . 2006, *PASP*, 118, 351
- Wang, B. & Han, Z. 2010, *A&A*, 515, A88
- Wang, X., Li, W., Filippenko, A. V., Foley, R. J., Smith, N., & Wang, L. 2008, *ApJ*, 677, 1060
- Warner, B. 2003, *Cataclysmic Variable Stars* (Cataclysmic Variable Stars, by Brian Warner, pp. 592. ISBN 052154209X. Cambridge, UK: Cambridge University Press, September 2003.)
- Webbink, R. F. 1984, *ApJ*, 277, 355
- Weiler, K. W. & Panagia, N. 1978, *A&A*, 70, 419
- Weingartner, J. C. & Draine, B. T. 2001, *ApJ*, 548, 296
- Weisskopf, M. C., Hester, J. J., Tennant, A. F., Elsner, R. F., Schulz, N. S., Marshall, H. L., Karovska, M., Nichols, J. S., Swartz, D. A., Kolodziejczak, J. J., & O'Dell, S. L. 2000, *ApJL*, 536, L81
- Welch, D. L., Clayton, G. C., Campbell, A., Barlow, M. J., Sugerman, B. E. K., Meixner, M., & Bank, S. H. R. 2007, *ApJ*, 669, 525
- Westerlund, B. 1961, *PASP*, 73, 72
- Wheeler, J. C. & Harkness, R. P. 1990, *Reports on Progress in Physics*, 53, 1467
- Wheeler, J. C., Maund, J. R., & Couch, S. M. 2008, *ApJ*, 677, 1091
- Whelan, J. & Iben, Jr., I. 1973, *ApJ*, 186, 1007
- Williams, D. R. W. 1973, *A&A*, 28, 309

Winkler, P. F., Gupta, G., & Long, K. S. 2003, *ApJ*, 585, 324

Woosley, S. & Bloom, J. 2006, *Annual Review of Astronomy and Astrophysics*, 44, 507

Wyckoff, S. & Murray, C. A. 1977, *MNRAS*, 180, 717

Xu, J. & Crots, A. P. S. 1999, *ApJ*, 511, 262

Xu, J., Crots, A. P. S., & Kunkel, W. E. 1994, *ApJ*, 435, 274